

Government Arts & Science College
RESEARCH JOURNAL

Vol 9 • Issue 1 • December 2018

**Essays In
Contemporary Science**

Editor: Dr. Binitha M P
Department of Physics



Govt Arts & Science College
Kozhikode- 18



Government Arts & Science College
RESEARCH JOURNAL

(Bi-annual)

Vol. 9. Issue 1 December 2018

ISSN: 2277-4246

Peer-reviewed

Advisory Board

Dr. A K Abdul Gafoor	Dr. V. M. Kannan
Dr. A Rajan Nambiar	Dr. Joby K Jose
Prof. M. K. Remesh Babu	Dr. Sini. P

Editorial Board

Dr. Sangeetha. C	Dr Z. A. Ashraf
Dr. Jayasree S.	Abdul Riyas. K
Gireesh Babu. M	

Managing Editor

Dr. Jayasree S
Editor: Dr. Binitha M P

**This publication is funded by The Parent and Teachers Association
2018-19, GASC Kozhikode**

© All rights reserved. No part of this publication may be reproduced, stored in a retrieval system or transmitted in any form or by any means, electronic, mechanical, photocopying, recording or otherwise, without prior permission of the authors. The authors are responsible for the views expressed in their articles.

Book layout & cover design: Print X World, Calicut
Published by Dr. Jayasree S, Principal, Govt. Arts & Science College, Calicut

Contents

1. PROCESS CAPABILITY INDICES AND ITS APPLICATIONS

● Swalih K., Bindu Punathumparambath | Pages 9-25

2. STRUCTURAL, THERMAL AND ELECTRICAL CHARACTERIZATION ON GEL GROWN COBALT SUCCINATE TETRAHYDRATE SINGLE CRYSTALS

● M.P Binitha and P.P Pradyumnan | Pages 26-41

3. HYBRID BIONANOCOMPOSITE MATERIALS FOR WATER PURIFICATION

● Mujeeb Rahman P. | Pages 42-52

4. GENERALIZATIONS OF THE WEIBULL DISTRIBUTION AND ITS APPLICATIONS IN LIFETIME DATA ANALYSIS

● Nihala N. C., Bindu Punathumparambath | Pages 53-68

5. GREEN SYNTHESIS OF SILVER NANO PARTICLE USED FOR ANTIMICROBIAL APPLICATIONS

● Jeena Chalikuzhi, Archana Ashokan, Binitha M P | Pages 69-79

6. A REVIEW ON THE GREEN SYNTHESIS OF ZINC OXIDE NANOPARTICLES

● Dr.Nisha M | Pages 80-87

7. SYNTHESIS & CHARACTERIZATION OF Mn DOPED ZnS NANOPARTICLES

● Parvathy T, Sabira K | Pages 88-109

Contents

8. DEGREE POLYNOMIAL OF A GRAPH
● Annie Sabitha Paul |Pages 110-120
9. SUPERCAPACITOR APPLICATION OF ELECTROSPUN
PVA – PANI COMPOSITE NANOFIBER ELECTRODES
● Dr. Sindhu S, Akhil P |Pages 121-138
10. ON STRENGTH OF FUZZY GRAPHS
● Reshmi K M |Pages 139-149
11. STRENGTH OF A FUZZY GRAPH AS ITS STRENGTH
OF CONNECTIVITY
● Reshmi K M |Pages 150-159
12. COMPLEMENT TREE DOMINATION NUMBER
● Raji Pilakkat, Roopa.V.K |Pages 160-169
13. SOME MORE RESULTS ON COMPLEMENT TREE
DOMINATION NUMBER
● Raji Pilakkat, Roopa.V.K |Pages 170-178
14. CALCULATION OF BETWEENNESS CENTRALITY OF
SOME GRAPHS
● Shiny Joseph |Pages 179-192
15. DIRECT SUM OF WEAK SPECTRAL SYNTHESIS SETS
● Muraleedharan T. K |Pages 193-196

Foreword

It is my privilege to write the forward to the 9th volume of the research journal of our college. This issue includes a collection of research manuscripts related to findings in different fields of science and gives an honest look at the progression of science and technology in this rapidly growing technological world. I am sure that the articles in this issue will improve one's knowledge in all these aspects in a very efficient way and will provide the primary forum for advancement and dissemination of scientific knowledge. I would like to praise all the people who put their efforts for the making and publication of this journal.

Dr. S. Jayasree

Principal

Govt. Arts and Science College

Preface

I am delighted to introduce the new issue of the science journal of Government Arts & Science Journal. This journal provides a really exciting opportunity to consider the truly interdisciplinary nature of different science topics at a time of great change across the wider technology world.

The objective of this journal is to publish up-to-date, high-quality and original research papers along with relevant and insightful reviews. As such the journal tries to be captivating and accessible, and in the meantime integrative and challenging. This journal issue consists of two types of papers, original research articles and review papers. Research Papers are more traditional in form and demonstrate theoretical and experimental works in the different research areas and gives a clear contribution to knowledge in the respective field. Critical Reviews, provide a critical and concise yet comprehensive and contemporary review of a particular theme.

An overview of the contents of this issue is discussed as follows. The issue is opened with a research article in Statistics entitled "Process Capability Indices and Its Applications". In this paper the authors have identified certain process capability indices which are suitable for normal and non-normal data. Also they have compared two different types of processes using capability indices for decision making.

In the second paper entitled "Structural,

Thermal and Electrical Characterization on Gel Grown Cobalt Succinate Tetrahydrate Single Crystals” the authors describe the growth features of Cobalt Succinate Tetrahydrate crystals in silica gel medium and detailed structural study of the grown crystals.

The next article deals with the preparation and characterization of hybrid bionanocomposite materials for water purification. Hybrid Chitosan-ZnO composites were prepared by sol-gel method, and characterized by Fourier transform infrared spectrometer, X-ray diffraction and Scanning Electron Microscopy. The composites were found to behave as an excellent adsorbent and antimicrobial material.

The fourth paper entitled “Generalizations of the Weibull Distribution and its Applications in Lifetime Data Analysis” the authors have investigated the various generalizations of the Weibull distribution and have illustrated the applications of the Weibull distribution with resilient and tilted parameter.

The next paper describes the synthesis of silver nanoparticle using leaf extracts of *Azadirachta Indica* and *Terminalia catappa* and the demonstration of antibacterial activity of the prepared samples. The sixth paper is a review paper on the green synthesis of zinc oxide nanoparticles and various applications of nanoparticles in different fields. In the article entitled “Synthesis & Characterization of Mn doped ZnS Nanoparticles”, the authors have focussed on the synthesis of pure and doped zinc sulphide nano particles and their photo luminescent properties.

In the next paper k-nodal set of a graphs are discussed and Degree Polynomial of a graph is introduced.

Some properties of this polynomial are observed and degree polynomial of some specific graphs is computed. Supercapacitor application of electrospun PVA – PANI composite nanofiber electrodes is discussed in the next article.

In the next article entitled “On Strength of Fuzzy Graphs” the authors describes some basic definitions and terminologies of fuzzy graphs, which have generated interest in many researchers in mathematics as well as in engineering. In the next paper the strength of various fuzzy graphs are determined in terms of order of the graph/ the number of its weakest edge, using the concept of strength of connectivity. The next two articles are related to complement tree domination numbers. In the next paper the betweenness centrality of graphs obtained by some graph operations in the star graph and some construction of betweenness uniform graphs are discussed. Last article is an analysis paper in mathematics.

I take this opportunity to thank all the journal's collaborators and supporters. On behalf of the Editorial Board and the whole Editorial Office, I would like to express our gratefulness to the authors of articles published in this issue.

Dr. Binitha M P

Department of Physics

PROCESS CAPABILITY INDICES AND ITS APPLICATIONS

■ Swalih K¹, Bindu Punathumpambath²

¹Department of Statistics, Govt. Arts and Science College, Kozhikode.

²Assistant Professor, Department of Statistics,
Govt. Arts and Science College, Kozhikode
Email:ppbindukannan@gmail.com

Abstract

Process capability indices (PCIs) have lot of applications in the manufacturing industry as it provides measures of process quality. Several basic process capability indices such as C_p , C_{pk} , and C_{pm} were used to monitor the process potential and process performance. In the present study we identified indices which are suitable for normal and non-normal data. Also we compared two different types of processes using capability indices such as C_p , C_{pk} , C_{pk}^* , and C_{pm} for decision making. We illustrated this with real datasets related to two suppliers, who provided aluminium foil materials to an electronic company in Taiwan. The analysis is carried out using R Package.

1. INTRODUCTION

Quality is one of the most important consumer decision making factors in the selection among competing products and services. Understanding and improving quality is a key factor leading to business success, growth and an enhanced competitive position. Quality control requires an environment in which both management and employees strive for perfection. This is done by training personnel, creating benchmarks for product quality, and testing products to check for statistically significant variations. The first significant attempt to understand and remove process

variation in a scientific way was made by Walter A. Shewhart of Bell Telephone Laboratories in the 1920's.

Shewhart developed the concept of statistical control chart in 1924 and the final conclusions were available in Shewhart (1931). Shewhart's system of Statistical Process Control was developed further by his colleague, W. Edwards Deming. By the middle of 1930's Statistical Quality Control (SQC) methods were widely in use. SQC is one of the most important applications of statistical techniques in industry. It is a set of statistical tools used by quality professionals.

A search for providing proof of quality via process capability study naturally ends up with the construction of one or the other of a set of process capability measures more commonly known as process capability indices (PCIs). The concept of PCIs was introduced by Juran et al. (1974). They realized the need for a single ratio or index to compare the specification interval with the actual process spread or variation as a measure of process capability. Detailed references on PCIs are available in Kotz and Johnson (2002), Kotz and Johnson (1993), Kotz and Lovelace (1998), Spiring et al. (2003) and Pearn and Kotz (2007).

Process capability analysis is a very valuable engineering decision tool. Quality engineers and managers are often faced with decision problems such as whether to accept or scrap a batch of process output, to intervene or not to intervene in a production process, or to review or not to review a managerial decision to intervene in a production process etc. Process capability analysis can be defined as the quantification of process variability, as the analysis of this variability relative to product specifications, and as an aid in eliminating or greatly reducing this variability in development and manufacturing.

In the present paper, we studied different types of process capability indices and its applications. Section 2 describes various process capability indices. Process capability indices for non-normal cases were studied in section 3. Section 4 is devoted to the applications of process capability indices. Finally, some concluding remarks were given in section 5.

2. PROCESS CAPABILITY INDICES (PCIs)

A process capability index is a unit-free measure that quantifies the relation between the actual performance of the process and its specified requirements. These indices are proved to be extremely useful in attaining various production targets when used in conjunction with Engineering Quality Control methods. A process is capable if the capability index exceeds a threshold value which can never be less than one in any case. Its value can be used to measure the extent to which the process meets the specifications. In general, higher the value of the index, lower the amount of products outside the specification limits. If the value is not up to the requirements, improvement efforts can be initiated based on the value of the index.

$$\text{General form of PCIs} = \frac{\text{specification interval}}{\text{process spread}} \quad (2.1)$$

Table 2.1: Classification of processes based on the value of the capability index.

Capability value	Grading
Less than 1	Inadequate
1 and less than 1.33	Capable
1.33 and less than 1.5	Satisfactory
1.5 and less than 2	Excellent
2 and above	Super

Next we discuss the different types of process capability indices.

2.1 The C_p index

The history of PCIs began with the introduction of the C_p index by Juran et al. in 1974, though it did not get considerable acceptance, until early 1980s. They defined the

index as index as

$$C_p = \frac{USL - LSL}{6\sigma} = \frac{\text{allowable range of measurements}}{\text{actual range of measurements}} \quad (2.2)$$

Finley (1992) refers to this index as Capability Potential Index (CPI), and Montgomery (2005) as Process Capability Ratio (PCR).

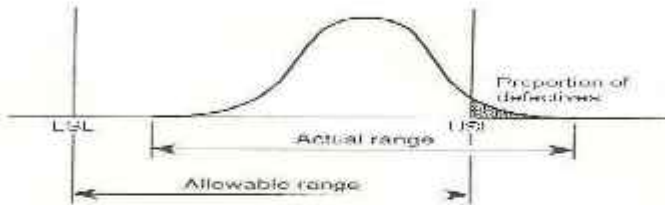


Figure 2.1: Comparison of actual and allowable variation ranges.

The numerator of C_p gives the size of the range over which the process measurements can vary. The denominator gives the size of the range over which the process is actually varying. Obviously, it is desirable to have a C_p as large as possible to attain high capability. But even when C_p is large, the process may not be capable, unless the process mean is located at safer positions between LSL and USL as can be seen in figure 2.1.

2.2 The C_{pu} Index

A capacity index that takes into account the change in both the process mean and process variation was felt by many, and that resulted in the proposal of the C_{pk} index by Kane (1986). C_{pk} is defined by a three-step procedure as follows:

Let

$$C_{pu} = \frac{USL - \mu}{3\sigma} = \frac{\text{allowable upper spread}}{\text{actual upper spread}}$$

and

$$C_{\mu} = \frac{\mu - LSL}{3\sigma} = \frac{\text{allowable lower spread}}{\text{actual lower spread}}$$

then

$$\begin{aligned} C_{pk} &= \min \{ C_{pl}, C_{pu} \} \\ &= \min \left\{ \frac{\mu - LSL}{3\sigma}, \frac{USL - \mu}{3\sigma} \right\} \\ &= \frac{d - |\mu - M|}{3\sigma}; \quad d = \frac{USL - LSL}{2}, \quad M = \frac{USL + LSL}{2} \end{aligned}$$

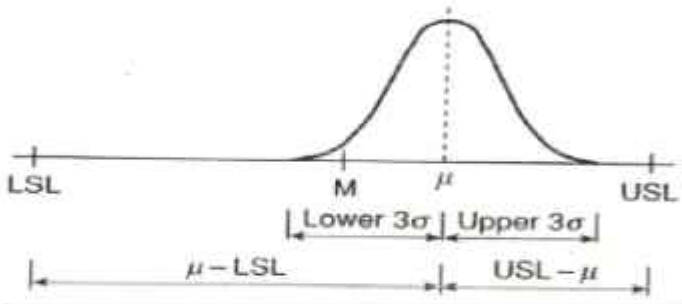


Figure 2.2: Comparison of amount of room available to amount of room needed.

Figure 2.2 illustrates the C_{pk} index. Gunter (1989) describes C_{pk} as a way to measure the ratio of the amount of room needed to the amount of room available to produce product within specifications.

2.3 The C_{pm} Index

The indices C_p and C_{pk} do not take into account the fact that the process mean μ may differ from some other more interested target value T . As per modern quality improvement theories, it is important to use target values and to keep the process on target.

The case when $\mu = \frac{USL + LSL}{2} = M$ referred to as asymmetric tolerances and most of the earlier PCIs were designed for

symmetric tolerances, PCIs, free of target values T , generally assume their maximum value when $\mu = \frac{USL + LSL}{2}$ and hence in such cases process conditions are so arranged that μ is at M , as far as possible. This is not the case of indices incorporating a target value.

Chan, Cheng and Spiring (1988) introduced such a capability index that incorporates a target value into its formula. The index proposed by them can be taken as a measure of process centering, and it is called C_{pm} .

$$\text{if } T = \frac{USL + LSL}{2}, C_{pm} = \frac{USL - LSL}{6\sigma'} = \frac{USL - LSL}{6\sigma \sqrt{1 + \left(\frac{\mu - T}{\sigma}\right)^2}} \quad (2.4)$$

where

$$\begin{aligned} \sigma' &= \sqrt{E(X - T)^2} \\ &= \sqrt{E(X - \mu + \mu - T)^2} \\ &= \sqrt{E(X - \mu)^2 + 2E(X - \mu)(\mu - T) + (\mu - T)^2} \\ &= \sqrt{E(X - \mu)^2 + (\mu - T)^2} \\ &= \sqrt{\sigma^2 + (\mu - T)^2} \\ &= \sigma \sqrt{1 + \left(\frac{\mu - T}{\sigma}\right)^2} \\ &= \sigma \sqrt{1 + \left(\frac{\mu - T}{\sigma}\right)^2} \end{aligned}$$

Since $E(X) = \mu, \sigma^2 = E(X - \mu)^2$

$$\text{If } T \neq \frac{USL + LSL}{2}, C_{pm} = \min\left\{\frac{USL - T}{3\sigma}, \frac{T - USL}{3\sigma}\right\} \quad (2.5)$$

2.4 The C_{pk} Index

A process is said to be centred or to have a symmetric tolerance if the target value T is the midpoint of the specification interval $T = M$. Though symmetric cases are common, asymmetric cases do occur in the manufacturing industry as just seen in the case of C_{pm} .

To overcome this problem, Pearn and Chen (1998) proposed the C_{pk}^* index, defined by

$$C_{pk}^* = \frac{d^* - A^*}{3\sigma} \quad (2.6)$$

Where

$$d^* = \min \{USL - T, T - LSL\} \text{ and } A^* = \max \left[\frac{d^* (\mu - T)}{USL - T}, \frac{d^* (T - \mu)}{T - LSL} \right]$$

Now we discuss the process capability indices for non-normal approach.

3. PROCESS CAPABILITY INDICES OF NON NORMAL APPROACH

Recently, research on non-normal process capability indices has emerged. Gunter (1989) pointed out the following three non-normal distributions with the same mean and standard deviation as those of a normal distribution: (1) chi-squared distribution with 4.5 d.f.; (2) t distribution with 8 d.f. and (3) uniform distribution. Although having the same C_p and C_{pk} indices, the defects falling outside $\pm 3\sigma$ are significantly different.

Clements (1989) used a Pearson distribution curve to estimate the non-normal process capability index. If the distribution of measurements of a quality characteristic belongs to the Pearson family of probability curves consisting of normal, lognormal, t, F, beta and gamma distributions, then let

$$P(LPL \leq \mu \leq UPL) = 1 - 0.0027 = 0.9973,$$

where the process mean is replaced by median, UPL is the 99.865 percentile, and LPL is the 0.135 percentile of the Pearson family. The non-normal process capability indices are defined as:

$$C_p = \frac{USL - LSL}{x_{0.9865} - x_{0.135}} \quad (2.7)$$

$$C_{pu} = \frac{USL - x_{50}}{x_{0.9865} - x_{50}} \quad (2.8)$$

$$C_{pl} = \frac{x_{50} - LSL}{x_{50} - x_{0.135}} \quad (2.9)$$

$$C_{pk} = \min \{ C_{pu}, C_{pl} \} \quad (2.10)$$

Where $x_p = p \cdot 100^{\text{th}}$ percentile.

When the collected data do not belong to a specific distribution of Pearson family of probability curves, we can use the Chebycheff inequality listed below to estimate UPL and LPL:

$$p(|X - \mu| < k\sigma) \geq 1 - \frac{1}{k^2} \quad \text{where } k > 1.$$

This means that when we use \bar{x} to estimate μ at least $100(1 - (1/k^2))\%$ of the observed values will fall within $\mu \pm k\sigma$

regardless of what distribution it is. For example, if $k = 5$, at least 96% of the observed value will fall within $\mu \pm 5\sigma$, and then we can use $UPL = x_{98}$, $LPL = x_2$ and $\mu = x_{50}$. The formulae for calculating normal and non-normal process capability indices can be summarized, according to three types of specifications: (1) bilateral specification; (2) unilateral specification with target value; and (3) unilateral specification without target value, as in Tables 3.1-3.4.

Table 3.1: The formulae of process capability indices to calculate normal and non-normal data for bilateral specification if $T = (USL+LSL)/2$.

	Normal	Non-Normal
\hat{C}_p	$\frac{USL - LSL}{6s}$	$\frac{USL - LSL}{x_{90.885} - x_{0.135}}$
\hat{C}_{pk}	$\min\left\{\frac{USL - \bar{X}}{3s}, \frac{\bar{X} - LSL}{3s}\right\}$	$\min\left\{\frac{USL - x_{70}}{x_{92.805} - x_{50}}, \frac{x_{50} - LSL}{x_{70} - x_{0.135}}\right\}$
\hat{C}_{pm}	$\frac{USL - LSL}{6\sqrt{s^2 + (\bar{X} - T)^2}}$	$\frac{USL - LSL}{\sqrt{\left(\frac{x_{90.885} - x_{0.135}}{6}\right)^2 + (x_{50} - T)^2}}$

Table 3.2: The formulae of process capability indices to calculate normal and non-normal data for bilateral specification if $T \neq (USL+LSL)/2$.

	Normal	Non-Normal
\hat{C}_p	$\frac{USL - LSL}{6s}$	$\frac{USL - LSL}{x_{90.800} - x_{0.115}}$
\hat{C}_{pk}	$\min\left\{\frac{USL - \bar{X}}{3s}, \frac{\bar{X} - LSL}{3s}\right\}$	$\min\left\{\frac{USL - x_{50}}{x_{92.865} - x_{50}}, \frac{x_{50} - LSL}{x_{50} - x_{0.135}}\right\}$
\hat{C}_{pm}	$\min\left\{\frac{USL - T}{3\sqrt{s^2 + (\bar{X} - T)^2}}, \frac{T - LSL}{3\sqrt{s^2 + (\bar{X} - T)^2}}\right\}$	$\min\left\{\frac{\frac{USL - T}{\sqrt{\left(\frac{x_{90.885} - x_{0.135}}{6}\right)^2 + (x_{50} - T)^2}}}{T - LSL}, \frac{T - LSL}{\sqrt{\left(\frac{x_{90.885} - x_{0.135}}{6}\right)^2 + (x_{50} - T)^2}}\right\}$

Table 3.3: The formulae of process capability indices to calculate normal and non-normal data for unilateral specification if target value does not exist.

	Normal	Non-Normal
\hat{C}_{pu}	$\frac{USL - \bar{X}}{3s}$	$\frac{USL - x_{70}}{x_{92.805} - x_{50}}$
\hat{C}_{pl}	$\frac{\bar{X} - LSL}{3s}$	$\frac{x_{50} - LSL}{x_{50} - x_{0.135}}$

Table 3.4: The formulae of process capability indices to calculate normal and non-normal data for unilateral specification if target value exists.

	Normal	Non-Normal
\hat{C}_p	$\frac{USL - T}{6s}$	$\frac{USL - T}{x_{99.865} - x_{0.135}}$
\hat{C}_{pu}	$\frac{USL - \bar{X}}{3s}$	$\frac{USL - x_{50}}{x_{99.865} - x_{50}}$
\hat{C}_{pl}	$\frac{\bar{X} - T}{3s}$	$\frac{x_{50} - T}{x_{50} - x_{0.135}}$
\hat{C}_p	$\frac{T - LSL}{6s}$	$\frac{T - LSL}{x_{99.865} - x_{0.135}}$
\hat{C}_{pl}	$\frac{\bar{X} - LSL}{3s}$	$\frac{x_{50} - LSL}{x_{99} - x_{0.135}}$
\hat{C}_{pu}	$\frac{T - \bar{X}}{3s}$	$\frac{T - x_{50}}{x_{99.865} - x_{50}}$

3.1 Lower Confidence Limits for C_{pk}

As C_{pk} is the most widely used PCI, majority of the work on the confidence interval estimation of PCIs are on that of C_{pk} . When the true value of C_{pk} is unknown then construction of its confidence interval becomes necessary. Construction of confidence intervals for C_{pk} is complicated since the process mean μ and process standard deviation σ is unknown (Kotz and Johnson (1993)). The usual estimator of C_{pk} is given by,

$$C_{pk} = \min\{C_{pu}, C_{pl}\} = \min\left\{\frac{\mu - LSL}{3\sigma}, \frac{USL - \mu}{3\sigma}\right\} \quad (3.1)$$

3.2 Confidence Limits for difference between PCI's

In this section we discuss procedure for constructing a confidence interval of process capability indices, to select a better supplier using the difference between two process capability indices. The manufactures necessity to satisfy the customer demand and extend after-sales support has made them truly quality conscious. Therefore, effective total quality

management and accurate evaluation of manufacturer's process capabilities have become important in industry. Different methods have been developed for evaluating whether a single supplier's item conforms to the requirements of a customer.

4. APPLICATIONS OF PROCESS CAPABILITY INDICES

In this section, we discuss two applications of process capability indices. First we analyse the data of the inside diameter measurements on forged piston rings given in Montgomery (2005).

A confidence interval can be used to assess the two supplier's capabilities if the confidence interval of the difference between two supplier's process capabilities can be obtained. If both the lower and upper confidence limits for the difference between two process capability indices ($C_{pk1} - C_{pk2}$), is positive. Then supplier 1 has a better process capability than supplier 2, if both confidence limits is negative, then supplier 2 has a better process capability than supplier 1; if one confidence limit is positive and the other negative, then no significance difference exists between the two supplier's process capabilities.

Then we compared the process capability indices for two supplier's data, given in Chen and Tong (2003).

4.1 Forged Piston Rings Data Analysis

We analysed the inside diameter measurement on forged piston rings data set taken from Montgomery (2005). The analysis is carried out by using 'qcc' package in R-programming. The xbar chart and process capability analysis were given in figure 4.1 and 4.2.

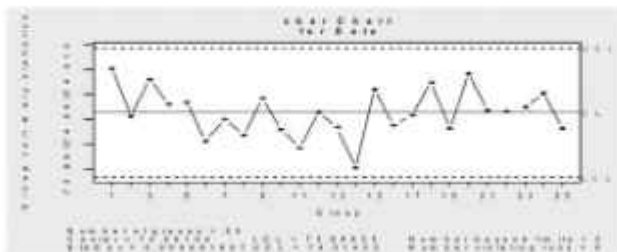


Figure 4.1: xbar chart for Inside diameter measurements on forged piston rings

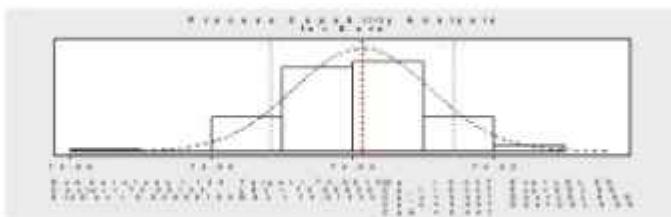


Figure 4.2: process capability analysis for Inside diameter measurements on forged piston rings

Table 4.1: Capability indices of inside diameter measurement on forged piston rings.

	Value	2.5%	97.5%
C_p	0.4472	0.3916	0.5028
C_{pk}	0.4474	0.3796	0.5151
C_{pm}	0.4471	0.3794	0.5148
C_{pk}	0.4471	0.3664	0.5278
C_{pm}	0.4472	0.3918	0.5026

From the table 4.1 we can see that the values of C_p , C_{pk} and C_{pm} were 0.4472, 0.4471, 0.4472 respectively. These values are all less than 1, so the process is inadequate.

4.2 Analysis of Supplier's Data

Now we analyze the data taken from Chen and Tong (2003). The data is related to two suppliers, who provided aluminium foil materials to an electronic company in Taiwan. Aluminium foil is a key component that governs the quality of capacitors and the voltage. The production specifications (U, T, L) of the voltage are (530, 520, 510). If the voltage falls outside this interval, the aluminium of foil will break and thus rejected. 45 random samples are taken from suppliers 1 and 2 by quality inspector. The data is analysed using R-package and obtained the values of process capability indices of the two data sets separately and compared the two indices values C_{pk1} and C_{pk2} .

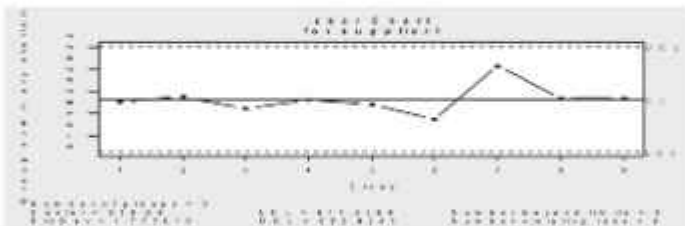


Figure 4.3: xbar chart for supplier 1.

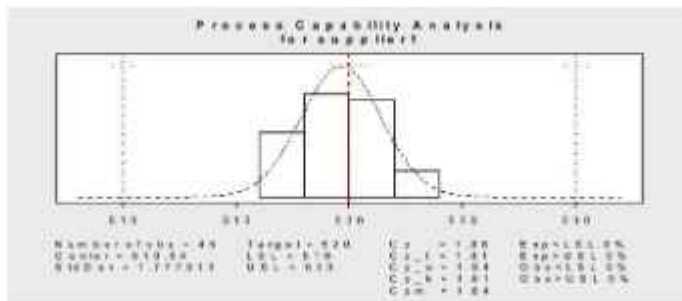


Figure 4.4: Process capability analysis for supplier 1.

Table 4.2: Capability indices of supplier1.

	Value	2.5%	97.5%
C_p	1.876	1.485	2.266
C_{pl}	1.808	1.481	2.136
C_{pu}	1.943	1.593	2.294
C_{pk}	1.808	1.418	2.198
C_{pm}	1.838	1.452	2.224

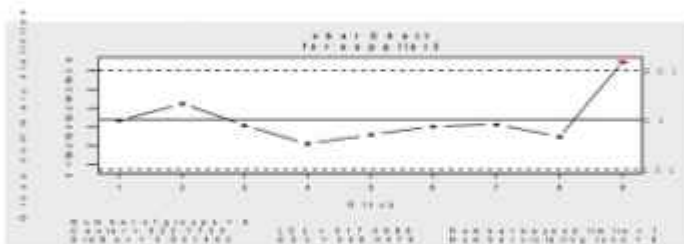
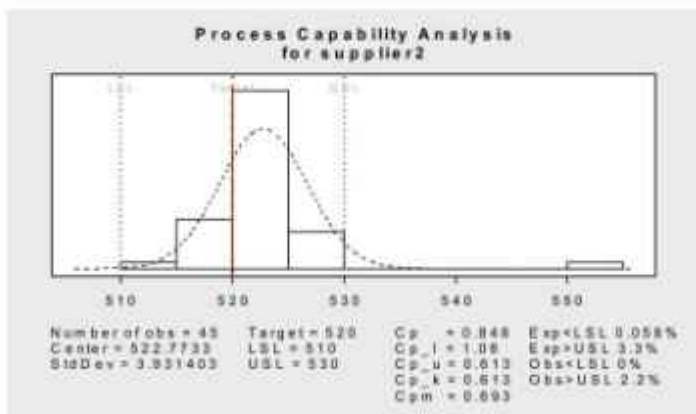
**Figure 4.5: xbar chart for supplier2.****Figure 4.6: process capability analysis for supplier2.**

Table 4.3: Capability indices of supplier2.

	Value	2.5%	97.5%
C_p	0.8479	0.6712	1.0242
C_{pi}	1.0830	0.8763	1.2898
C_{pu}	0.6127	0.4777	0.7477
C_{pk}	0.6127	0.4519	0.7736
C_{pm}	0.6928	0.5283	0.8571

From the table 4.2 and 4.3 we can see that process of each supplier is approximately normally distributed and both the lower and upper confidence limits for the difference between two process capability indices $(1.808 - 0.6127) = 1.1953$, are positive, the supplier 1 has a better process capability than supplier 2.

SUMMARY

In the present study we identified indices which are suitable for normal and normal data. We compared two different types of processes using capability indices such as C_p, C_{pk}, C_{pk}^* , and C_{pm} for decision making. We analyzed datasets given in Montgomery (2005) and Chen and Tong (2003). We found that the production process related to forged piston ring is inadequate and it needs correction. For the second datasets related to two suppliers who provided aluminium foil materials to an electronic company in Taiwan. The values of process capability indices C_{pi} for supplier1 and C_{pk} for supplier2 are 1.4227 and 1.2582 respectively. The difference between two process capability indices $(1.4227 - 1.2582) = 0.1645$, is positive. So the supplier1 has a better process capability than supplier2. Hence process capability analysis is an important tool in decision making and for taking corrective measures.

REFERENCE

1. Clements, J.A., Process capability calculations for non-normal distributions. Quality progr., 1989.
2. Chan, L.K., Cheng, S.W and Spring, F.A., A new measure of process capability: C_{pm} . J. Quality Technology., 1998.
3. Chen, J.P. and Tong, L.I. (2003). Bootstrap Confidence Interval of the Difference Between Two Process Capability Indices, International Journal of Advanced Manufacturing Technology, 21, 249–256.
4. Gunter, B.H., *The use and abuse of Cpk: Parts 1–4*, Qual. Progr. 22 (January) (1989), pp. 72–73; March, pp. 108–109; May, pp. 79–80; July, pp. 86–87.
5. Juran, J.M., Gryna, F.M. and Bingham, R.S. Jr. Quality Control Hand book, McGraw-Hill, New York, 1974.
6. Kane, V.E. (1986). Process capability indices. *Journal of Quality Technology*, 18(1), 41–52.
7. Kotz, S. and Johnson, N.L. Process Capability Indices, Chapman and Hall, London, 1993.
8. Kotz, S. and Lovelace, C.R. Process Capability Indices in Theory and Practice, Arnold, London, 1998.
9. Krishnamoorthi, K.S., Capability indices for processes subject to unilateral and positional tolerances. Quality Engineering, 1990.
10. Montgomery, D.C. Introduction to Statistical Quality Control. 5th edn. New York Wiley, 2005.
11. Pan, J.N and Wu, S. L., Process capability analysis for non-normal relay test data, department of statistics, national cheng-kung university, Tainan. publication in 2 April 1996. PII:SOO26-2714(96)00071-6 (research journal)
12. Pearn, W.L. and Kotz, S., Encyclopedia and handbook

of PCIs. World Scientific Publishing Society, 2007.

13. Shewhart, W.A. *Economic Control of Quality Manufactured Product*, Van Nostrand, New York, 1931.
14. Spiring, F., Leung, B., Cheng, S. and Yeung, A. (2003). A bibliography of process capability papers. *Quality and Reliability Engineering International*, 19,445-460.

STRUCTURAL, THERMAL AND ELECTRICAL CHARACTERIZATION ON GEL GROWN COBALT SUCCINATE TETRAHYDRATE SINGLE CRYSTALS

■ M.P Binitha¹ and P.P Pradyumnan²

¹ Department of Physics, Govt. arts & Science College, Kozhikode
binithamp@gmail.com

² Department of Physics, University of Calicut

Abstract

Cobalt succinate tetrahydrate ($\text{CoC}_4\text{H}_4\text{O}_7 \cdot 4\text{H}_2\text{O}$) crystals were grown by controlled diffusion in silica gel medium and rectangular plate like single crystals of size up to $4.4 \times 3.8 \times 2.4 \text{ mm}^3$ were obtained. Single-crystal X-ray diffraction studies showed that it crystallizes in monoclinic space group $P2_1/c$ with unit cell dimensions of $a = 7.3806 \text{ \AA}$, $b = 14.7622 \text{ \AA}$, $c = 7.7646 \text{ \AA}$, $\alpha = 90^\circ$, $\beta = 99.781^\circ$ and $\gamma = 90^\circ$. Infrared spectra of the grown crystals were recorded in $400\text{--}4000 \text{ cm}^{-1}$ frequency regions and different vibrational modes of the title compound are assigned and discussed. The thermal degradation behavior of the crystal is studied by thermo gravimetric - differential thermo gravimetric (TG-DTG) and differential thermal calorimetric (DTA) analysis. The electrical characterization was done and the variations of dielectric constant and ac conductivity with frequency of the applied field were discussed.

Key words: Single crystal growth, X-ray diffraction, Dielectric studies

1. Introduction

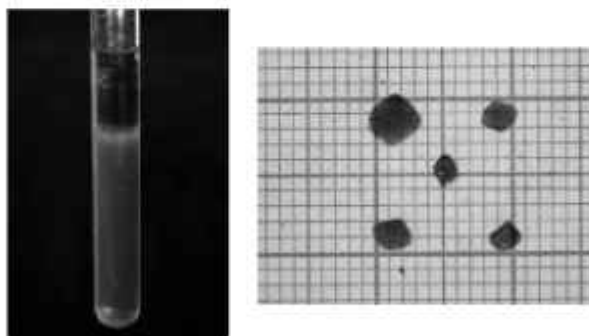
Hybrid inorganic-organic materials are an emerging class of structures with a crucial role in the development of advanced functional materials and with potential applications in hydrogen storage, electrical and magnetic

devices, non linear optical devices, luminescence and use as catalysts [1-3]. The growing interest in such materials attracts the attention of chemists, physicists, biologists and material scientists who are looking forward to exploit them for creating new smart materials. The succinate ion is a dicarboxylic ligand exhibiting diverse coordination modes and flexible stereochemistry. The succinate anion is a versatile ligand and offers the possibility of different modes of coordination towards different metal ions. It can behave as a monodentate, bidentate, multidentate or bridging ligand and it is used for designing compounds with desired magnetic properties [4]. One dimensional, two dimensional and three dimensional metal organic coordination polymers bridged by succinate ligands have been fabricated by several investigators [5-7]. The succinate derivatives of certain metals can provide the framework of supramolecular crystal engineering [8-9]. Majority of the reported metal succinates are synthesized by precipitation or aqueous reaction methods [10-12]. Precipitation is a fast reaction process, often accompanied by undesired agglomeration. A crude precipitation process can be transformed into crystallization process by careful control of the degree of supersaturation which will yield defect free single crystals. There is an accentuating demand for purest single crystals in scientific and industrial spheres as a result of which crystallographers were directed to focus their attention on novel varieties of unsullied crystals, free of flaws, existing in their purest form. In this paper we report the growth of cobalt succinate tetrahydrate single crystals by gel aided solution growth techniques for the first time. The gel growth technique is one kind of modified alternative version of solution growth technique in which the growth occurs due to reaction between two suitable reactants in a gel medium or achieving super-saturation by diffusion in gel medium. It is a simple, elegant and room temperature growth method yielding a variety of single crystals and is well suited for the crystal growth of compounds, which are sparingly soluble and decompose at fairly low temperatures.

2. Experimental

Crystals of cobalt succinate were grown by gel technique by single diffusion method in hydro silica gel. "Analytical reagent (AR grade)" succinic acid and cobalt chloride were used as the reagents. Silica gel was prepared by adding sodium metasilicate solution of specific gravity 1.03 to 0.25 M succinic acid. The pH of the gel was adjusted between a value of 5 and 6. This solution was then transferred to several glass tubes. The gel was found to set in one day. A supernatant solution of 0.5 M cobalt chloride was then carefully placed over the set gel so that the Co^{2+} ions diffuse slowly through the narrow pores of the gel to react with the succinate ions, giving rise to the formation of single crystals of cobalt succinate tetrahydrate. The crystal growth process was completed in about six weeks, with an ultimate crystal size of $0.44 \times 0.38 \times 0.24 \text{ cm}^3$. The crystal growth set up and grown crystals of cobalt succinate are shown in figure 1

Figure 1. Photograph of growth set up and as grown crystals of cobalt succinate.



After harvesting the fully grown cobalt succinate crystals, structural characterization was performed using single crystal X ray diffraction technique and X-ray powder

diffraction technique. The single crystal X-ray diffraction data were collected using a Bruker Kappa Apex II diffractometer, with graphite-monochromator Mo-K α ($\lambda = 0.71073 \text{ \AA}$) radiation. The unit cell dimensions were recorded at 296K. The powder X-ray diffraction studies were carried out by Rigaku Miniflex 600 using Cu-K α monochromator of wavelength 1.541 \AA . Jasco FT IR 4100 spectrophotometer was employed to obtain IR spectrum. Thermo-analytical techniques such as thermogravimetry (TG), derivative thermogravimetry (DTG) and differential thermal analysis (DTA) were carried out using Perkin Elmer TGA instrument. The A.C. electrical conductivity measurements were carried out on the grown crystals in the temperature range of 30° to 110° using the LCR meter (LCR HiTESTER 3532-50).

3. Results and Discussion

3.1. X-ray diffraction studies

A good single crystal of size $0.35 \times 0.30 \times 0.30 \text{ mm}^3$, was chosen for the single crystal XRD analysis. The program SAINT/XPREP was used for data reduction and APEX2/SAINT for cell refinement. The structure was solved using SIR92 and refinement was carried out by full-matrix least squares on F^2 using SHELXL-97. Based on 6446 reflections and 151 parameters, the residuals is converged to $R(\text{int}) = 0.0334$.

From single crystal XRD studies it is confirmed that the crystal structure of cobalt succinate is monoclinic (space group P21/c) with unit cell dimensions of $a = 7.3806 \text{ \AA}$, $b = 14.7622 \text{ \AA}$, $c = 7.7646 \text{ \AA}$, $\alpha = 90^\circ$, $\beta = 99.781^\circ$ and $\gamma = 90^\circ$. Figure 2 represents the ORTEP of the molecules with thermal ellipsoids at 50% probability and the packing diagram of the molecule down b axis is shown in figure 3. The crystal data and structure refinement parameters are presented in Table 1.

The structure consists of isolated cobalt atoms that are octahedrally coordinated to oxygen atoms of four coordinated water molecules and two succinate oxygens, resulting in a one dimensional coordination polymer. The corresponding bond lengths range from 2.0763 to 2.1358 Å. The carboxylic groups are monodentate and one of the oxygen atoms is a free terminal oxygen. The Powder X-ray diffraction spectrum along with the simulated powder pattern obtained from single crystal data using Mercury software is plotted in figure 4, which are in good agreement, showing very good crystallinity for the powdered samples as well

In each asymmetric unit there are four coordinated water molecules which serve as receptors or donors of O-H...O hydrogen bonds and are hydrogen bonded to oxygen of other coordinated water molecule and carboxylate oxygen of succinate group. Thus these coordinated water molecules in the structure of cobalt succinate are involved in the extensive network of hydrogen bonds amongst themselves and are responsible for the stability of the structure

Figure 2 ORTEP diagram of cobalt succinate 50% probability

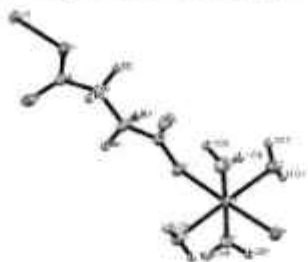


Figure 3 Packing of the molecules down b-axis

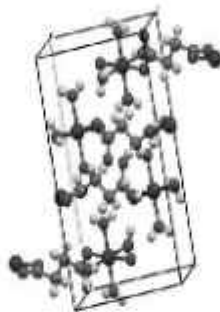


Figure 4 Simulated and experimental X ray diffraction spectrum of cobalt succinate

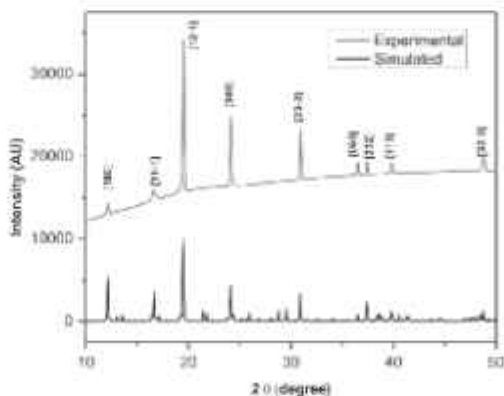


Table 1. Crystal data and structure refinement parameters for cobalt succinate

Identification code	shelxl
Empirical formula	$C_4 H_{12} Co O_4$
Formula weight	247.07
Temperature	296(2) K
Wavelength	0.71073 Å
Crystal structure, space group	Monoclinic, P21/c
Unit cell dimensions	$a = 7.3806(3) \text{ \AA}$, $b = 14.7622(7) \text{ \AA}$, $c = 7.7646(4) \text{ \AA}$, $\alpha = 90^\circ$,
Volume	$\beta = 99.781(2)^\circ$, $\gamma = 90^\circ$ $833.69(7) \text{ \AA}^3$
Z, Calculated density	4, 1.968 Mg/m ³
Absorption coefficient	2.074 mm ⁻¹
F(000)	508
Crystal size	0.35 x 0.30 x 0.30 mm
Theta range for data collection	2.76 to 28.31 deg.
Limiting indices	$-9 \leq h \leq 9$, $-19 \leq k \leq 19$, $-10 \leq l \leq 9$
Reflections collected / unique	6446 / 2066 [R(int) = 0.0334]
Completeness to theta	28.31 99.5 %
Absorption correction	Semi-empirical from equivalents
Max. and min. transmission	0.5750 and 0.5305
Refinement method	Full-matrix least-squares on F ²
Data / restraints / parameters	2066 / 12 / 151
Goodness-of-fit on	0.699

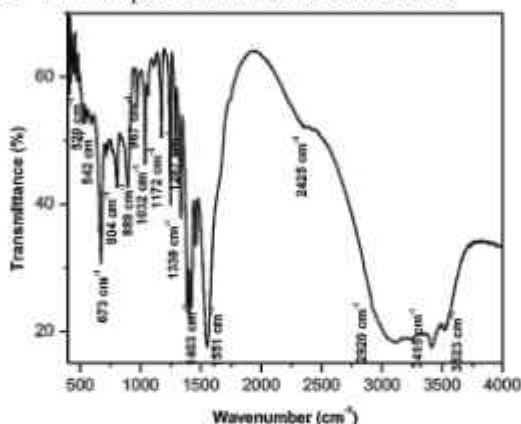
F ² Final R indices [$I > 2\sigma(I)$]	$R_1 = 0.0221$, $wR_2 = 0.063$
R indices (all data)	$R_1 = 0.0233$, $wR_2 = 0.0615$
Extinction coefficient	0.0254 (14)
Largest diff. peak and hole	0.482 and -0.305 e.Å ⁻³

3.2 FT-IR studies

FT-IR analysis of cobalt succinate tetrahydrate crystals was performed in KBr medium using powdered samples, in the region 400–4000 cm^{-1} . The FT-IR spectrum at room temperature is shown in figure 5. The IR absorption peak observed at 3523 and 3415 cm^{-1} are assigned to asymmetric and symmetric stretching vibration of O-H group respectively, confirming the existence of strong hydrogen bonds in the crystal. The shoulder band observed at 2920 cm^{-1} is due to asymmetric stretching of $\nu_{\text{as}}(\text{CH}_2)$. The asymmetric and symmetric stretching vibrations of carboxylate group give strong vibrations at 1551 and 1403 cm^{-1} respectively. The strong vibrational band observed at 1287 cm^{-1} is assigned to the C-O stretching of the OCO group. The observed vibrational frequency at 1330 cm^{-1} and 1245 cm^{-1} are due to the C-H vibrations of $\delta(\text{C-H})$ of the CH_2 group. The vibrational band at 1172 cm^{-1} is ascribed to the asymmetric C-C stretching vibration. The medium bands observed at 967 cm^{-1} and 804 cm^{-1} also are assigned to C-H bending $\delta(\text{C-H})$ of the methylene group. The strong band at 715 cm^{-1} corresponds to the bending vibration of the OCO group. The medium band at 889 cm^{-1} is assigned to the O-H deformation of the water molecule. The vibration at 673 cm^{-1} is assigned to the wagging mode, $\rho_{\text{w}}(\text{C-H})$ of the

methylene group. The weak band at 542 cm^{-1} is assigned to the wagging and twisting modes of water and deformation mode of methylene group. The absorption at 520 cm^{-1} is associated with metal-oxygen bonding [13-14].

Figure 5 FT-IR spectrum of cobalt succinate



3.3 Thermal decomposition studies

The thermal properties of the material were studied by thermogravimetric (TGA) and differential thermal analyses (DTA) and are shown in figure 6 and figure 7 respectively. The TGA was carried out between 37° and 800°C in the nitrogen atmosphere at a heating rate of $10^\circ\text{C min}^{-1}$. The material exhibits sharp weight loss starting at 65°C and ending at 150°C . This corresponds to a weight loss of 28.02% and can be attributed to the loss of four coordinated water molecules. Cobalt succinate obtained remains stable up to 372°C and there is an exotherm at 290.56°C in DTA curve in this region which corresponds to the phase transition [15]. The next stage of decomposition starts at 372°C and ends at 492°C and results a mass loss of 37% giving the end product Co_3O_4 . The endotherm at

440°C in the DTA curve and 443°C in the DTG curve can be assigned to this degradation process with a theoretical weight loss of 38% [16].

Figure 6 TG-DTG curve of cobalt succinate

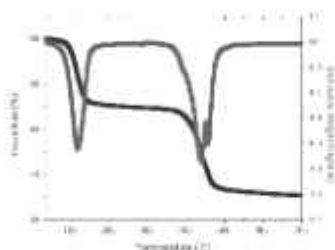
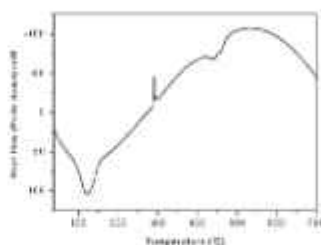


Figure 7 DTA curve of cobalt succinate



3.4 Dielectric studies

Capacitance (C) and $\tan \delta$ values of cobalt succinate samples were measured by using a LCR Meter, model LCR HiTESTER 3532-50, in the temperature range from 30° to 110°C and frequency range from 100Hz to 50 kHz. Dielectric constant (ϵ_r) was evaluated by using the following relation:

$$\epsilon_r = \frac{cd}{\epsilon_0 A} \quad (1)$$

and the ac conductivity is calculated by the relation

$$\sigma_{ac} = \epsilon_0 \epsilon_r \omega \tan \delta \quad (2)$$

Where C is the capacitance, d is the thickness, A is the area of cross section of pellet and $\tan \delta$ is the dielectric relaxation of the sample and ω is the angular frequency, which is equal to $2 \pi f$ (where f is the frequency). If M is the molecular weight of the crystal and ρ its density, the valance electron plasma energy $\hbar \omega_p$ is given by

$$\hbar\omega_p = 28.8 \left[\frac{Z\rho}{M} \right]^{1/2} \quad (3)$$

Where Z is the total number of valance electrons in the crystal. The valence electron plasma energy $\hbar\omega_p$ is related to the Penn gap (E_p) and Fermi energy E_f by the equations [17-18]

$$E_p = \frac{\omega_p}{(\epsilon_\infty - 1)^{1/2}} \quad (4)$$

Where ϵ_∞ is the high frequency dielectric constant and

$$E_f = 0.2948(\hbar\omega_p)^{4/3} \quad (5)$$

Polarizability (α) is obtained using the relation [19]

$$\alpha = \left[\frac{(\hbar\omega_p)^2 S_0}{(\hbar\omega_p)^2 S_0 + 3\epsilon_p^2} \right] \times \frac{M}{\rho} \times 0.396 \times 10^{-24} \text{ cm}^3 \quad (6)$$

Where S_0 is a constant for the material, which is given by

$$S_0 = 1 - \frac{E_f}{4E_p} + \frac{1}{3} \left[\frac{E_f}{4E_p} \right]^2 \quad (7)$$

Also from Clausius–Mossotti equation,

$$\alpha = \frac{3M}{4\pi N_a \rho} \left(\frac{\epsilon_\infty - 1}{\epsilon_\infty + 2} \right) \quad (8)$$

From the plot of dielectric constant with frequency of the applied field (figure 8), it is clear that dielectric constant decreases with increase of frequency which is the normal dielectric behavior. When an alternating field is applied to a dielectric material, polarization requires a time to form which is often of the same order of magnitude or greater than the period of the alternating current. This results in the polarization not being able to form completely before the

direction of the field is reversed and causes the magnitude of dielectric polarization and dielectric constant to decrease with frequency of the applied field. When the frequency of the applied field is increased, the dipoles present in the sample cannot reorient themselves fast enough and therefore dielectric constant becomes a constant.

The different types of polarization mechanisms in a crystal are electronic, atomic, orientational or dipolar and interfacial. The electronic and atomic polarizations are temperature independent whereas the dipolar and interfacial polarizations are temperature dependent. When temperature is increased the action of the electric field in aligning the dipoles is opposed by the thermal motion, which acts as an influence tending to keep them oriented at random. As the temperature is increased the thermal energy becomes larger and the polarization becomes smaller resulting in a negative temperature coefficient of dielectric constant. The ac conductivity of the crystal is found to be increasing with frequency and decreasing with temperature as shown in figure 9. When increasing the temperature the thermal expansion reduces the density of the crystal and this cause the reduction in conductivity [20-21]. The values of plasma energy, penn gap (E_p), fermi energy (E_f) and polarizability (α) are determined from the collected data for the grown crystal and the values of parameters are depicted in Table 2.

Figure 8 Variation of ϵ_r with frequency

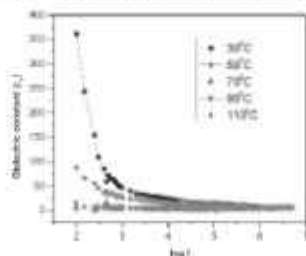


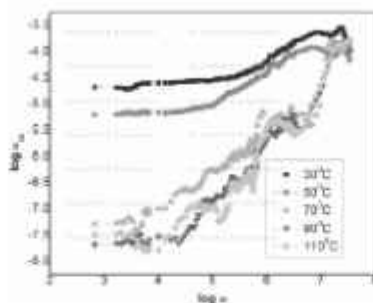
Figure 9 Variation of $\alpha\epsilon_s$ with angular frequency

Table 2 Some theoretical data for grown crystal.

Parameters	Values
Plasma energy ($\hbar\omega_p$)	23.69 eV
Penn gap (E_p)	9.524 eV
Fermi energy (E_f)	20.05 eV
Polarizibility (α)	
By Penn analysis	$3.2 \times 10^{22} \text{ cm}^{-3}$
By Clausious–Mossotti	$3.35 \times 10^{23} \text{ cm}^{-3}$

Conclusions

Cobalt succinate single crystals have been successfully grown by single diffusion gel growth technique and powder X-ray diffraction analysis was carried out to verify the crystallinity of the grown crystals. Single crystal XRD studies revealed the polymeric one dimensional crystal structure of the compound. The FTIR studies confirmed the major functional groups in the crystal. The thermal decomposition pattern of the material suggests a two stage decomposition process and the end product is cobalt oxide (Co_2O_3). The dielectric constant is

decreasing with frequency and temperature, attaining a constant value at higher frequencies. The ac conductivity is found to be increasing with frequency and decreasing with temperature. The physical parameters like valance electron plasma energy, Penn gap, Fermi energy and electronic polarizability had been determined for the grown crystal from the dielectric study as well as structural information.

Acknowledgments

The authors would like to acknowledge UGC-SAP and FIST 2 (DST, Govt. of India), for the research facilities in the Dept. of Physics, University of Calicut. The authors also express sincere gratitude to Dr. Shibu M. Eapen, SAIF, Cochin University of Science and Technology for providing single crystal X-ray diffraction data.

REFERENCE

- [1] Kenji Sumida et al., R. Long Chem. Sci, 1 (2010) 184
- [2] Corinne A. Allen, Jake A. Boissonnault, Jordi Cirera, Ryan Gulland, Francesco Paesani and Seth M. Cohen (2013) Chem Comm
- [3] Mark D. Allendorf, Adam Schwartzberg, Vitalie Stavila and Alec Talin AChem. Eur. J. 17 1(2011) 1372
- [4] Honghan Fei, Andrew D. LaForge, Tedmann M. Onyango, Jeremy C. Robins, Peter Y. Zavalij, Arthur P. Ramirez and Scott R. J. Oliver J. Mater. Chem. C 1 (2013) 1099
- [5] Paul M. Forster,^aAndrea R. Burbank,^aCarine Livage,^bGérard Férey^b and Anthony K. Cheetham Chem. Commun. (2004) 368
- [6] Siau Gek Ang, Bai Wang Sun, Song Gao Inorganic Chemistry Communications 7 (2004) 795
- [7] O.M. Yaghi, Guangming and T.L Groy Journal of solid state Chemistry 11 (1995) 7256
- [8] M. Padmanabhan, S. Meena Kumary, Xiaoying Huang, Jing Li *in* Acta Chimica Acta 358 (2005) 3537
- [9] Sadhika khullar and Sanjay K Mandal CrystEngComm 15 (2013) 6652
- [10] Zakariae Amghouz, Laura Roces, Santiago Garcí'a-Granda, Jose' R. Garcí'a, Badredine Souhail, Luí's Mafra, Fa-nian Shi, Joao Rocha Journal of Solid State Chemistry 182 (2009) 3365
- [11] Carine Livage, Chrystelle Egger, Marc Noguez^b and Gérard Férey J. Mater. Chem. 8 (1998) 2743
- [12] P. M. Forster, A. K. Cheetham, Angew. Chem. 114 (2002) 475
- [13] Bon Kweon Koo Bull. Korean Chem. Soc. 33 (2012) 72299

- [14] Brusau, E.V, Pedregosa, J.C, Narda, G.E The Journal of the Argentine Chemical Society 92 (2004) 43
- [15] B. Malecka, A. Łącz, J. Therm. Anal. Calorim. 88 (2007) 295–299
- [16] M P Binitha, P P Pradyumnan Phys. Scr. 87 (2013) 065603
- [17] S.K. Arora, Vipul Patel, Bhupendra Chudasama, Brijesh Amin J. Cryst. Growth 275 (2005) e657–e661..
- [18] S. Krishnan, C. Justin Raj, S.M. Navis Priya, R. Robert, S. Dinakaran, S. Jerome Das Cryst. Res. Technol. 43 (2008) 845–850
- [19] N.M. Ravindra, V.K. Srivastava Infrared Phys. 20 (1980) 67–69.
- [20] Samy A. Rahman Egypt. J. Solids 29 1 (2006) 131
- [21] Arora SK, Patel V, Patel RG, Amin B and Kothari AJ. Phys. Chem. Solids 65 (2004) 965

HYBRID BIO NANOCOMPOSITE MATERIALS FOR WATER PURIFICATION

■ **Mujeeb Rahman P**

Department of Chemistry, Government Arts & Science College,
Meenchanda, Kozhikode.
mujeebparammel@gmail.com

Abstract

Hybrid Chitosan-ZnO composites were prepared by sol-gel method, and characterized by Fourier transform infrared spectrometer (FT-IR), X-ray diffraction (XRD) and Scanning Electron Microscopy (SEM). Adsorption of methylene blue from aqueous solutions by the resulting composites was studied by batch adsorption experiments. Antimicrobial efficacy of composite powder was analysed well diffusion method. The composites were found to behave as an excellent adsorbent and antimicrobial material.

1. Introduction

Chitosan is the second-most abundant natural polymer and has widely studied in large number of applications (1) and the properties of chitosan can be modified by tuning its structure as well as adding nanoparticles to its polymer matrix (2). In recent years much attention has been devoted to the hybrid materials of nano metal oxides and chitosan owing to their unique properties such as photo catalysts, antimicrobial agents,

adsorbent etc. This hybridization could enhance the properties of each single component counterpart of composites. (3-4). It is already known that chitosan has inherent antimicrobial activity against gram negative and gram positive bacteria, but the exact mechanism of its antimicrobial activity is not clearly known. The inherent antimicrobial activity of chitosan is believed to be due to the presence of the positively charged amino groups which interact with negatively charged cell membranes of pathogens, leading to the leakage of proteinaceous and other intracellular constituents and finally to the death of microorganism (5).

Recently, adsorbents have been developed from naturally occurring materials. These adsorbents have become a focus of environmental investigations because of their low cost and biodegradability (6). Chitosan is, highly insoluble in water and in many organic solvents, shows low chemical reactivity, and it is a non-toxic biodegradable and biocompatible polymer. Over the last several years, chitinous polymers, especially chitosan, have received increased attention as one of the promising adsorbent for wastewater treatment (7). Since it contains a large number of reactive hydroxyl (-OH) and amino (-NH₂) groups and exhibit unique adsorption and chelating properties for all kinds of heavy metal ions (8).

The present work involves the fabrication of a novel, eco-friendly composite containing chitosan and ZnO nanoparticles by in situ sol-gel conversion. The objective of this work was to formulate a simple and cost effective bionanocomposite as a potential antimicrobial agent and dye adsorbent.

2. Experimental

2.1 Materials

Chitosan with 85 percent degree of deacetylation was purchased from Sigma Aldrich Co. Ltd (USA). Acetic acid, Sodium hydroxide, and Zinc acetate dehydrate, Methylene blue were purchased from Merck (Germany). All the chemicals were analytical grade and used without further purification. Deionized water was used to prepare all the solutions in this paper.

2.2 Preparation

Chitosan solution was prepared by dissolving 0.5 g of chitosan in 2% Acetic acid solution under room temperature. To this solution 30 mL of 15% zinc acetate dihydrate solution was added. With this solution, 30 mL of Sodium hydroxide solution (45%) was added at the temperature 70°C and chitosan was started to settle, the entire mixture was kept under stirring at 70 °C for four hours. The white precipitate obtained was allowed to settle for 24 h. The supernatant solution was discarded and the precipitate was rinsed with distilled water for several times to remove excess NaOH, finally precipitate was filtered and dried at 50 °C in an oven for 12h. The white dried precipitate was powdered well and sample was designated as CN 45. The above process was repeated with decreasing Sodium hydroxide concentration to 30% and 15% and corresponding composites were designated as CN 30 and CN 15 respectively.

2.3 Characterization

The structure and morphology of the samples were analysed by Fourier transform infrared spectrometer (FT-IR, JASCO -4100), X-ray diffraction (XRD, Rigakudiffractor with Cu K α radiation), Scanning Electron

Microscopy (Model: Hitachi SU-6600 FESEM). The absorption spectra were recorded by using UV-visible spectrophotometer (Model: Jasco V-550)

2.4 Antibacterial activities

The antimicrobial activity of chitosan and chitosan-based nanocomposite powders were evaluated by Agar well diffusion method. Gram-negative bacteria *E.coli* (MTCC 1687) and Gram-positive bacteria *S.aureus* (MTCC 737) were used as test organisms. Sterile NA plates were prepared and 0.1 mL of the inoculums of test organism was spread uniformly over it. Wells were prepared by using a sterile borer of diameter 6mm and the samples of pure chitosan (C), CN15, CN30 and CN45 were added in each well separately. The plates were incubated at 35-37°C for 24 h, a period of time sufficient for the growth. The zone of inhibition around the well was measured in mm.

2.5 Adsorption experiments

A stock solution of Methylene Blue (10^{-5} M) was prepared in 1 L of deionised water. The desired concentrations were obtained by dilution. For each adsorption experiment, 50 mL of the dye solution with adsorbent was stirred at uniform speed in a glass flask. 0.1gm CN45, CN30 and CN15 were present in each flask with the dye solution. At predetermined time intervals, samples were withdrawn by a pipette, centrifuged and the residual concentration was determined using a spectrophotometer. The experiments were repeated with 0.2gm and 0.3gm composite powders.

3. Results and discussions

3.1. FTIR spectroscopy analysis

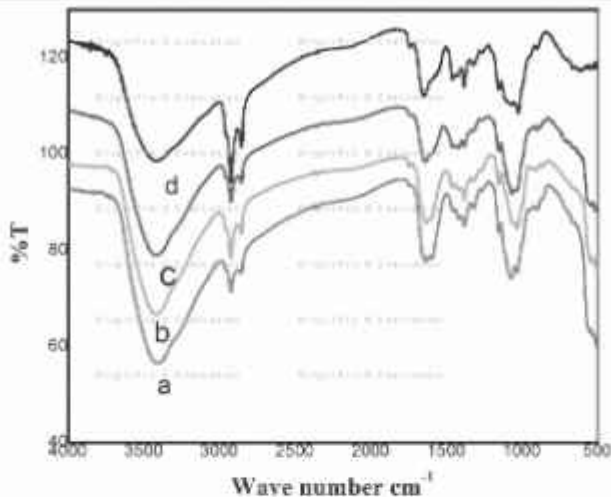


Fig-1

FTIR spectra of (a) CN45, (b) CN30, (c) CN15 (d) pure chitosan

Figure-1 shows the FTIR spectra of pure chitosan and nanoZnO composites powder. In Fig-1d the characteristic broad band at 3367cm^{-1} is attributed to the stretching vibrations of $-\text{NH}_2$ group and $-\text{OH}$ group of chitosan. The band at 2876cm^{-1} is due to asymmetric stretching vibration of $-\text{CH}$ group and the bands at 1656 and 1588cm^{-1} are designated to the stretching vibrations of $\text{C}=\text{O}$ and the scissoring vibrations of $-\text{NH}_2$ of chitosan. The bands at $1150\text{-}1040\text{cm}^{-1}$ is due to the stretching vibration of $-\text{C}-\text{O}-\text{C}-$ of glycosidic linkage of the polymer. The FTIR spectrum of ZnO composites (fig 1-a, b and c) are similar to that of pure chitosan but in contrast to fig-1d, the band corresponding to stretching vibrations of $-\text{NH}_2$, $-\text{OH}$, $\text{C}=\text{O}$, $-\text{C}-\text{O}-\text{C}-$ and asymmetric stretching vibrations of $-\text{CH}$ groups are shifted to lower wave number region indicating the strong interaction of these groups with ZnO particles. The decrease in the width of the band corresponding to $-\text{OH}$ and $-\text{NH}_2$ group is ascribed to the reduction of hydrogen bond due to impregnation of ZnO groups.

Moreover, the intense bands at 470 cm^{-1} in fig (a-c) are ascribed to the starching mode of Zn-O vibrations strongly supporting the presence of nanoparticles (9).

3.2 XRD analysis

Figure-2 shows the XRD patterns of pure chitosan (C) and composite powders. The typical peak of pure chitosan at 19.9° in (fig-2a) is not visible in composites, this may be due the loss of semi crystalline behavior of chitosan in the presence of nanoparticles

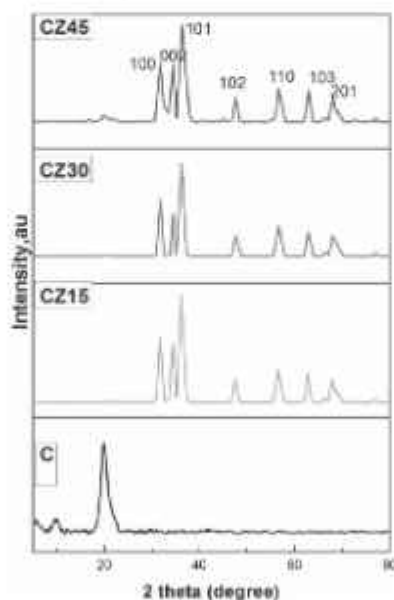


Fig-2.

XRD patterns of (a) pure chitosan, (b) CN15, (c) CN30, (d) CN45

The major peaks at 31.78° , 34.44° , 36.27° , 47.5° , 56.56° , 62.87° , and 67.96° in fig (b,c and d) of composites were assigned to diffraction from the planes (100), (002),

(101) , (102), (110) , (103) and (201) respectively. And these results are consistent with the data base of (JCPDS No 36-1451). The XRD results support the formation of ZnO with hexagonal structure.. The average sizes of particles were calculated using Debye-Scherrer equation.

$$D = \frac{K\lambda}{\beta \cos\theta} \quad (1)$$

3.3 SEM analysis

The direct evidence of the immobilization of nano-ZnO particles in the chitosan matrix was given by SEM photographs. Fig-3, displays the SEM photographs of the pure chitosan and its composites CN 45, CN 30 and CN 15. As shown in (fig 3a),the surface of the chitosan was rather smooth.However the in situ formation of ZnO particles break the smooth surfaces of chitosan and nanoZnO particles are get impregnated over the matrix. SEM images in fig 3 (b-d) clearly displays the formation of nanoZnO particles, but the distribution of particles are varying when concentration of NaOH was changed.In CN 45 (fig-3b) and CN15 (fig-3d) particles are found as agglomerated.

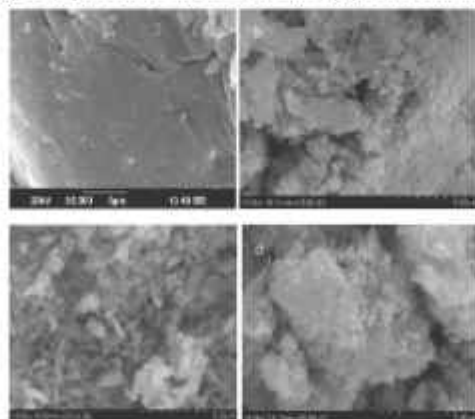


Fig-3.

SEM photographs of pure chitosan (a), CN15 (b), CN30 (c) and CN45 (d).

3.4 Antimicrobial properties

The antibacterial properties of composites were measured by Agar well diffusion method. Figs. 4(a,b) show the antimicrobial activity of pure chitosan (C), CN 45, CN 30 and CN 15 against *E.coli* and *S.aureus* respectively. The data show that chitosan ZnO composite has enhanced antimicrobial activity as compared to pure chitosan. The presence of nanoparticles in chitosan matrix is expected to promote the columbic interaction with outer cell wall of microorganisms and leads to increased antimicrobial activity. The composites show higher activity towards *E.coli*, compared to *S.aureus*, which may be due to the presence of a thick layer of peptide glycans in the cell wall of *S.aureus* [39].

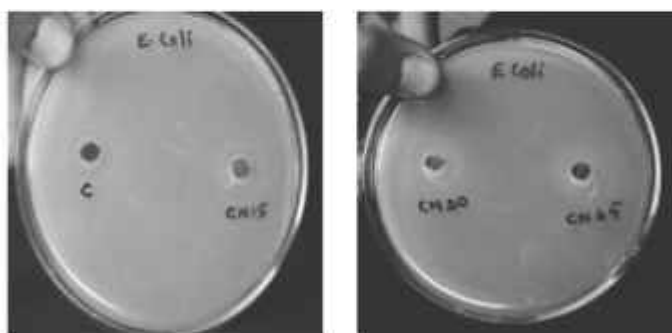


Fig .4a

Antimicrobial activity against *E.coli* - pure chitosan-(C), CN15, CN30 and CN 45

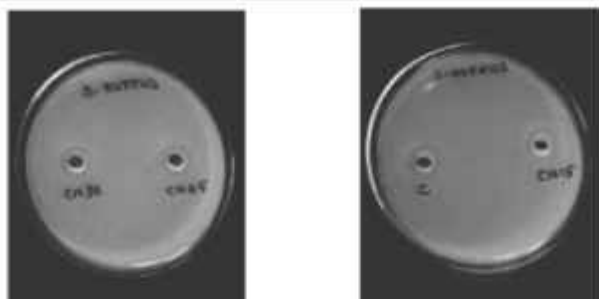


Fig.4b

Antimicrobial activity against *S.aureus* pure chitosan-(C), CN15, CN30 and CN 45

3.5 Adsorption of Methylene Blue

The adsorption of methylene blue on chitosan composites was evaluated by using a batch procedure. As shown in fig 5(a-d) higher adsorption tendency was exhibited by CN45 composites and this may be due to higher surface area present in CN45 composite powder.

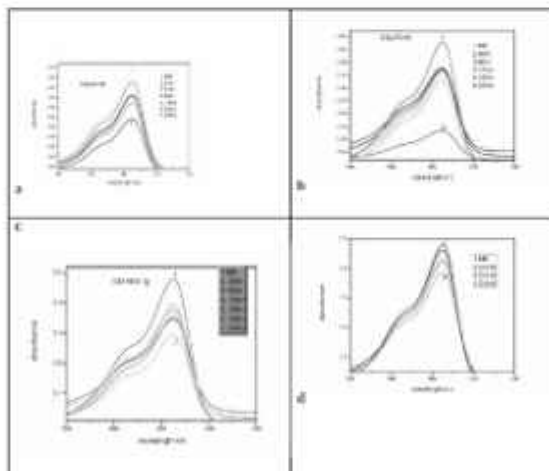


Fig-5

- a) UV-Vis spectrum of 0.3gm Cn30
- b) UV-Vis spectrum of 0.3gm Cn45
- c) UV-Vis spectrum of 0.1gm cn45
- d) UV-vis spectrum of 0.1 gm composites after 2h.

4. Conclusion

Three different chitosan –nanoZnO composites were prepared by sol-gel method and designated as CN15, CN30 and CN45. The composites were characterized using Fourier transform infrared spectrometer (FT-IR), X-ray diffraction (XRD) and Scanning Electron Microscopy (SEM). Adsorption and antimicrobial properties of composites were evaluated. All the composites were found to be better adsorbents as well as excellent antimicrobial agent. The experiment proved that CN45 is the better choice as an adsorbent and antimicrobial agent

REFERENCES

- (1) F. Shahidi, J.K.V. Arachchi, Y.J. Jeon, Trends Food Sci. Technol. **1999**, 10, 37-51.
- (2) R. Khan, A. Kaushik, P.R. Solanki, A.A. Ansari, M.K. Pandey, B.D. Malhotra, Chim. Acta, **2008**, 616, 207-213
- (3) C. Petchthanasombat, T. Tiensing, P. Sunintaboon, J. Colloid Interf. Sci. **2012**, 369, 52-57.
- (4) K. Vimala, M. Yallapu, K. Varaprasad, N. Reddy, S. Ravindra, N. Naidu, K. Raju, jbnb, **2011**, 1, 55-64.
- (5) A.El. Shafei, A. Abou-Okeil, Carbohydr. Polym., **2013**, 83, 920-925
- (6) M.P. Elizalde-González, Trends Chem. Eng. **2006**, 10, 55-66
- (7) J. Zhang, C.G. Xia, J. Mol. Catal. A **2003**, 206, 59
- (8) S. WanNgah, S. Fatinathan, Chem. Eng. J **2003**, 153-166
- (9) Leceta, P. Guerrero, I. Ibarburu, M.T. Duenas, K. de la Caba, J. Food Eng., **2013**, 116, 889-899

GENERALIZATIONS OF THE WEIBULL DISTRIBUTION AND ITS APPLICATIONS IN LIFETIME DATA ANALYSIS

■ Nihala N. C.¹, Bindu Punathumpambath²

¹Department of Statistics, Govt. Arts and Science College, Kozhikode.

²Asst. Professor, Department of Statistics,
Govt. Arts and Science College, Kozhikode

Email:ppbindukannan@gmail.com

Abstract

Lifetime or response time data analysis has got more importance in areas such as engineering, medicine, and the biological sciences. Recently there has been lot of research works under going in this area. Lifetime data is a term used for describing data that measures time to occurrence of some event. Lifetime or time to event is usually considered as a positive real valued random variable having a continuous distribution function. In the present paper we study various generalizations of the Weibull distribution and its applications in lifetime data analysis. Finally, we illustrate the applications of the Weibull distribution with resilient and tilted parameter. The analysis is carried out using R Package.

1. INTRODUCTION

Lifetime data is a term used for describing data that measures time to occurrence of some event. The event may be death, appearance of some disease, relapse from

remission, equipment breakdown etc. The development of models and methods to deal with lifetimes took place in the second half of the twentieth century. The development proceeded into two main inter mingling streams; through reliability theory and survival analysis. The reliability theory concerns with models for lifetimes of components and systems in the engineering and industrial fields and the survival analysis concerns with medical and similar biological phenomena. Lifetime distribution methodology is widely used in the biomedical and engineering sciences.

Lifetime or time to event is usually considered as a positive real valued random variable having a continuous distribution function. The definition of lifetime includes a time scale and time origin, as well as specification of the event that determines lifetime. In some instances, time may represent age, with the time origin as the birth of the individual. In other instances, the natural time origin may be occurrence of some event such as entry into a study or diagnosis of a particular disease. In some situations, it is difficult to say precisely when the event occurs, for example, the case of appearance of tumour. The time scale is not always real or chronological time, especially where machines or equipments are considered. It could be the number of operations a component performs before it breaks down. Applications of lifetime distribution methodology range from investigations of the durability of manufactured items to studies of human diseases and their treatment.

In present paper, we study generalizations of the Weibull distribution and its applications in life time data analysis. Section 2 describes survival function, hazard rate function and cumulative hazard rate functions of Weibull

distribution. Parametric extensions of the Weibull distribution were studied in section 3. Section 4 is devoted to the applications of parametric extensions of Weibull distribution to two lifetime datasets. Finally, some concluding remarks were given in section 5.

2. WEIBULL DISTRIBUTION

Weibull distribution is a continuous probability distribution. It is named after Waloddi Weibull (1951), although it was first identified by Fréchet (1927) and first applied by Rosin & Rammler (1933) to describe a particle size distribution. Weibull distribution is the most widely used lifetime distribution model, since it can be used to model situations having increasing, decreasing or constant hazard rate. Weibull distribution is used as a lifetime model for diverse types of items, such as ball bearings, automobile components, and electrical insulation. It is also used in biological and medical applications, for example, in studies on the time to the occurrence of tumors in human populations or in laboratory animals.

Weibull distribution is a generalization of exponential distributions, but it does not assume a constant hazard rate and therefore it has broader applications. It has many applications in Reliability and human disease modeling. The probability density function of a Weibull random variable is:

$$f(t; \gamma, a) = \frac{\gamma}{a} \left(\frac{t}{a} \right)^{\gamma-1} \exp\left(-\left(\frac{t}{a}\right)^\gamma\right), \quad (2.1)$$

where $t \geq 0$, $\gamma, \alpha > 0$, γ is the *shape parameter* and α is the *scale parameter* of the distribution. Its complementary cumulative distribution function is a stretched exponential function. The Weibull distribution is related to a number of other probability distributions; in particular, it interpolates between the exponential distribution ($\gamma = 1$) and the Rayleigh distribution ($\gamma = 2$). If the quantity T is a "time-to-failure", the Weibull distribution gives a distribution for which the failure rate is proportional to a power of time.

The cumulative distribution function for the Weibull distribution is:

$$F(t) = 1 - e^{-(t/\alpha)^\gamma}, \quad t \geq 0, \gamma, \alpha > 0. \quad (2.2)$$

The failure function h (or hazard) is given by:

$$h(t) = (\gamma/\alpha)(t/\alpha)^{\gamma-1}, \quad t \geq 0, \gamma, \alpha > 0. \quad (2.3)$$

The survival function $S(t)$ for the Weibull distribution is:

$$S(t) = e^{-(t/\alpha)^\gamma}, \quad t \geq 0, \gamma > 0, \alpha > 0. \quad (2.4)$$

The plot of the Densities of Weibull distribution is given below in figure (2.1).

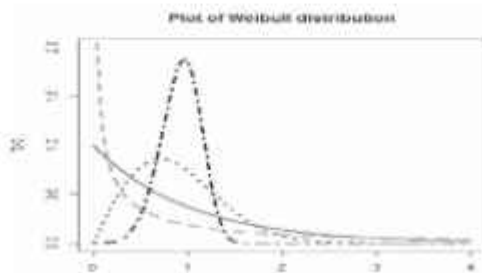


Figure 2.1: Density Function of Weibull distribution for

$\gamma = 1$ (red line), $\gamma = 2$ (blue dots), $\gamma = 5$ (black dash dot)

The plot of the Hazard Function of Weibull distribution is given below in figure (2.2).

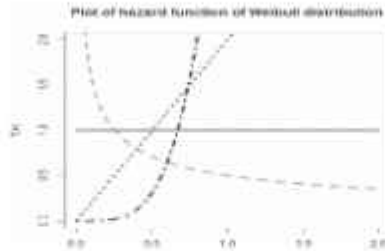


Figure 2.2: Hazard Function of Weibull distribution for $\gamma = 1$ (red line), $\gamma = 2$ (blue dot), $\gamma = 5$ (black dash dot)

3.1 Weibull Distribution with a Resilience Parameter

A special case of the Weibull distribution with resilience parameter was introduced by Burr (1942) as his Type X distribution. The general Weibull distribution with resilience has been introduced and studied under the name “exponentiated Weibull family” by Mudholkar and Srivastava (1993), Mudholkar, Srivastava and Freimer (1995), and Mudholkar and Hutson (1996). The distribution function of the Weibull with resilience parameter is defined as,

$$F(t; \lambda, \alpha, \eta) = [1 - e^{-(\lambda t)^\alpha}]^\eta \quad \lambda, \alpha, \eta > 0, t \geq 0, \quad (3.1)$$

and for $\lambda, \alpha, \eta > 0, x \geq 0$, its densities function is given by

$$f(t; \lambda, \alpha, \eta) = \lambda \alpha \eta (\lambda t)^{\alpha-1} [1 - e^{-(\lambda t)^\alpha}]^{\eta-1} [e^{-(\lambda t)^\alpha}]. \quad (3.2)$$

Mudholkar and Hutson (1996) show that this density is decreasing if $\alpha\eta \leq 1$, and is unimodal if $\alpha\eta > 1$. These results can be verified by examining the derivative of $\log f(t | \lambda, \alpha, \eta)$. From (3.1) and (3.2) it follows directly that the hazard rate is

$$h(t | \lambda, \alpha, \eta) = \frac{\lambda\alpha\eta(\lambda t)^{\alpha-1} [1 - \exp\{-(\lambda t)^\alpha\}]^{\eta-1} \exp\{-(\lambda t)^\alpha\}}{1 - [1 - \exp\{-(\lambda t)^\alpha\}]^\eta}, \lambda, \alpha, \eta > 0, t \geq 0 \quad (3.3)$$

The hazard rate takes on a variety of forms (see figure 3.2). In particular, Mudholkar and Hutson (1996) showed that the hazard rate is

- (i) increasing for $\alpha \geq 1$ and $\alpha\eta \geq 1$,
- (ii) decreasing for $\alpha \leq 1$ and $\alpha\eta \leq 1$,
- (iii) bathtub shaped for $\alpha > 1$ and $\alpha\eta < 1$,
- (iv) Inverted bathtub shaped (unimodal) for $\alpha < 1$ and $\alpha\eta > 1$.

The plot of Densities of Weibull Distribution with Resilience parameter given below in Figure (3.1)

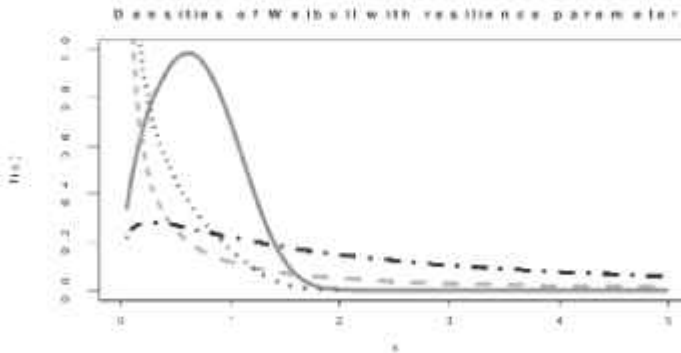


Figure 3.1: Densities of the Weibull distribution with resilience (i) red line ($\alpha = 3, \eta = 0.5$); (ii) green dash line ($\alpha = 0.5, \eta = 0.5$); (iii) blue dot line ($\alpha = 3, \eta = 0.1$); (iv) black dash dot ($\alpha = 0.5, \eta = 3$).

The plot of Hazard rates of Weibull Distribution with resilience parameter given below in figure (3.2)

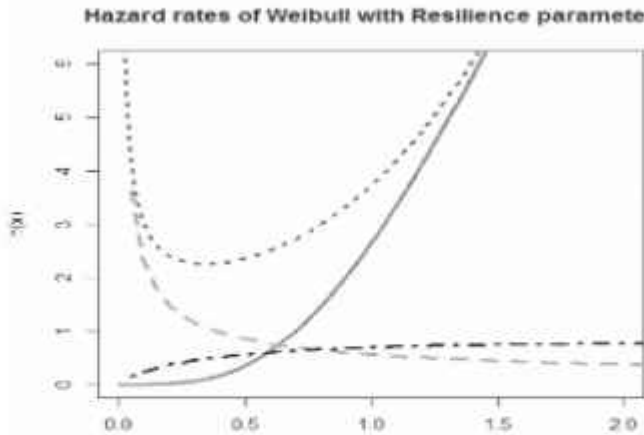


Figure 3.2: Hazard rates of the Weibull distribution with resilience (i) ($\alpha = 3, \eta = 1.5$);(ii) ($\alpha = 0.5, \eta = 0.5$); (iii) ($\alpha = 3, \eta = 0.1$); (iv) ($\alpha = 0.9, \eta = 2$)

3.2 Weibull Distribution with a Tilt Parameter

The survival function of the Weibull distribution with tilt parameter is given by,

$$\bar{F}(t/\lambda, \gamma, \alpha) = \frac{\gamma \exp[-(\lambda t)^\alpha]}{1 - (1-\gamma) \exp[-(\lambda t)^\alpha]}, t \geq 0, \lambda, \alpha, \gamma > 0 \quad (3.4)$$

and the hazard rate is

$$h(t | \lambda, \alpha, \gamma) = \frac{\lambda \alpha (\lambda t)^{\alpha-1}}{1 - (1-\gamma) \exp[-(\lambda t)^\alpha]}, t \geq 0, \lambda, \alpha, \gamma > 0. \quad (3.5)$$

From figure 3.3 we can see that hazard rate is increasing if $\gamma \geq 1, \alpha \geq 1$, and decreasing if $\gamma \leq 1, \alpha \leq 1$. If $\alpha > 1$ and $\gamma < 1$, then the hazard rate is initially increasing and eventually increasing, but there may be one interval where

it is decreasing. Similarly, if $\alpha < 1$ and $\gamma > 1$, then the hazard rate is initially decreasing and eventually decreasing, but there may be one interval where it is increasing. The plot of Hazard rates of Weibull Distribution with Tilt parameter given below in Figure (3.3)

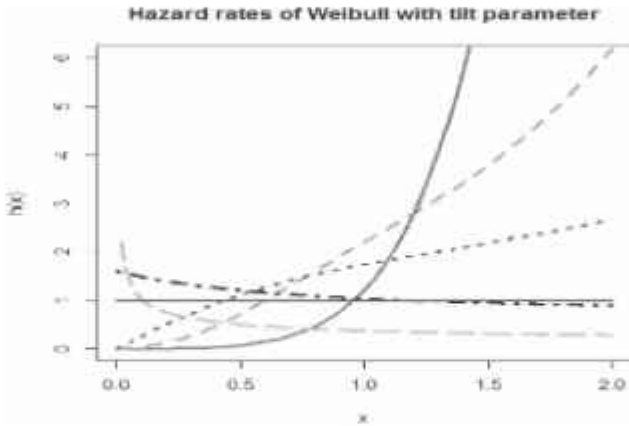


Figure 3.3: Hazard rates of the Weibull distribution with tilt parameter

(I) red line ($\alpha = 5, \gamma = 1.5$); (ii) green dash line ($\alpha = 3, \gamma = 0.5$); (iii) blue dot line ($\alpha = 2, \gamma = 0.5$); (iv) black dash dot ($\alpha = 1, \gamma = 0.5$); (v) cyan long dash line ($\alpha = 0.5, \gamma = 1.5$) and (vi) brown line ($\alpha = 1, \gamma = 1$).

4. APPLICATIONS

In this section we discuss the applications of Weibull with resilience and tilt parameter in the analysis of Lifetime data. We analyzed the Lifetime data using Exponential, Weibull, Weibull with resilience parameter, Weibull with tilt parameter and Lognormal distributions. Estimation of parameters are carried out using Maximum likelihood method of estimation and Kolmogorov-Smirnov goodness of fit test, using the R Package.

conditioning equipment time data is given below in Table 4.1 and their KS test is given below in Table 4.2

4.1 Analysis of successive failures of air-conditioning equipment

Proschan (1963) gave data on the time, in hours of operation, between successive failures of air-conditioning equipment in 13 aircraft, taken from Jerald F. Lawless (2003) by John Wiley & Sons. The data for plane number 3 are as follows:

90, 10, 60, 186, 61, 49, 14, 24, 56, 20, 79, 84, 44, 59, 29, 118, 25, 156, 310, 76, 26,

44, 23, 62, 130, 208, 70, 101, 208.

Here we fitted exponential, Weibull, Weibull distribution with resilience parameter, Weibull distribution with tilt parameter and lognormal distribution for the data and is given in figure 4.1. Maximum likelihood estimators of the parameters for the

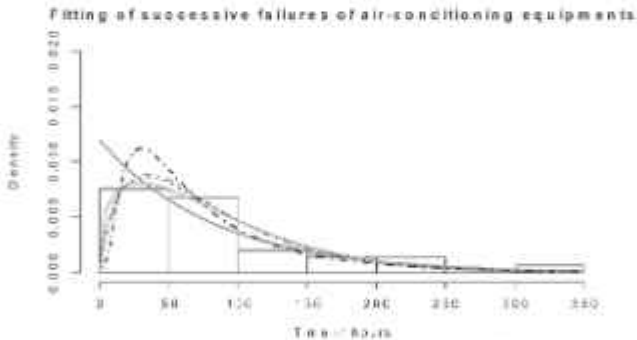


Figure 4.1: Fitted Exponential (red line), Weibull (red dash dot), Weibull distribution with resilience parameter (green line), Weibull distribution with tilt parameter (blue dot) and lognormal (black dash dot) distribution for failures of air-conditioning equipment time data.

Table(4.1) :Air-conditioning equipment time data analysis-- maximum likelihood estimates for exponential, Weibull, Weibull distribution with resilience parameter,

Weibull distribution with tilt parameter and lognormal distribution.

Parameter	Exponential	Weibull	Weibull with resilience parameter	Weibull with tilt parameter	Lognormal
μ	—	—	—	—	4.097
σ	—	—	—	—	0.836
λ	0.01197	—	0.644	0.021	—
γ	—	1.292	—	0.523	—
α	—	90.655	0.0197	1.799	—
H	—	—	2.237	—	—

Table 4.2: K-S Test

Distribution	K-S distance (D)	p-value
Exponential	0.1439	0.5851
Weibull	0.0955	0.9542
Weibull with resilience parameter	0.0865	0.9801
Weibull with tilt parameter	0.0918	0.9676
Lognormal	0.0931	0.9641

From table 4.2 we can see that the p-value for the Kolmogorov-Smirnov test for Weibull with resilience parameter (0.9801) is greater than that of Weibull, Weibull with tilt parameter and Gamma distribution. Hence from Kolmogorov-Smirnov test and figure 4.1, Weibull with resilience parameter is a good fit for the air-conditioning equipment time data.

4.2. Analysis of failure times of cycles

The data below show the number of cycles to failure for twenty-five 100-cm. specimens of yarn, tested at a particular strain level:

86, 146, 251, 653, 98, 175, 176, 76, 264, 15, 157, 220, 42, 321, 180, 198, 38, 20, 61, 121, 282, 224, 149, 180, 325.

Here we fitted Exponential distribution with a Resilience parameter, Weibull distribution with resilience and Weibull distribution with tilt, given in the figure.4.3. We used Akaike's Information Criterion (AIC) (Akaike, 1973) to assess the appropriateness of Exponential distribution with resilience parameter, Weibull distribution with resilience Weibull distribution with tilt parameter for the failure time data.

The AIC is given by

$$AIC = -2 \log L + 2K,$$

where $\log L = \log(Lf(\hat{\theta} | x_1, \dots, x_n))$ is the log-likelihood of the data x_1, \dots, x_n under the probability distribution f , K is the number of parameters being estimated $\hat{\theta}$ is the maximum likelihood estimate of the parameters of f . A smaller value of AIC indicates a better fit.

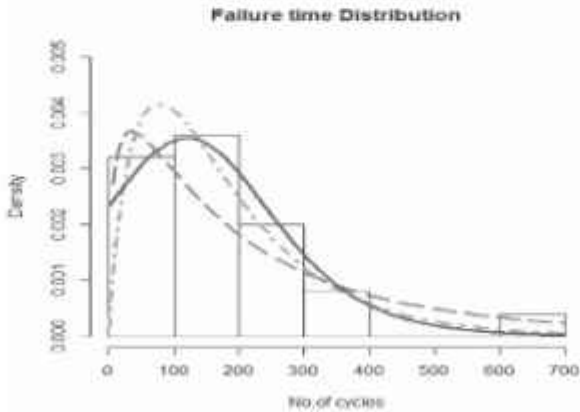


Figure 4.2: Fitted Exponential distribution with a Resilience parameter (red dash line), Weibull distribution with a Resilience parameter (blue line), Weibull distribution with tilt parameter (green dash dot line) for failure time data.

Table(4.3) :Failure time data analysis-- maximum likelihood estimates for exponential resilience parameter, Weibull distribution with resilience parameter and Weibull distribution with tilt parameter.

Parameter	Exponential With resilience parameter	Weibull with resilience parameter	Weibull with tilt parameter
λ	0.008	0.657	0.011
γ	—	—	0.523
α	1.865	0.009	1.859
H	—	2.27330	—
AIC	308.97	5.67	308.5

Table- 4.3 shows that the AIC for the Weibull distribution with resilience distribution had a lower value for the above dataset. A smaller value of AIC indicates a better fit, and hence, Weibull distribution with resilience seems to fit the data better than Exponential distribution with resilience parameter and Weibull distribution with tilt parameter.

5. CONCLUSION

In this paper we studied various parametric extensions of Weibull distributions, Weibull distribution with resilience and tilt parameter. In Weibull distribution

with resilience parameter, the density was decreasing if $a\eta \leq 1$, and was unimodal if $a\eta > 1$. The hazard rate takes on a variety of forms. In particular the hazard rate was increasing for $\alpha \geq 1$ and $a\eta \geq 1$, decreasing for $\alpha \leq 1$ and $a\eta \leq 1$, bathtub shaped for $\alpha > 1$ and $a\eta < 1$, inverted bathtub shaped (unimodal) for $\alpha < 1$ and $a\eta > 1$. In weibull distribution with tilt parameter hazard rate was increasing if $\gamma \geq 1$, $\alpha \geq 1$, and decreasing if $\gamma \leq 1$, $\alpha \leq 1$. If $\alpha > 1$ and $\gamma < 1$, then the hazard rate was initially increasing and eventually increasing, but there may be one interval where it is decreasing. Similarly, if $\alpha < 1$ and $\gamma > 1$, then the hazard rate was initially decreasing and eventually decreasing, but there may be one interval where it was increasing.

Therefore we could conclude that the hazard rates and the survival functions of the parametric extensions of Weibull distribution have explicit expressions, so that these distributions could provide useful models for most of the lifetime data.

In section 4.2 we discussed the analysis of Lifetime data set of successive failure times of air-conditioning equipment in 13 aircraft, taken from Proschan (1963) in Jerald F. Lawless (2003). We fitted Exponential distribution, Weibull, Weibull with resilience parameter, Weibull with tilt parameter and Lognormal distributions for these data sets. Maximum likelihood estimation of parameters were carried out using the R Package. For identifying the best model for the data we used Kolmogorov-Smirnov test. For this data set the Weibull

with resilience parameter has greatest p-value than that of Exponential, Weibull distribution, Weibull with tilt parameter and Lognormal. Here we found that Weibull distribution with resilience parameter is good fit for the data.

REFERENCES

1. Akaike, H., 1973. *Information theory and an extension of the maximum likelihood principle*. In: Kotz, Johnson, (Eds.), *Breakthroughs in Statistics*, vol. I. Springer Verlag, New York, pp. 610–624.
2. Burr, I.W. (1942). Cumulative frequency functions. *The Annals of Mathematical Statistics* **13**, 215–232.
3. Elisa T. Lee, John Wang, *Statistical methods for survival data analysis*, Third edition 2003
4. Fréchet, Maurice (1927). Sur la loi de probabilité de l'écart maximum. *Annales de la Société et Polonaise de Mathématique, Cracovie* **6**, 93–116.
5. Jerald F. Lawless (2003). *Statistical Models and Methods for Lifetime Data*, Wiley –Interscience, John Wiley & Sons, Inc., Publication.
6. Mudholkar, Govind S. and Alan D. Hutson (1996). The exponentiated Weibull family: Some properties and flood data application. *Communications in Statistics: Theory and Methods* **25**, 3059–3083.
7. Mudholkar, Govind S. and Deo Kumar Srivastava (1993). Exponentiated Weibull family for analyzing bathtub failure-rate data. *IEEE Transactions on Reliability* **42**, 299–302.
8. Mudholkar, Govind S., Deo Kumar Srivastava, and Marshall Freimer (1995). The exponentiated Weibull family: A reanalysis of the bus-motor-failure data.

Technometrics **37**, 436–445.

9. Mudholkar, Govind S., Deo Kumar Srivastava, and Georgia D. Kollia (1996). A generalization of the Weibull distribution with application to the analysis of survival data. *Journal of the American Statistical Association* **91**, 1575–1563.
10. Proschan, F. (1963). Theoretical explanation of observed decreasing failure rate. *Technomet-Has*, 5,375-383.
11. Rosin, P. and E. Rammler (1933). The laws governing the fineness of coal. *Journal of the Institute of Fuels* **6**, 29–36.

GREEN SYNTHESIS OF SILVER NANO PARTICLE USED FOR ANTIMICROBIAL APPLICATIONS

■ Jeena Chalikuzhi¹, Archana Ashokan², Binitha M P³

^{1,2}Department of Physics, Govt. Arts and Science College, Kozhikode.

³ Asst. Professor, Department of Physics,
Govt. Arts and Science College, Kozhikode

Email:binithamp@gmail.com

Abstract

Nanoparticles, compared to micro particles have distinctly different properties and advanced characteristics. Silver nanoparticles are one of the metal nanoparticles which have varied and different properties when compared to other materials. These unique properties of silver nanoparticle can be incorporated into antimicrobial applications, biosensor materials, composite fibers, cryogenic superconducting materials, cosmetic products, and electronic components. The synthesis of silver nanoparticles using plant extracts is very cost effective, and therefore can be used as an economic and valuable alternative for the large-scale production of metal nanoparticles. This work demonstrates synthesis of silver nanoparticle using leaf extracts of *Azadirachta Indica* (Neem) and *Terminalia catappa* (Badam). Silver

nanoparticle formation was confirmed by the colour change of plant extract. The formation is further confirmed by Ultraviolet-Visible (UV-vis) Spectrometric studies. The crystalline nature of silver nanoparticles is confirmed by X-ray Diffraction measurements. The synthesized silver nanoparticles were tested for antibacterial activity.

The formation is further confirmed by Ultraviolet-Visible (UV-vis) Spectrometric studies. The crystalline nature of silver nanoparticles is confirmed by X-ray Diffraction measurements. The synthesized silver nanoparticles were tested for antibacterial activity.

INTRODUCTION

In the past ten years silver nanoparticle (AgNPs) have been one of the extensively studied nanomaterials and have attracted a great deal of attention due to their unique physical, chemical, optical and biological properties and found tremendous application in biomedicine, drug delivery, electronics, optics, catalysis, food industry, agriculture, textile industry and water treatment [1-2].

Several chemical methods have been developed for the synthesis of silver nanoparticle including chemical reduction, aqueous solution chemical reduction, non aqueous chemical reduction, the template method, electrochemical reduction, ultrasonic assisted reduction, photo induced or photo catalytic reduction, microwave assisted synthesis, irradiation reduction, the micro emulsion method, biochemical method etc [3-4]. But those

chemical methods have been reported along with various drawbacks including the use of toxic solvents, generation of hazardous by-products and high energy consumption, which pose potential risk to human health and to the environment. Currently there is a growing need to develop an environment friendly nanoparticle synthesis [5] that does not use toxic chemicals in the process of its synthesis.

In recent years green chemistry and biosynthetic methods have become more attractive ways to obtain AgNPs. These unconventional methods use either biological microorganisms [6] (e.g.: bacteria, fungi, marine algae, yeasts) or different alcoholic or aqueous plant extracts. Plant-mediated synthesis of AgNPs is more advantageous compared to the methods that use microorganisms especially because they can be easily improved, are less bio hazardous and do not involve the elaborate stage of growing cell cultures [7].

MATERIALS AND METHODS

Around 2 gm each of fresh leaves of *Azadirachta Indica* (Neem) and *Terminalia catappa* (Badam), were boiled in 20 ml of distilled water for 15 min. Each of these 1ml extracts were mixed with 50ml of 1mM silver nitrate (AgNO_3) solution and colour change was observed indicating the formation of silver nanoparticles.

RESULTS AND DISCUSSION

Reduction of silver ions into silver nanoparticles during exposure to plant extracts was observed as a result of the color change. The color change is due to the Surface Plasmon Resonance (SPR) phenomenon. The metal nanoparticles have free electrons, which give the SPR absorption band, due to the combined vibration of electrons of metal nanoparticles in resonance with light wave.

It was observed that solution of silver nitrate turned yellowish brown on addition of leaves extract; it indicated the formation of AgNPs due to the reduction of Ag^+ to Ag^0 , while no color change was observed in the absence of plant extract. The change in colour was observed initially after 5 minutes of adding the solution to neem leaf broth. The colour intensity was increased with increasing the reaction time. In general, the conduction band and valence band lie very close to each other in metal nanoparticles like silver and gold. Due to the collective oscillation of electrons of silver nanoparticles in resonance with the light wave, the free electrons give rise to a surface plasmon resonance absorption band. The formation of silver nanoparticles was monitored periodically using UV-Vis spectroscopy which has proved to be a useful technique.

Figure(1) and figure (2) show the absorption spectra of AgNPs obtained from the reaction of Neem leaf extract (*Azadirachta indica*) and $AgNO_3$, and that between Badam leaf extract (*Terminalia catappa*) and $AgNO_3$,

recorded in the range of 300-800 nm at different reaction time. The sharp bands of silver nanoparticles were observed around 437 nm in case of *Azadirachta indica* that confirmed the synthesis of AgNPs. Past studies suggested that a SPR peak located between 410 and 450 nm has been observed for AgNPs. Absorption maximum is observed at 425 nm in the case of *Terminalia catappa* and it is observed that there is an increase in the absorbance with the passage of time, indicating the enhancement in the formation of AgNPs.

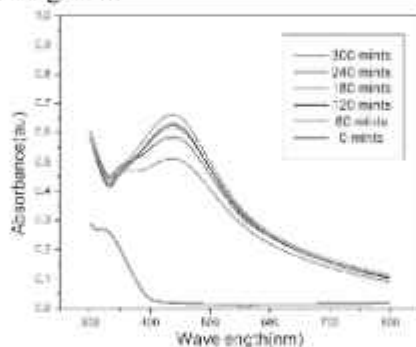


Figure (1): Absorption spectra of AgNPs observed at 6 different reaction times of 1 mM AgNO_3 solution with Neem leaf broth

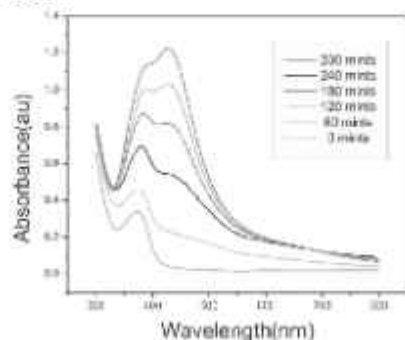


Figure (2): Absorption spectra of AgNPs observed at 6 different reaction times of 1 mM AgNO₃ solution with badam leaf broth X-Ray diffraction analysis

The structure of prepared silver nanoparticles has been investigated by X-ray diffraction (XRD) analysis. The XRD pattern of silver nanoparticles prepared from neem leaf extract given in figure 3.

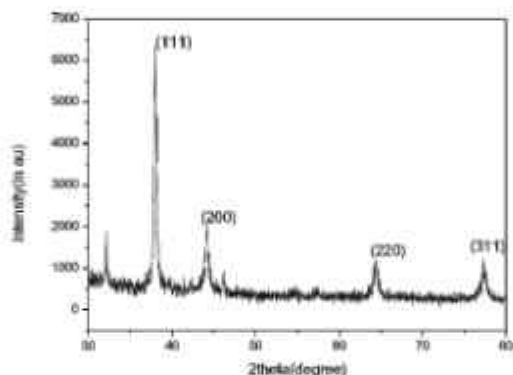


Figure 3.

XRD of silver nanoparticles synthesized by using neem extract

The peak intensities were recorded from $2\theta = 30^\circ$ to 80° . Four distinct diffraction peaks at 37.98° , 44.14° , 64.34° and 77.21° corresponding to the (111), (200) and (220) and (311) Bragg reflections of face centered cubic (fcc) crystal structure of silver. The interplanar spacing, d values are 2.36, 2.05, 1.44, and 1.234 Å for (111), (200), (220) and (311) planes respectively. The d values from XRD pattern of silver nanoparticles are matched with standard values. The high intense peak for fcc materials is

generally (1 1 1) reflection, which is observed in the sample. The intensity of peaks reflected the high degree of crystallinity of the silver nanoparticles. However, the diffraction peaks are broad which indicating that the crystallite size is very small. The XRD shows that silver nanoparticles formed are crystalline. The crystallite size of silver nanoparticles is calculated as 21 nm from FWHM of the high intense diffraction peak using Scherrer's formula. Figure 4. shows the XRD pattern of silver nano particle formed from badam leaf extract.

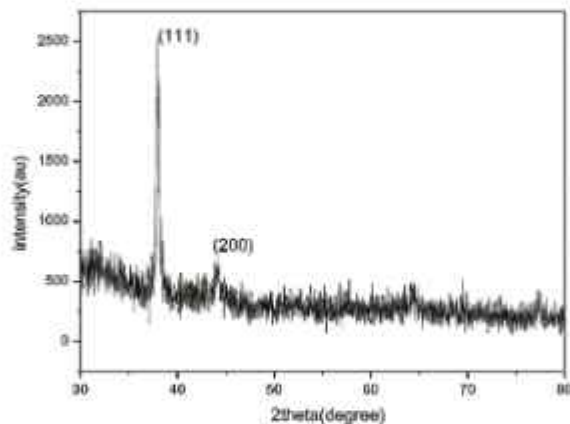


Figure 4: XRD pattern of silver nanoparticle formed from Terminalia catappa leaf extract

Bragg reflections can be seen which correspond to the (111) and (200) reflections of fcc structure. The size of nanoparticle formed is calculated as 32.25 nm using Scherrer's formula.

Antimicrobial activity

Anti microbial activity is carried out in gram negative bacteria *E.coli* and gram negative bacteria *Staphylococcus aureus* using silver nanoparticle produced using neem leaves extract. Figure 5 and 6 shows the zone of inhibition around the disc for the synthesized Ag NPs and obtained values are presented in the Table 1 and 2. It was observed that the synthesized Ag NPs showed better antibacterial activity.

The size of silver nanoparticles is about 21 nm. They can easily enter into bacterial cell (size is 100-1000 nm) and then combine with thiol, hydroxyl, and carboxyl group in cell and deactivate the function by releasing the silver ion. Silver nanoparticles combined with respiratory enzyme, protease enzyme and DNAs of bacteria to cause suffocation, indigestion and inhibition of cell replication respectively. Bacterial cell functions were disturbed by these silver nanoparticles which damaged the cell and lead to the death of bacterial cell [8].

1. GRAM NEGATIVE

Organism: *E.coli*

Sample	Concentration ($\mu\text{g/mL}$)	Zone of inhibition (mm)
Silver Nanoparticle	Streptomycin (100 μg)	22
	25	Nil
	50	Nil
	100	2

Table 1: table showing zone of inhibition for *E.coli*



Figure 5 :Antibacterial activity of Ag NPs against E.coli

2 .GRAM POSITIVE

Organism: Staphylococcus aureus

Sample	Concentration (µg/mL)	Zone of inhibition (mm)
Silver Nanoparticle	Streptomycin (100µg)	26
	25	Nil
	50	10
	100	13

Table2: table showing zone of inhibition for E.coli



Figure 6: Antibacterial activity of Ag NPs against Staphylococcus aureus

GENERAL CONCLUSIONS

We have synthesized silver nanoparticle from plant leaves extract of *Azadirachta Indica* (Neem) and *Terminalia Catappa* (Badam). Color changes occurred in the silver nitrate solution after the addition of leaf extract due to the excitation of NPs Surface Plasmon Resonance (SPR), which strongly indicates the formation of Ag NPs. The formation of AgNPs is further confirmed by UV-Visible spectroscopy. The absorption spectra of AgNPs obtained from the reaction of leaf extract and AgNO_3 and the sharp bands of silver nanoparticles were observed in the range of 420 to 440 nm. The intensity of absorption peak is found to be increasing with reaction time, which indicates the increase in concentration of silver nanoparticles. X-ray diffraction studies confirmed the fcc structure of silver nanoparticles. The high-intensity peak for fcc materials is generally (111) reflection, which is observed in the sample.

REFERENCES

1. Klaus, T.J., R.; Olsson, E.& Granqvist, C.Gr., Proc Natl Acad Sci USA., 1999. 96:p. 13611-13614
2. Senapati, S., "Biosynthesis and immobilization of nanoparticles and their applications.". University of pune, India, 2005.
3. Harekrishna Bar, D.K.B., Gobinda sahoo P, priyanka Sarkar, Sankar PD., Colloid surface A, 2009. 39(3): p. 134-139.
4. Cassandra D, N.N., Jodi H, Linfeng G, Tan, Li, et al.
5. Kaviya S, S.J., Viswanathan B., Journal of nanotechnology, 2011: p. 1-5
6. Mukherjee P, A.A., Mandal DS, Senapati S, Sainkar R, Khan MI, Parishcha R, Ajaykumar PV, Alam M, Kumar R, Sastry M, Nano Lett, 2001. 1: p. 515-519.
7. Spring H, S.K., Syst Appl Microbiol, 1995. 18(2): p. 147-153.
8. L. Kvitek, A. Panacek, J. Soukupova, M. Kolar, R. Vecerova, R. Prucek, J. Phys. Chem. C, 112 (2008) 5825-5834.

A REVIEW ON THE GREEN SYNTHESIS OF ZINC OXIDE NANOPARTICLES

■ Dr.NISHA M.,

Assistant Professor, Department of Physics,
Govt.Arts and Science College Kozhikode
nisha77@gmail.com

Abstract

Nanomaterials play an important role in technological advancements because of their tunable physical, chemical and biological properties such as melting point, wettability, electrical and thermal conductivity, catalytic activity light absorption and scattering. Nanotechnology and biomedical sciences open the possibility for a wide variety of biological research topics and medical uses at the molecular and cellular level. The biosynthesis of nanoparticles has been proposed as a cost-effective and environmentally friendly alternative to chemical and physical methods. Plant-mediated synthesis of nanoparticles is a green chemistry approach that connects nanotechnology with plants. Among the biological alternatives, plants and plant extracts seem to be the best option The present review gives an overview of green synthesis of ZnO nanoparticles, and various applications of nanoparticles in different fields.

Introduction

Nanotechnology deals with the production and usage of materials with nanoscale dimension. Nanoscale dimension provides nanoparticles a large surface area to volume ratio and thus very specific properties. Most of the current nanoparticles are classified into four material based categories namely carbon based nanomaterials, inorganic based nanomaterials, organic based nanomaterials and composite based nanomaterials. Among these, inorganic based nanomaterials include metal nanoparticles (Ag, Au etc) and metal oxide nanoparticles [1]. Several types of inorganic metal oxides have been synthesized and remained in recent studies like TiO_2 , CuO , and ZnO . Of all these metal oxides Zinc oxide Nanoparticles (ZnO NPs) is of maximum interest because they are inexpensive to produce, safe and can be prepared easily [2]. US FDA has enlisted ZnO as GRAS (generally recognized as safe) metal oxide [3]. ZnO is an n-type semiconducting Metal oxide. Zinc oxide NPs has drawn interest in past two–three years due to its wide range of applicability in the field of electronics, optics and biomedical systems [4], [5]. ZnO NPs exhibit tremendous semiconducting properties because of its large band gap (3.37 eV) and high exciton binding energy (60meV) [6,7]. Due to its UV filtering properties, it has been extensively used in cosmetics like sunscreen lotions. It has a wide range of biomedical applications like in drug delivery and has anticancer, antidiabetic, antibacterial and

antifungal properties [8,9]. ZnO NPs have a very strong antibacterial effect at a very low concentration of gram negative and gram positive bacteria as confirmed by the studies[10,11]. It is also employed for rubber manufacturing,, for removing sulfur and arsenic from water, protein adsorption and dental applications. It also exhibit piezoelectric and pyroelectric properties [12]. ZnO NPs have been reported in different morphologies like nanoflake, nanoflower, nanobelt, nanorod and nanowire[13,14,15]

The physical and chemical production of these NPs, require toxic chemicals and extreme environments. So green methods employing the use of plants, fungus, bacteria, and algae are becoming popular. Green synthesis of nanoparticles is an approach of synthesizing nanoparticles using microorganisms and plants having biomedical applications. This approach is an environment-friendly, cost-effective, biocompatible, and safe [16]. These methods allow large scale production of ZnO NPs free of additional impurities [17]. NPs synthesized from biomimetic approach show more catalytic activity and limit the use of expensive and toxic chemicals. Plant parts like roots, leaves, stems, seeds, fruits have also been utilized for the NPs synthesis as their extract is rich in phytochemicals which act as both reducing and stabilization agent [18,19,20]

Discussion

Pragati Jamdagni et al[21] optimized the synthesis conditions zinc oxide nanoparticles using aqueous flower extract of *Nyctanthes arbortristis* and resultant nanopowder was characterized structurally and optically. The nanoparticles were present in the form of aggregates with a particle size range of 12–32 nm. The role of a lesser intense capping layer on the NP surface was shown by the TEM. The NPs showed good activity against 5 tested fungal phytopathogens. The study showed that the Nps could be utilized for developing antifungal agents for commercial use in the field of agriculture. Studies on using an eco-friendly approach for synthesis of zinc oxide nanoparticles have potential for developing good fungicidal formulations having nanoparticles.

ZnO NPs synthesized using *Costus pictus* leaf extract as a reducing and capping agent caused the formation of pure hexagonal phase structures of ZnO NPs. The biosynthesized zinc oxide nanoparticles exhibited strong antimicrobial behavior against bacterial and fungal species when agar diffusion method was employed. It also exhibited anticancer activity against Daltons lymphoma ascites (DLA) cells [22].

ZnO NPs synthesized by Zinc acetate and sodium hydroxide utilizing the biocomponents of leaves of *Catharanthus roseus* were spherical in shape with an

average size of 23 to 57 nm. These ZnO-NPs were evaluated for antibacterial activity. The maximum diameter of inhibition zones around the ZnONPs disk used for *Bacillus thuringiensis* indicates the resistance to ZnO NPs followed by *Escherichia coli*. Among the four bacterial species tested, the *Pseudomonas aeruginosa* is more susceptible when compared with other three species. It is concluded that the biological synthesis of ZnO NPs is very fast, easy, cost effective and eco-friendly and without any side effects and ZnO NPs may be used for the preparation of antibacterial formulations against *Pseudomonas aeruginosa*[23].

The temperature dependent synthesis and particle growth have been reported where *Hibiscus subdariffa* leaf extract was used for the green synthesis of ZnO NPs[24]. The anti-bacterial activity of ZnO NPs was studied on *Escherichia coli* and *Staphylococcus aureus* and the NPs were found to be potential antibacterial agents. The authors also found that small sized ZnO NPs, stabilized by plant metabolites had better anti-diabetic effect on streptozotocin (STZ) induced diabetic mice than that of large sized ZnO particles. By employing enzyme linked immunosorbent assay (ELISA) and real time polymerase chain reaction (RT-PCR) it was seen that ZnO can induce the function of Th1, Th2 cells and expressions of insulin receptors and other genes of the pancreas associated with diabetes.

Literature shows the report on the novel green synthesis of

stable ZnO NPs using various concentrations of zinc nitrate (0.01M, 0.05M, 0.1M) and *Albizia lebbek* stem bark extracts as an efficient chelating agent. Antimicrobial, antioxidant, cytotoxic, and antiproliferative activities of the synthesized NPs on human breast cancer cell lines were evaluated using different assays[25].

A single step rapid synthesis of zinc oxide nanoparticles (ZnO NPs) in a green approach has been demonstrated *via* conjugating the natural product riboflavin by varying temperature[26]. Field emission scanning electron microscopy (FESEM) analysis and high-resolution transmission electron microscopy (HRTEM) showed that the average diameter of the synthesized nanoparticles is about 40 nm in spherical shape. ZnO NPs showed significant ameliorative efficiency against jaundice stress at molecular and cellular levels in mice models. Biochemical parameters, different cytokine profiling (Th1 & Th2 cells) and their corresponding m-RNA expressions have been studied by the enzyme-linked immunosorbent assay (ELISA) and real-time polymerase chain reaction (RT-PCR) in the presence of riboflavin conjugated ZnO NPs synthesized at 60 °C and 30 °C temperature (Ribo-ZnO30/Ribo-ZnO60). Substantial Ribo-ZnO60 assisted improvement ($p > 0.001$) of the thymus-dependent functions and protein expressions of other genes associated with jaundice were observed by Western blotting. The supplementation of Ribo-ZnO60 treatment is more active

in histologically recovering the liver and kidney tissues than Ribo-ZnO₃₀ due to their particle nature and more phases with uniform size.

Conclusion

Rapid industrialization and urbanization has led to the release of a large amount of hazardous, poisonous and unwanted chemicals, gases and substances causing a great deal of damage to the environment. Biological molecules are more suitable and less hazardous for nanotechnology applications, because of their exclusive properties. Green synthesis of nanoparticles makes use of environment friendly and non-toxic reagents like plant extracts. Thorough research is going on in this field for optimizing the synthesis parameters by employing various green agents as reducing agents and capping agents. From the above survey it can be seen that the green synthesis of ZnO NPs is environ friendly and at the same the synthesized nanoparticles has got wide range of applications in the medical field as antibacterial, anticancer and antidiabetic agents.

References

1. Jaison Jeevanandam, Ahmed Barhoum, Yen S.Chan, Alain Dufresne, Michael K.Danquah, Beilstein J.Nanotechnol. 2018,9,1050-1074
2. C. Jayaseelan, A.A. Rahuman, A.V. Kirthi, S. Marimuthu, T. Santhoshkumar, A. Bagavan, *et al.*, Spectrochim. Acta A Mol. Biomol. Spectrosc, 90 (2012), pp. 78-84,
3. J. Pulit-prociak, J. Chwastowski, A. Kucharski, M. Banach, Appl. Surf. Sci, 385 (2016), pp. 543-553,
4. M. Anbuvaran, M. Ramesh, G. Viruthagiri, N. Shanmugam, N. Kannadasan, Spectrochim. Acta A Mol. Biomol. Spectrosc, 143 (2015), pp. 304-308,
5. M. Sundarajan, S. Ambika, K. Bharathi, Adv. Powder Technol, 26 (2015), pp. 1294-1299
6. H. Mirzaei, M. Darroudi, Ceram. Int, 43 (2017), pp. 907-914,
7. V. Patel, D. Berthold, P. Puranik, M. Gantar, Biotechnol. Reports, 5 (2015), pp. 112-119,
8. F. Movahedi, H. Masrouri, M.Z. Kassaei, J. Mol. Catal. A Chem., 395 (2014), pp. 52-57,
9. L. Martinková, B. Uhnáková, M. Pátek, J. Nešvera, V. Křen, Environ. Int, 35 (2009), pp. 162-177
10. K. Vimala, S. Sundarraj, M. Paulpandi, S. Vengatesan, S. Kannan, Process biochem, 49 (2014), pp. 160-172
11. P. Venkatachalam, M. Jayaraj, R. Manikandan, N. Geetha, E.R. Rene, N.C. Sharma, *et al.*, Plant Physiol. Biochem, 110 (2016), pp. 59-69,
12. A.K. Jha, Nano, 2 (2007), pp. 239-242
13. K. Paulkumar, S. Rajeshkumar, G. Gnanajobitha, M. Vanaja, C. Malarkodi, G. Annadurai, *et al.*, ISRN Nanomater, 2013 (2013), pp. 1-8,

SYNTHESIS & CHARACTERIZATION OF Mn DOPED ZnS NANOPARTICLES

■ Parvathy T, Sabira K

Dept. of Physics, Govt Arts and Science College, Calicut

E mail: parvathysivadass@gmail.com

Abstract

Researchers take keen interest in the semiconductor of Group II-VI compounds because of their important unique properties and potential applications. ZnS is an important group II-VI semiconductor having different application in the field of optical coatings, field effect transistor, optical sensors, electroluminescence displays, phosphors and other light emitting applications. Luminescent ZnS quantum dots have great potential for use in biological imaging and diagnostic applications. Zinc sulphide and Manganese doped nanoparticles having different concentration were synthesized via wet chemical route method. The structure of nanoparticle were characterized by an X-ray diffraction techniques and was also confirmed by using a microraman spectrometer. The band gap of ZnS was determined by using an UV-visible spectrometer and is found to be 3.74eV and it is observed that on doping with Mn, band gap is found to be varying. The emission spectrum of ZnS:Mn nanoparticles show two peaks in which the first peak is at 445nm and it is a blue emission peak and the second peak lies at 598 nm and it correspond to

orange emission. The emission spectrum centered at 598 nm is the characteristics of Mn^{2+} ion which can be attributed to a $4T_1 \rightarrow 6A_1$ transition. Concentration quenching is observed when Mn^{2+} concentration is increased more than 7%.

INTRODUCTION

Nanoscience and nanotechnology are the study and application of extremely small things and can be used across all the other science fields such as, physics, chemistry, biology material science and engineering. It involves the ability to see and control individual atoms and molecules. In its popular use nano refers to length and the nanoscale usually refers to a length from the atomic level from around 0.01 nm up to 100 nm. In general nanoscience is defined as the study of the phenomenon on the scale of 1-100 nm. A nanometer is the SI unit of length 10^{-9} m or a distance of one-billionth of a meter. Atoms are a few tenths of a nanometer in diameter and molecules are typically a few nanometer in size. Nanocrystals of group II-VI semiconductors, known as Qdots, in which electrons and holes are three dimensionally confined within the exciton Bohr radius of the material, are characterized by the exceptional optical properties, such as broad absorption and sharp emission bands as well as size-tunable photoluminescence in the visible spectral range. II-VI compound semiconductors include the cations of zinc, cadmium and/or mercury combined with anionic oxygen, sulfur, selenium and/or tellurium. These semiconductors generally crystallize in both a face-centered cubic (zinc blende) and a hexagonal (wurtzite) crystal structure. For

example, the equilibrium crystal structure of both ZnO and ZnS is hexagonal, although ZnS often also exhibits a metastable cubic or a mixed hexagonal/cubic structure. The II-VI compound semiconductors may exhibit good luminescence because they have a direct band gap. In addition, many of the II-VI semiconductors are often used as a host for luminescent activators, for example, ZnS doped with Mn^{2+} , which emits yellow light. Near band edge emission from excitons can be observed from II-VI semiconductors, especially at low temperatures, from those materials with a low exciton binding energy.

ZnS quantum dots

ZnS Qdots are considered to be one of the most important Qdots because of their unique lighting, sensors and lasers. In addition, transition metal and/or rare earth metal ion doped ZnS is one of the most popular semiconductor phosphors. ZnS is a wide band-gap compound semiconductor ($E_g = 3.6$ eV or 340 nm). The luminescence characteristic of impurity-activated ZnS Qdots differ markedly from those of the bulk ZnS. Yang *et al.* hypothesized that these differences result from the size dependence of the properties and their high dispersion [5].

Doped ZnS Qdots

Doped ZnS Qdots are important semiconductor nano materials, With Mn^{2+} doped ZnS Qdots being one of those most studied as a phosphors [6-7]. In 1994, Bhagrava *et al.* reported high PL quantum yields (18%) from ZnS :Mn Qdots [8]. Coincident with the intensity enhancement, they reported shorter luminescent lifetimes for the Mn^{2+}

emission (decrease from hundreds of microseconds for the bulk to nanoseconds in nanocrystals) [9, 10]. The increased intensity was attributed to an efficient energy transfer from the ZnS host to Mn^{2+} ions facilitated by mixed electronic states. Hybridization of atomic orbitals of ZnS and d -orbitals of Mn^{2+} in the nanoparticles was suggested to also be responsible for the relaxation of selection rules for the spin-forbidden $4T_1 \rightarrow 6A_1$ transition of Mn^{2+} , leading to the short emission lifetimes of atomic orbitals of ZnS and d -orbitals of Mn^{2+} in the nanoparticles. Subsequent research demonstrated that while the quantum yield of passivated ZnS:Mn Qdots could be high, the luminescent lifetimes were not significantly smaller from those of the bulk material. However, the luminescence properties were found to be dependent upon the S^{2-} and Mn^{2+} concentrations as well as the structural properties of the Qdots.

Materials and methods

In the present work, zinc acetate [$Zn(CH_3COO)_2 \cdot 2H_2O$] (purity >98%), manganese acetate, [$Mn(CH_3COO)_2 \cdot 4H_2O$] (purity >99.5%), (purity >99.5%) and sodium sulphide [$Na_2S \cdot 9H_2O$] (purity >98%) were purchased from Merck specialties private limited, Mumbai. Chemical route technique has number of advantages including easy process ability at ambient conditions, very easy to control the particle size, use of simple equipment, large area uniform production, environmental friendliness and less hazardous..

Synthesis of manganese doped ZnS

Pure ZnS and manganese doped ZnS nanoparticles (ZnS:Mn) were synthesized by simple technique of

chemical co-precipitation method. Freshly prepared, aqueous solutions of zinc acetate, manganese acetate and sodium sulphide were used for the synthesis. In a typical reaction, 50 ml of 1 M solution of zinc acetate was mixed with 50 ml of 0.01 M solution of manganese acetate in a conical flask. To this solution, 50 ml of 1 M sodium sulphide solution was added drop by drop, with vigorous stirring for 11 hrs at room temperature. The precipitate was washed several times with distilled water and dried in an oven at 80 °C and thoroughly ground in a mortar to get a fine powder of the samples [11-12]. The experiment was repeated with 0 M, 0.005M, 0.01M, 0.03M, 0.05M, 0.07M, 0.09M, 0.11M and 0.13M manganese acetate solution without varying the molarity of zinc acetate or sodium sulphide.

Results and discussion

X-Ray Diffraction (XRD) analysis

The crystalline structure of the synthesized nanoparticles was analyzed by x-ray diffraction (XRD) with Cu K_α radiation (wavelength = 1.5418 Å). A step size of 0.05° and time-per-step of 0.6s was used for each scan. The x-ray diffraction pattern of pure ZnS is shown in figure 1. The observed diffraction peaks correspond well with the standard powder diffraction data of cubic ZnS. The XRD pattern shows three prominent peaks at 29.18°, 48.1° and 57.36° corresponding to (111), (220) and (311) lattice planes of the zinc blend structure of ZnS (JCPDS No.

050566) [13].

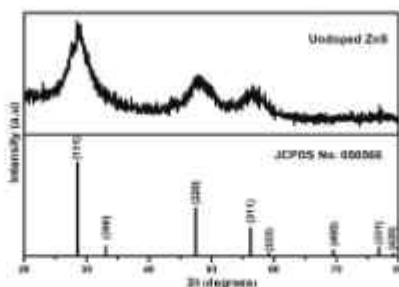


Figure 1: XRD pattern of undoped ZnS nanoparticles

There is an obvious broadening of the XRD peaks which indicates the formation of nanosized ZnS:Mn. The average particle size of the nanostructured ZnS:Mn is found to be in the range of 2 to 4 nm from Scherrer equation. Since the crystallite size is comparable to exciton Bohr radius of ZnS (2.5 nm), the resulting quantum confinement effects facilitate the formation of ZnS quantum dots.

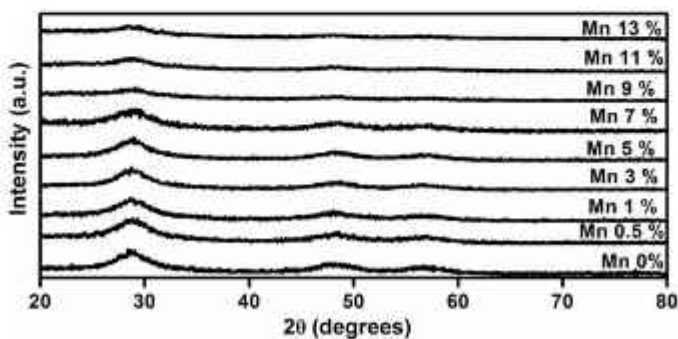


Figure 2: XRD pattern of pure ZnS and ZnS:Mn nanoparticles with different doping concentration

XRD pattern of Mn doped ZnS nanoparticles with doping concentration 0.5%, 1%, 3%, 5%, 7%, 9%, 11% and 13% are as shown in figure 2. All the peaks again matched well with the standard powder diffraction data of cubic ZnS. The presence of any other secondary phases is not found by XRD results which confirms the successful incorporation of Mn into ZnS lattice and hence the doping of ZnS is verified.

UV-visible absorption spectroscopic studies

Optical absorption study plays an important role to understand the behavior of semiconductor nanocrystals. A fundamental property of semiconductors is the band gap, which is the energy separation between the filled valance band and the empty conduction band. In fact, optical excitation of electrons across the band gap is strongly allowed, producing an abrupt increase in absorption at the wavelength corresponding to the band gap energy. Such feature in the optical spectrum is known as the optical absorption edge.

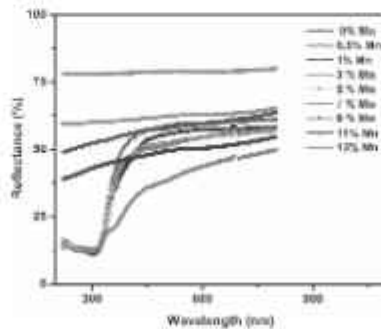


Figure 3: Diffuse reflectance spectra of pure and Mn doped ZnS nanoparticles

Optical characterisation of the nanoparticles was carried out using diffuse reflectance spectroscopy (DRS). All spectra were taken in the range of 220-800 nm with a JASCO V 570 spectrophotometer. The figure 3 shows the diffuse reflectance spectra of undoped and doped ZnS nanoparticles. From the spectra, it is seen that the absorption edge of ZnS nanoparticles is fairly red shifted when compared with that of bulk ZnS ($3.77 \text{ eV} \approx 311 \text{ nm}$). Pure ZnS and lightly doped ZnS nanoparticles have good absorption for light in the wavelength of 220 nm - 350 nm[14]. The absorption edge of the doped samples is shifted towards longer wavelength when compared with undoped ZnS and this shift slightly increases with increase in Mn^{2+} concentration. This red shift is mainly due to the quantum confinement effect caused by the reduction in particle size [15]. The shift towards longer wavelength indicates a decrease in the optical band gap.

It is well known that the fundamental absorption is due to the transition of electron excitation from the valence band to the conduction band which can be used to determine the value of the optical band gap of the nanoparticles. The most direct way of extracting the optical band gap from the figure is to simply determine the wavelength at which the extrapolation of the base line and the absorption edge crossed [16]. Thus knowing wavelength, the energy band gaps of all the prepared samples were calculated by using a simple wave-energy equation

$$E = \frac{hc}{\lambda}$$

where h is the Planck's constant, c is the velocity of light, λ is the absorption wavelength. The energy band gaps of all the prepared samples is given in table 1.

Table 1: Energy bandgap of undoped and doped ZnS nanoparticles

Doping concentration of Mn	Wavelength(nm)	Bandgap(eV)
Pure	311.74	3.77
0.05%	313.76	3.74
1%	315.78	3.72
3%	317.8	3.70
5%	319.82	3.67
7%	323.71	3.63
9%	325.73	3.61
11%	327.76	3.58
13%	328.94	3.57

The variation of bandgap of ZnS nanoparticles with Mn doping is shown in figure 4. The band-gap energy is found to decrease from 3.77 eV to 3.57 eV with increasing in doping concentration of Mn is due to the quantum confinement effects. It implies that with decreasing particle size a strong hybridisation of the s-pstates of the ZnS host and the d states of the Mn^{2+} impurity should occur. This hybridisation results in a faster energy transfer between the ZnS host Mn^{2+} impurity yielding a higher quantum efficiency and it was argued that through this hybridisation, the spin forbidden transition of the Mn^{2+} impurity become less forbidden, resulting in a shorter decay time.

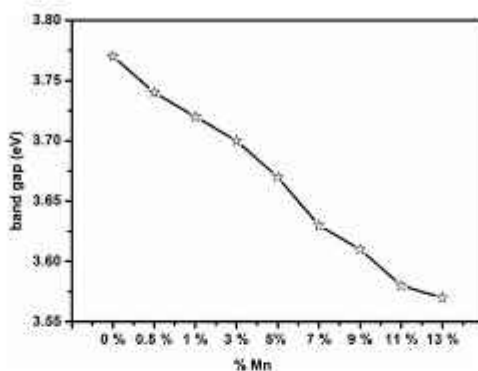
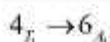


Figure 4: Variation of bandgap of ZnS with different doping concentration of Mn

Photoluminescence studies

The objective of this work is to study and discuss the luminescence enhancement effect of Mn^{2+} -doped ZnS nanoparticles. ZnS has attracted enormous interest because it has been commercially used for a variety of applications such as light-emitting diodes (LEDs), electroluminescence devices, flat panel displays, sensors, lasers, infrared windows, solar cells, bio-devices, and other optoelectronic devices. In addition, because of its wide band gap, ZnS is suitable for use as a host material for a variety of dopants. It is reported that the doping with Mn into ZnS nanocrystals results in the luminescence efficiency enhancement and the

lifetime shorting in comparison with that of the bulk material. Such results are explained on the basis of the interaction of the sp electron-hole of the host (ZnS) and the 3d electrons of the impurity (Mn) under condition of the quantum confinement for the sp states. It has been analyzed as a photoluminescence excitation (PLE) spectra in the ultraviolet- and visible-regions for the ZnS:Mn nanoparticle samples with different sizes and they have proposed a model for the energy transfer from the host ZnS lattice to Mn^{2+} d levels. It is concluded that the Mn^{2+} luminescence under the inter-band excitation occurs mostly by the energy transfer from the electron-hole pairs delocalized inside the ZnS host nanocrystals. As the chemical similarity between Zn^{2+} and Mn^{2+} facilitates the incorporation of the dopant ion, a lot of study has been made on doped ZnS:Mn nanoparticles. Since a significant part of the Mn^{2+} ions resides near the surface of the nanoparticle, the incorporated

Photoluminescence studies

The objective of this work is to study and discuss the luminescence enhancement effect of Mn^{2+} -doped ZnS nanoparticles. ZnS has attracted enormous interest because it has been commercially used for a variety of applications such as light-emitting diodes (LEDs), electroluminescence devices, flat panel displays, sensors, lasers, infrared

windows, solar cells, bio-devices, and other optoelectronic devices. In addition, because of its wide band gap, ZnS is suitable for use as a host material for a variety of dopants. It is reported that the doping with Mn into ZnS nanocrystals results in the luminescence efficiency enhancement and the lifetime shorting in comparison with that of the bulk material. Such results are explained on the basis of the interaction of the sp electron-hole of the host (ZnS) and the 3d electrons of the impurity (Mn) under condition of the quantum confinement for the sp states. It has been analyzed as a photoluminescence excitation (PLE) spectra in the ultraviolet- and visible-regions for the ZnS:Mn nanoparticle samples with different sizes and they have proposed a model for the energy transfer from the host ZnS lattice to Mn^{2+} d levels. It is concluded that the Mn^{2+} luminescence under the inter-band excitation occurs mostly by the energy transfer from the electron-hole pairs delocalized inside the ZnS host nanocrystals. As the chemical similarity between Zn^{2+} and Mn^{2+} facilitates the incorporation of the dopant ion, a lot of study has been made on doped ZnS:Mn nanoparticles. Since a significant part of the Mn^{2+} ions resides near the surface of the nanoparticle, the incorporated concentration of Mn^{2+} is consistently lower than the intended dopant concentration. Also the emission spectrum in $ZnS:Mn^{2+}$ is almost size-independent. Consequently, the growth of an inorganic (ZnS) shell around ZnS:Mn effectively reduces non-

radiative decay paths whereby the enhancement in the luminescence takes place more efficiently as compared to the organic passivation of the surface. Due to its wide band gap, ZnS has a high index of reflection and high transmittance in the visible range particular suitable for host material for a large variety of dopants. The synthesis of Mn^{2+} doped ZnS nanoparticles have been primarily investigated because of the luminescence of manganese ions inside the ZnS host. In fact, in Mn^{2+} doped ZnS nanoparticles, the luminescence quantum efficiency is expected to increase as a result of greater interaction between the electron and hole of the host ZnS nanoparticles with localized dopant levels. Basically, in photoluminescence the electrons are excited from the ZnS valence band to conduction band by absorbing the energy equal to or greater than their band gap energy and subsequent relaxation of these photo-excited electrons to some surface states or levels is followed by radiative decay enabling luminescence in the visible region.

Photoluminescence(PL) emission spectra were recorded using Jobin Yvon Fluoromax-3 spectrometer equipped with 150 W xenon lamp. PL emission spectra of undoped ZnS nanoparticles is given in figure 5. The spectra of pure ZnS nanoparticles showed emission at 430nm which is blue emission, which was originated from the defect site of ZnS itself and also sulphur deficiency

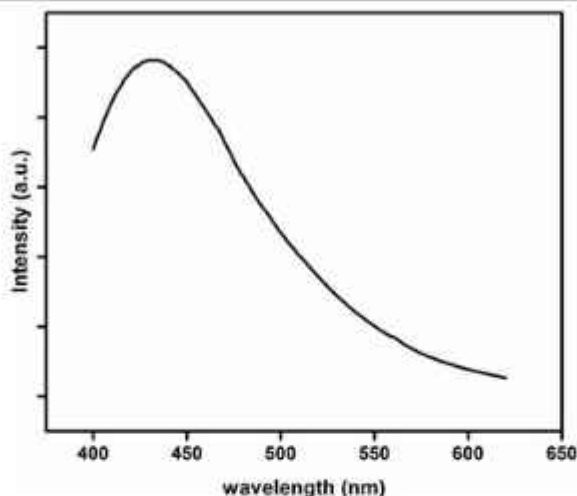


Figure 5 :PL emission spectra from undoped ZnS nanoparticles

Figure 6 shows the PL spectra of ZnS:Mn nanoparticles with different Mn doping concentration. The PL spectra of ZnS:Mn nanoparticles with % of Mn 0.05%, 1%, 3%, 5%, 7%, 9%, 11% and 13% are measured in which excitation wavelength is same for all the samples. The experiment is performed at room temperature.

Two peaks were found for each sample. Two peaks are obtained in the emission spectra of ZnS:Mn nanoparticles, in which the first peak is at 445nm and it is a blue emission peak which is attributed due to the transition of electrons from the shallow states near the conduction band to sulphur vacancy present near the valence band and the second peak lies at 598 nm and it correspond to orange

emission, and it does not shift with Figure 6 shows the PL spectra of ZnS:Mn nanoparticles with different Mn doping concentration. The PL spectra of ZnS:Mn nanoparticles with % of Mn 0.05%, 1%, 3%, 5%, 7%, 9%, 11% and 13% are measured in which excitation wavelength is same for all the samples. The experiment is performed at room temperature.

Two peaks were found for each sample. Two peaks are obtained in the emission spectra of ZnS:Mn nanoparticles, in which the first peak is at 445nm and it is a blue emission peak which is attributed due to the transition of electrons from the shallow states near the conduction band to sulphur vacancy present near the valence band and the second peak lies at 598 nm and it correspond to orange emission, and it does not shift with reducing size of the nanocrystals. The orange emission from the Mn doped ZnS nanoparticles is given inset of figure 6. The blue emission at 445nm, called PL peak I or PL type I, is very broad and originates from the radiative recombination involving defect states in the ZnS nanocrystals. The orange emission centered at 598 nm, called PL peak II or PL type II, is the characteristics emission of Mn^{2+} ion which can be attributed to a $4T_1 \rightarrow 6A_1$ transition. The intensity of first peak in the PL spectra increases with increase in the concentration. The intensity of second peak also increases

with the doping concentration. The intensity increases as Mn doping concentration varies from 0.05% to 7% of Mn and decreases for 9%, 11%, 13% of Mn. The PL intensity drops for these higher concentration of Mn i.e. quenching occurs here. From the figure 6, concentration quenching is observed when Mn^{2+} concentration is increased more than 7% where there is a decrease in the intensity of Mn^{2+} for 4T1 - 6A1 transition. Concentration quenching has been mainly attributed to the migration of the excitation energy between Mn^{2+} ions pairs in the case of Mn^{2+} doping. Thus the existence of Mn^{2+} pairs is important for the occurrence of the concentration effect. During the concentration process, the excitation energy is transferred from one Mn^{2+} ion to its nearest Mn^{2+} ion by non-radiative transitions and a via a number of transfer steps, finally to a quenching site [17].

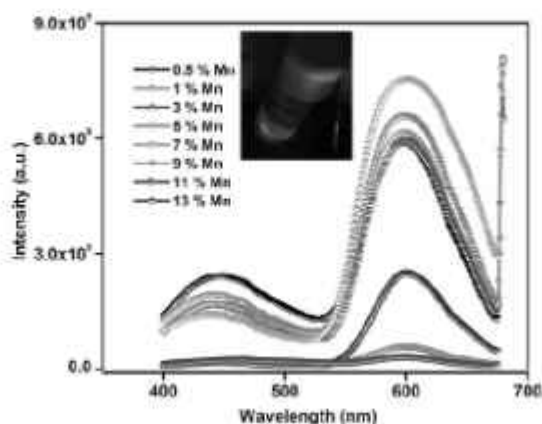


Figure 6: PL emission spectra of Mn doped ZnS nanoparticles

Color characterization

Color characterization of a spectral distribution is done to gauge the quality of its chromaticity. This is accomplished using color coordinates [18]. In 1931, the Commission Internationale de l'Eclairage (CIE) established an international standard for quantifying color known as CIE color coordinates. The chromaticity coordinates map all the visible colors with respect to hue and saturation on a two-dimensional chromaticity diagram. The CIE coordinates are obtained from the three CIE tristimulus values, X, Y and Z. These tristimulus values are computed by integrating the product of the spectrum of the light source, $P(\lambda)$, and standard observer functions called the CIE color matching functions, $x\lambda(\lambda)$, $y\lambda(\lambda)$ and $z\lambda(\lambda)$ over the entire visible spectrum.

Table 2: CIE coordinates of doped and pure ZnS samples

ZnS	CIE	
	X	Y
Pure ZnS	0.1764	0.1674
Mn doped Zns	0.497	0.389

The CIE coordinate of the PL emission of ZnS and Mn doped sample was calculated by above-mentioned method. The CIE coordinate for Mn doped samples is given in the table 2. These coordinates can be represented inside a gamut drawn from the standard x, y values (figure7). This

clearly indicates the purity of the pinky orange color of the Mn doped ZnS while the undoped samples show blue emission.

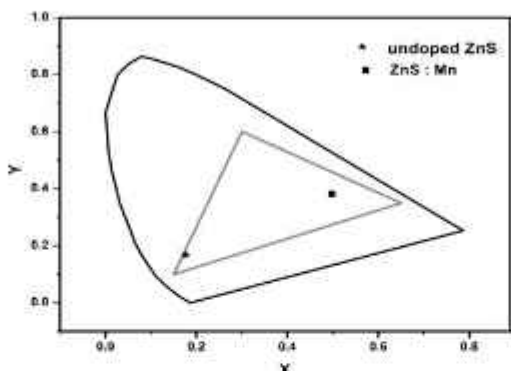


Figure 7:
CIE coordinates of PL emission spectra of pure and doped samples.

Conclusion

ZnS and ZnS:Mn nanoparticles were prepared by wet chemical route using zinc acetate, manganese acetate and sodium sulphide as precursors. The cubic structure of pure ZnS and ZnS:Mn are confirmed by XRD. The Mn has been successfully incorporated into the ZnS host lattice as evident from the increase in lattice constant. The average crystalline size of the ZnS samples to be 3 nm. The manganese doped ZnS shows red shift in the band gap with increase in Mn concentration. The energy corresponding to the absorption ranges from about 3.57 eV to 3.77 eV. The PL spectrum of the pure sample shows an emission in the blue

region at 430nm corresponding to the sulfur vacancy for an excitation wavelength of 325nm. The PL spectra of ZnS:Mn shows a orange emission at 598nm under same excitation. This can be attributed to the radiative transition between Mn 4T1 and 6A1 levels. The CIE color coordinates calculated from the PL spectrum confirms the pinky orange emission of ZnS:Mn nanoparticles

References

- [1] M.B.Rao, K.K.Reddy, Encyclopedia of Nanotechnology vol1, Introduction to Nanotechnology,Campus book International 2 (2005).
- [2] M.Jaros, Physics And Application Of Semiconductor Nanostructures, Clarendon press, Oxford(1989)
- [3] K .Barnham and D.Vvedensky (Eds), Low-Dimensional Semiconductor structures, Cambridge University Press,Cambridge(2001)
- [4] Bang, J., Yang, H. and Holloway, P.H. (2006) 'Enhanced and stable green emission of ZnO nanoparticles by surface segregation of Mg', Nanotech. 17(4): 973–8.
- [5] Yang, P., et al. (2001) 'ZnS nanocrystals co-activated by transition metals and rare-earthmetals – a new class of luminescent materials', J. Lumin. 93(2): 101–5.
- [6] Qu, S.C., et al. (2002) 'Photoluminescence properties of Eu³⁺ doped ZnS nanocrystals prepared in a water/methanol solution', App. Phys. Lett. 80(19): 3605–7.
- [7] Suyver, J.F., et al. (2001) 'Synthesis and photoluminescence of nanocrystalline ZnS : Mn²⁺', Nano Lett. 1(8):429–33.
- [8] Bhargava, R.N., et al. (1994) 'Optical-Properties of

- Manganese-Doped Nanocrystal ZnS', *Phys. Rev. Lett.* 72(3): 416–19.
- [9] Bol, A.A. and Meijerink, A. (1998) 'Long-lived Mn^{2+} emission in nanocrystalline ZnS: Mn^{2+} ', *Phys. Rev. B* 58(24): R15997–6000.
- [10] Su, F.H., et al. (2003) 'Pressure dependence of Mn^{2+} luminescence in differently sized ZnS: Mn nanoparticles', *J. Phys. Chem. B* 107(29): 6991–6.
- [11] M. Sajimol Augustine, P.P. Manzur Ali, K. Sapna, K.K. Elyas, S. Jayalekshmi, Size dependent optical properties of bio-compatible ZnS:Mn nanocrystals and their application in the immobilisation of trypsin, *Spectrochim. Acta ,Part A, Mol. Biomol. Spectrosc* 108 (2013) 223–228. doi:10.1016/j.saa.2013.01.066.
- [12] R. Kripal, A.K. Gupta, S.K. Mishra, R.K. Srivastava, A.C. Pandey, S.G. Prakash; Photoluminescence and photoconductivity of ZnS : Mn^{2+} nanoparticles synthesized via co-precipitation method; *Spectrochim. Acta Part A Mol. Biomol. Spectrosc* 76 (2010) 523–530. doi:10.1016/j.saa.2010.04.018.
- [13] Z. Delghani, S. Nazerdeylami, E. Saievar-Iranizad, M.H. Majles Ara, Synthesis and investigation of nonlinear optical properties of semiconductor ZnS nanoparticles, *J. Phys. Chem. Solids.* 72 (2011)

1008–1010. doi:10.1016/j.jpccs.2011.05.005.

- [14] Chen, Jianfeng; Li, Yaling; Wang, Yuhong; Yum, Jimmy; Cao, Depeng, *Mater. Res. Bulletin*, 2004, 39, 185.
- [15] Thambidurai, M.; Muthukumarasamy, N; Agilan, S.; Murugan, N.; Vasantha, S.; Balasundaraprabhu, R.; Senthil, T.S., *J. Mater. Sci.*, 2010, 45, 3254.
- [16] Martinez- Castanon, G.A.; Sanchez- Lorendo, M.G.; Martinez-Mendoza, J.R.; Facundo Ruiz, *Advances in Tech. Mat. and Mat. Processing*, 2005, 7(2), 171
- [17] Elham, Mohaghehpour; Mohammad, Rabiee; Fathollah ,Moztarzadeh; Mohammardreza, Tahriri, *Journal of Ceramic Processing Research*, 2010, 11(2), 144
- [18] G. Wyszecki and W. S. Stiles, *Color Science: concepts and methods, quantitative data and formulae*, Second edition, p.131, John Wiley & Sons Inc., New York (1982). 52

DEGREE POLYNOMIAL OF A GRAPH

■ Annie Sabitha Paul

Assistant Professor, Department of Mathematics,
Govt. College of Engineering, Kannur.
Email:anniesabithapaul@gmail.com

Abstract

In this paper k -nodal set of a graph G for $\delta(G) \leq k \leq \Delta(G)$, is defined. Also Degree Polynomial of a graph is introduced. Some properties of this polynomial are observed and degree polynomial of some specific graphs is computed.

INTRODUCTION

Graphs $G = (V(G), E(G))$ discussed in this paper are finite, simple and undirected. Any undefined term in this paper may be found in [1,7]. The degree [1] of a vertex v in graph G is denoted by $d(v)$, which is the number of edges incident with v . The maximum and minimum degrees of G are denoted respectively by $\Delta(G)$ and $\delta(G)$. An empty graph [1] is a graph with no edges. An isolated vertex [7] is one whose degree is zero. A vertex in a graph is called a pendant vertex [10] if its degree is one. Any vertex adjacent to a pendant

vertex is called a support vertex. A simple graph in which each pair of distinct vertices is joined by an edge is called a complete graph [1]. A complete graph on n vertices is denoted by K_n . A bipartite graph G is one whose vertex set can be partitioned into two subsets X and Y so that each edge has its ends in X and Y respectively. Such a partition (X, Y) is called a bipartition of G . A complete bipartite graph [1] is a simple bipartite graph with bipartition (X, Y) in which every vertex of X is joined to every vertex of Y . The complete bipartite graph with $|X| = m$ and $|Y| = n$ is denoted by $K_{m,n}$. The graph H is said to be an induced subgraph [2] of the graph G if $V(H) \subseteq V(G)$ and two vertices in H are adjacent if and only if they are adjacent in G . If two vertices u and v are connected in G , the length of the shortest u - v path in G is called the distance [1] between u and v and is denoted by $d(u, v)$. The diameter [1] of G is the maximum distance between two vertices of G and is denoted by $\text{diam}(G)$. A tree [1] is a connected acyclic graph. A cut edge [1] of a graph G is an edge such that whose removal makes the graph disconnected. The corona [6] of two graphs G_1 and G_2 is the graph $G = G_1 \circ G_2$ formed from one copy of G_1 and $|V(G_1)|$ copies of G_2 , where the i^{th} vertex of G_1 is adjacent to every vertex in the i^{th} copy of G_2 . There are several polynomials associated with a graph G . Polynomials play an important role in the study of graphs as

it encode various information about a graph, such as the number of trees, number of cliques, cycles etc., in G . Also some graph polynomials count the number of occurrences of certain graph features and some others make an attempt to find complete graph invariants and so on. In this paper degree polynomial of a graph is defined and some of its properties are observed.

2. DEGREE POLYNOMIAL

In this section we first define k -nodal set, $\delta(G) \leq k \leq \Delta(G)$ of a graph and then introduce degree polynomial of a graph. Also some properties of degree polynomials are observed.

Definition 2.1. Let $G(V, E)$ be any graph of order n . For $\delta(G) \leq k \leq \Delta(G)$, the k -nodal set of a graph G is defined as the set of all vertices of degree k in G . It is denoted by $V(G, k)$.

ie., $V(G, k) = \{u \in V : d(u) = k\}$

Some Simple observations of degree polynomials are;

- (1) $V(G, 0)$ is the set of all isolated vertices in G .
- (2) $V(G, 1)$ is the set of all pendant vertices in G .
- (3) For any graph G of order n , $0 \leq |V(G, k)| \leq n-1$, where $\delta(G) \leq k \leq \Delta(G)$.
- (4) For a nontrivial cycle C_n , $|V(C_n, k)| = n$ if $k = 2$
0 if $k \neq 2$
- (5) For a complete graph K_n , $|V(K_n, k)| = n$ if $k = n-1$
1 if $k \neq n-1$
- (6) For a path P_n , $|V(P_n, k)| = n-2$ if $k = 2$
2 if $k = 1$
0 if $k \neq 1$ or 2

Definition 2.2. Let G be any graph of order n . The Degree Polynomial of G is denoted by $D[G, x]$ and is defined as, $D[G, x] = \sum_{k=0}^{n(G)} |V(G, k)| x^k$ where $|V(G, k)|$ is the cardinality of k -nodal set of G .

Observation 2.3.

- (1) For any graph G of order n , if $V(G, 0) \neq \emptyset$ then $V(G, n-1) = \emptyset$ and viceversa.
- (2) If G_1 and G_2 are isomorphic graphs, then $D[G_1, x] = D[G_2, x]$.
- (3) If H is an induced subgraph of G , then $\deg(D[G, x]) \geq \deg(D[H, x])$
- (4) The constant term in $D[G, x]$ is the number of isolated vertices in G .
- (5) If a graph G has no isolated vertices, then zero is a root of its degree polynomial.

Theorem 2.4. Let G be a nontrivial graph of order n . Then $D[G, x]$ is a constant polynomial if and only if G is an empty graph.

Proof.

Let $D[G, x]$ is a constant polynomial. Then, $D[G, x] = \sum_{k=0}^{n(G)} |V(G, k)| x^k = C$, a constant. Hence $|V(G, k)| = 0$ for $0 \leq k \leq n-1$. Therefore, $d(v) = 0$ for all v in $V(G)$. Converse is obvious.

Theorem 2.5. Let G be any graph of order n . Then $\deg(D[G, x])$ is maximum if and only if G has a vertex of degree $n-1$.

Proof. The maximum possible degree of $D[G, x]$ of any graph G of order n is $n-1$. Hence $\deg(D[G, x])$ of G is $n-1$ if

and only if $\Delta(G) = n-1$ Since the maximum degree of a complete graph, Wheel graph, star graph etc, on n vertices is $n-1$, Corollary 2.6 follows.

Corollary 2.6. $\deg(D[K_n, x]) = n-1, \deg(D[W_n, x]) = n-1, \deg(D[S_n, x]) = n-1$, where K_n , W_n , and S_n are complete graph, Wheel graph, and star graph on n vertices.

Remark 2.7. For any graph G , $\deg(D[G, x])$ is maximum if and only if $\Delta(G) = n-1$ and $\deg(D[G, x])$ is minimum if and only if $= C$, a constant. Hence $|V(G, k)| = 0$ for $0 \leq k \leq n-1$. Therefore, $d(v) = 0$ for all v in $V(G)$. Converse is obvious.

Theorem 2.5. Let G be any graph of order n . Then $\deg(D[G, x])$ is maximum if and only if G has a vertex of degree $n-1$.

Proof. The maximum possible degree of $D[G, x]$ of any graph G of order n is $n-1$. Hence $\deg(D[G, x])$ of G is $n-1$ if and only if $\Delta(G) = n-1$ Since the maximum degree of a complete graph, Wheel graph, star graph etc, on n vertices is $n-1$, Corollary 2.6 follows.

Corollary 2.6. $\deg(D[K_n, x]) = n-1, \deg(D[W_n, x]) = n-1, \deg(D[S_n, x]) = n-1$, where K_n , W_n , and S_n are complete graph, Wheel graph, and star graph on n vertices.

Remark 2.7. For any graph G , $\deg(D[G, x])$ is maximum if and only if $\Delta(G) = n-1$ and $\deg(D[G, x])$ is minimum if and only if $\Delta(G) = 0$.

Theorem 2.8. The degree polynomial $D[G, x]$ of any graph G of order n contains at most $n-1$ terms.

Proof. The general expression for the degree polynomial $D[G, x]$ of any graph G is $D[G, x] = \sum_{d \in \{0\}} |P(G, k)| x^d$. When $\Delta(G) = n-1$, $\delta(G) \neq 0$ and when $\delta(G) = 0$, $\Delta(G) \neq n-1$. Therefore, $D[G, x]$ of G can have at most $n-1$ terms.

Theorem 2.9. For a graph G , the degree polynomial $D[G, x]$ is an even polynomial if and only if G is Eulerian.

Proof. Since $D[G, x] = \sum_{k=0}^{n(G)} |P(G, k)| x^k$, $D[G, x]$ is an even polynomial if and only if

$|V(G, k)| = 0$ for all odd powers of k . That is if and only if cardinality of all k -nodal sets is zero for all odd values of k . i.e., if and only if G has no odd degree vertices. i.e., if and only if G is Eulerian.

Theorem 2.10. For any cycle C_n , $D[C_n, x] = D[L(C_n), x]$ where $n \geq 3$

Proof. It is proved first that $L(C_n)$ is isomorphic to C_n . Then it follows that, $D[C_n, x] = D[L(C_n), x]$. Any cycle C_n has n vertices and n edges. Hence $L(C_n)$ has order n . Every edge in G is adjacent to exactly two edges in G . Therefore, every vertex in $L(C_n)$ has degree two. Hence both C_n and $L(C_n)$ same order, same size and same degree sequence. Hence the proof.

Theorem 2.11. A graph G is k -connected for $k \geq 2$ if and only if the lowest exponent of x in $D[G, x]$ is k .

Proof. Suppose that G is k -connected, i.e., if and only if $\delta(G)$ is k . Hence the proof.

Remark 2.12. Theorem 2.11 need not be true when $k = 1$. Suppose that $V(G, 1) \neq 0$. Then G has at least one pendant vertex, whose removal does not disconnect G .

3. DEGREE POLYNOMIAL OF SOME GRAPHS

In this section the degree polynomials of some graphs are computed. The polynomial expression is obtained using the definition.

Proposition 3.1. For any complete graph K_n , $D[K_n, x] = nx^{n-1}$, $n = 1, 2, 3, \dots$

Proposition 3.2. For any cycle C_n , $D[C_n, x] = nx^2$, $n \geq 3$

Proposition 3.3. For any path P_n , $D[P_n, x] = (n-2)x^2 + 2x$, $n \geq 2$

Proposition 3.3. For a Wheel graph $W_n = C_{n-1} + K_1$, $D[W_n, x] = x^{n-1} + (n-1)x^2$, $n \geq 4$

Definition 3.4 [5]. A Helm graph H_n , $n > 3$ is obtained from a wheel graph W_n by attaching a pendant edge at each vertex on the rim of the wheel W_n .

Proposition 3.5. For a Helm graph, $D[H_n, x] = x^{n+1} + (n-1)x^4 + (n-1)x$

Definition 3.6 [5]. A closed helm graph CH_n , $n > 3$ is obtained by taking a helm graph H_n and adding edges

between the pendant vertices.

Proposition 3.7. For a closed helm graph, $D[CH_n, x] = x^{n-1} + (n-1)x^4 + (n-1)x^1$

Definition 3.8 [5]. A Lollipop graph $L_{n,m}$, is obtained by joining $K_n, n \geq 3$ to a path P_m on m vertices with a bridge.

Proposition 3.9. For $D[L_{n,m}, x] = x^n + (n-1)x^{n-1} + (m-1)x^2 + x$

Definition 3.10 [5]. A Windmill graph $W_n^{(m)}$, is the graph obtained by taking m copies of the complete graph $K_n, n \geq 3$ with a common vertex. $W_n^{(3)}$ is called the friendship graph and is denoted by F_n

Proposition 3.11. For $D[W_n^{(m)}, x] = x^{m(n-1)} + m(n-1)x^{n-1}$

Corollary 3.12 $D[F_n, x] = x^{3(n-1)} + 3(n-1)x^{n-1}$

Definition 3.13 [3]. A Shell graph S_n is defined as the graph obtained from the cycle C_n by adding the edges corresponding to the $n-3$ concurrent chords of the cycle. The vertex at which all chords are concurrent is called the apex of the shell

Proposition 3.14 $D[S_n, x] = x^{n(n-1)} + (n-3)x^2$

Definition 3.15 [8]. A bow graph is a double shell with same apex in which each shell has any order.

Corollary 3.16. Let B_N be a bow graph of order $N \geq 5$, which includes shells S_n and S_m such that $N = m + n - 1$ then $D[B_N, x] = x^{m(n-2)} + (n+m-6)x^3$

Definition 3.17 [11]. A butterfly graph BF is a bow graph

with exactly two pendant edges at the apex.

Corollary 3.18. Let BF be a butterfly graph of order $N \geq 7$, then

$$D[BF, x] = x^{m+n} + (n+m-6)x^3 + 2x$$

Proposition 3.14. For a complete bipartite graph $K_{m,n}$,

$$D[K_{m,n}, x] = mx^n + nx^m$$

4. DEGREE POLYNOMIAL OF SOME GRAPH OPERATIONS

In this section the degree polynomial of some graph operations and graph modifications are obtained.

Since the disjoint union of two graphs will not affect the degree of any vertex in the union of the graphs, we have:

Theorem 4.1. Let G and H be any two graphs of order n and m respectively and let $G \cup H$ be the disjoint union of G and H . Then $D[G \cup H, x] = D[G, x] + D[H, x]$

Corollary 4.2. If a graph G has n components G_1, G_2, \dots, G_n , then $D[G, x] = D[G_1, x] + D[G_2, x] + \dots + D[G_n, x]$

Definition 4.3 [7]. The join of two graphs G_1 and G_2 , denoted by $G_1 \vee G_2$, is a graph with vertex set $V(G_1) \cup V(G_2)$ and edge set $E(G_1) \cup E(G_2) \cup \{uv | u \in V(G_1) \text{ and } v \in V(G_2)\}$.

Theorem 4.4 For any graph G of order n , $D[G \vee K_1, x] = x^n + xD[G, x]$

Proof. Since in $G \vee K_1$, the degree of each vertex in G is

increased by one and a new vertex of degree n is introduced, the result follows.

Theorem 4.5. Let G and H be any two graphs of order n and m respectively. Then

$$D[G \vee H, x] = x^m D[G, x] + x^n D[H, x]$$

Proof. Since in $G \vee H$ the degree of each vertex in G is increased by cardinality of H and the degree of each vertex in H is increased by cardinality of G , The result follows.

Let G be any graph with vertex set $\{v_1, \dots, v_n\}$. Add n new vertices $\{u_1, \dots, u_n\}$ and join u_i to v_i for $1 \leq i \leq n$. By the definition of the corona of two graphs, we shall denote this graph by $G \circ K_1$.

Theorem 4.6. If G is any graph of order n , then $D[G \circ K_1, x] = xD[G, x] + nx$

Proof. In the corona $G \circ K_1$, the degree of each vertex in G is increased by one and n vertices of degree one are introduced.

REFERENCE

- [1] Bondy J. A, Murty U.S.R, Graph Theory with Applications; Mac millan, 1978.
- [2] G. Chartrand, P. Zhang, Chromatic Graph Theory; CRC Press, USA, 2009
- [3] E.J. Cockayne, S.T. Hedetniemi, K.J. Miller, Properties of hereditary hypergraphs and middle graphs, *Canad. Math. Bull.* 21, 1978, pp.461-468
- [4] P.K. Deb, N.B. Limaye, On harmonious labelling of some cycle related graphs, *ArsCombinatorica* 65 (2002), 177– 197.
- [5] J. A. Gallian, A dynamic survey of graph labelling, *The Electronic journal of Combinatorics*, DS6. 2018
- [6] C.E Go, S.R Canoy Jr, Domination in the corona and join of Graphs; *International Mathematical Forum*, 6 (2011), 763-771.
- [7] F. Harary Graph theory ;Addison Wesley (1969)

SUPERCAPACITOR APPLICATION OF ELECTROSPUN PVA – PANI COMPOSITE NANOFIBER ELECTRODES

■ Dr. Sindhu S¹, Akhil P²

¹Department of Nanoscience and Technology, University of Calicut.
sindhu.swaminath@gmail.com

²Department of Physics, Govt. Arts & Science College, Calicut
akhbh1995@gmail.com

Abstract

Nanomaterials are widely explored area as they offer better properties than their bulk counterparts. Nanofibers are one such class which have high surface to volume ratio, mechanical strength, flexibility, thermal properties used for applications like filtration, nanocatalysis, medicine delivery, and as electrode material for energy storage devices. In this study we produce polymer solutions of polyvinyl alcohol (PVA) and polyvinyl alcohol-polyaniline (PVA-PANI) combined solutions and used for electrospinning. The PVA- PANI polymer nanofibers were tested for application as solid electrode material for supercapacitor. From this PVA-PANI polymer solution was prepared for different volume ratios and electrospun onto conducting PET substrates. Two of such PET substrates were taken and a piece of gel electrolyte was sandwiched between them which acted as an electrochemical pseudocapacitor. Also PET substrates were electrodeposited by PANI and a gel electrolyte was sandwiched between two of such substrates as before. Cyclic voltametry analysis gives the specific capacitance value of these capacitors. FTIR analysis of the fibers

confirmed presence of PVA and PANI. SEM images confirmed the formation of nanofibers and their diameter was found.

1. Introduction

Energy production is a greatest concern of mankind. Fossil fuels are a good source of energy but their increasing pollution effects force us to switch to renewable energy resources. So the electrical energy storage devices like Electrochemical cell and Supercapacitors plays a significant role. Batteries and capacitors seem similar as they both store and release electrical energy but their potential applications are different. An approach to utilize the benefits of both capacitor and batteries and fabricating into a single device is of present research interest. Such a device with much higher energy density comparable to batteries and with larger discharge time and power density is called a Supercapacitor. Ordinary capacitor uses solid dielectric whereas supercapacitors uses ElectricDouble Layer Capacitance (EDLC), Electrochemical Pseudocapacitance and a combination of these two is called hybrid capacitors [1-5].

In this study we look forward to improve the surface area of the electrode material by using nanostructured materials. We make PVA/PANI composite nanofibers by Electrospinning technique. The network porosity of the nanofibers can act as excellent surface for charge

accumulation. Thus the large surface area to volume ratio of nanofibers makes them promising material for supercapacitor electrodes.

2. Experimental

2.1 Materials and chemicals

The chemicals used for this work are Poly vinyl alcohol (PVA, MW = 89,000- 98000, 99+% hydrolyzed), Poly aniline (Emeraldine salt average MW > 15000, particle size= 3-100 μm) purchased from Sigma Aldrich, Dimethyl sulfoxide (DMSO), Aniline ($\text{C}_6\text{H}_5\text{NH}_2$), sulfuric acid (H_2SO_4), double distilled water and ITO (Indium doped tin oxide) coated PET (polyethylene terephthalate) substrates.

2.2 Preparation of PVA solution

9wt% solution of PVA was prepared by adding 4.5069 g of PVA to 50 ml distilled water. The above solution is heated to 80°C with constant stirring for 45 minutes till the solute is completely soluble and forms a clear viscous solution. The above viscous solution is used to make PVA nanofibers using electrospinning technique.

2.3 Production of PVA nanofibers using E-spin technique

The solution for E- spinning is taken in a 5 ml syringe and the collector drum is covered with a sheet of aluminium foil. The parameters like volume, flow rate, voltage are set in the E- spin unit. The constant parameters are Volume = 2 ml, flow rate = 0.1 μ l/s, voltage = 25 KV and time = 4 hours. The tip to collector distance was set to 15 cm. The collector drum was kept rotating at 650 rpm. Electrospinning was performed with horizontal scanning(y scan) for forming random fibers and to induce porosity in the network and without y- scan for aligned fibers.

2.4 Preparation of PVA-PANI solution at different volume ratios.

2 wt% solution of PANI (polyaniline-emeraldine salt) was prepared by adding 0.022g PANI to 1ml DMSO(dimethyl sulfoxide) and with constant stirring for 5 minutes. This PANI solution and the above prepared PVA solution were combined in different volume ratios to vary concentration. These solutions were taken for E-spinning.

PVA : PANI = 2ml : 20 μ l, 2ml : 50 μ l, 2ml : 100 μ l

2 ml of the above PVA solution (9 wt%) is taken separately in three beakers. To each of these beakers add 20 μ l, 50 μ l

and 100 μl of PANI solution (2 wt%) using micropipette. The resultant solution is stirred for 5 minutes.

2.5 Production of PVA-PANI composite nanofibers for different volume ratios.

The PVA-PANI solutions of different volume ratios were separately electrospun onto different pieces of conducting PET substrates attached on the rotating collector drum. The electrospinning parameters like volume = 1 ml, flow rate = 0.1 $\mu\text{l/s}$, voltage = 25 KV, drum rotation speed = 650 rpm were applied and E-spun for 1 hour. The three samples of composite PVA-PANI fibers were named as PP20, PP50 and Pp100.

2.6 Electrodeposition of PANI onto PET substrates

For electrodeposition, 0.06 M solution of Aniline with 0.2 M sulfuric acid was prepared in a standard flask taken as electrolyte. The electropolymerization were conducted by a three electrode set up. The FTO coated conducting PET substrate taken as the working electrode, Platinum wire as counter electrode and Ag/AgCl in saturated NaCl as reference electrode. There are several methods for electropolymerization. Here we use potentiostatic method of electropolymerization by applying a constant potential of 0.75 volts. Aniline is polymerised to Polyaniline and is electrodeposited for 15 minutes on PET substrate gives green colour coating as shown in figure 1, a& b

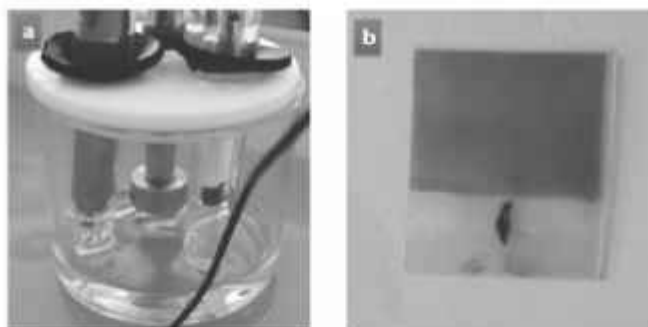


Figure 1

- (a) The electrodeposition of PANI on conducting PET substrate in three electrode system
 (b) The green colour coated PANI film on PET substrate.

3. Results & Discussion

3.1 Scanning electron microscopy analysis

Figure 2(a) shows the SEM images of PVA nanofibers produced at a tip collector distance of 15 cm. The polymer nanofibers have diameters 377.2 nm, 355.7 nm and 417.4 nm. The average diameter of the fibers is ~360 nm. The images show good network porosity and random arrangement of fibers. Figure 2(b) shows the SEM images of PVA – PANI nanofiber composite formed at the same conditions of E – spinning as that of PVA. The diameters of the fibers are 151.3 nm, 166.1 nm and 137.2 nm. The diameters of the composite fibers are lesser than pure PVA fibers. It is because addition of PANI to PVA polymer solution lowers the viscosity and hence diameter of fibers is decreased. Also the SEM images indicate the presence of agglomerated PANI particles in the fiber network.

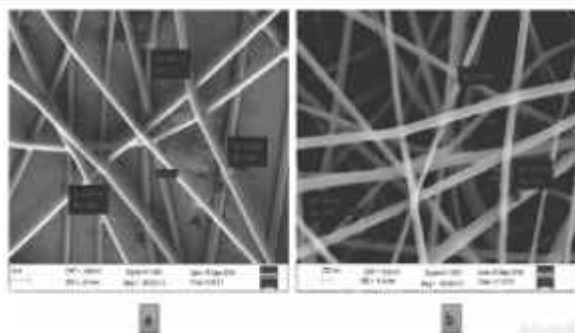


Figure 2 (a) The SEM image of PVA fiber
(b) The SEM image of PVA-PANI composite fiber

3.2 Fourier transform infrared spectroscopy analysis

Figure 3(a) and 3(b) shows the FTIR spectrum of pure samples of PVA and PANI (emeraldine salt) and their characteristic peak positions in the interferogram is marked.

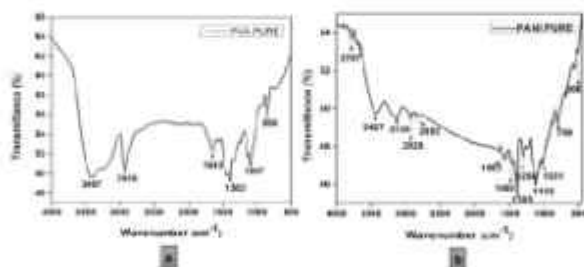


Figure 3

(a) FTIR spectrum of pure PVA (b) FTIR spectrum of pure PANI

Figure 4 shows the FTIR spectra of PVA fiber, electrodeposited PANI (EP), PP20, PP50 and PP100 (composite nanofibers) samples and their peaks are compared with that of figure 3.

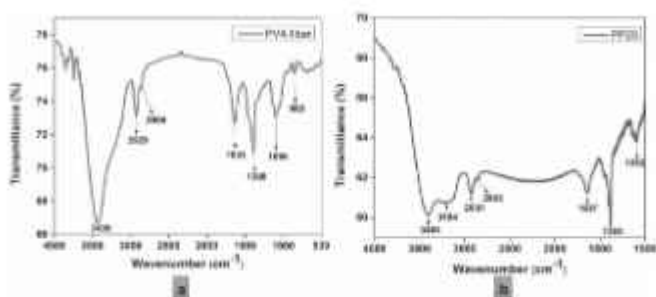


Figure 4 (a) FTIR spectrum of PVA nanofiber
 (b) FTIR spectrum of composite nanofiber ,
 PVA:PANI = 2ml:20µl.

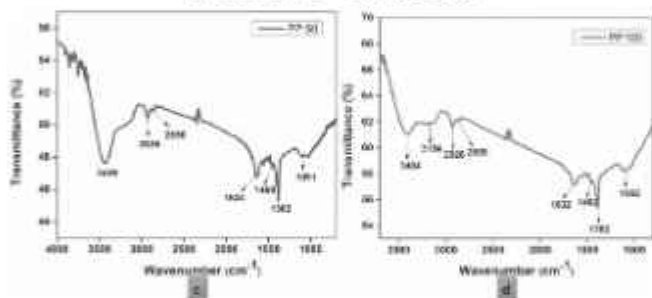


Figure 4 (c) FTIR spectrum of composite fiber,
 PVA:PANI = 2ml:50µl (d)) FTIR spectrum of
 composite fiber, PVA:PANI = 2ml:100µl

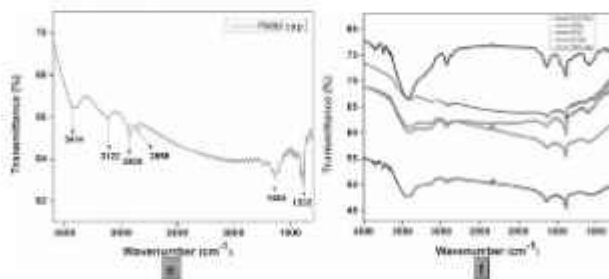


Figure 4 (e) FTIR spectrum of electrodeposited PANI
 (f) FTIR spectrum of PVA fiber, PP20, PP50, PP100 and EP.

In PVA fiber, the intense peak at 3436 cm^{-1} corresponds to O-H stretching vibrations of hydroxyl group in PVA. The peaks at 2929 cm^{-1} and 2855 cm^{-1} are due to C-H asymmetric and symmetric stretching vibrations respectively. The peak at 1635 cm^{-1} correspond to C-C group and can be explained on basis of intra or inter molecular hydrogen bonding with adjacent O-H group in PVA. The peak at 1388 cm^{-1} is due to C-H vibration and that at 1094 cm^{-1} is due to C-O stretching vibration. Characteristic peak at 853 cm^{-1} is from CH_2 stretching. [7,8] In the electrodeposited PANI sample peak positioned at 3414 cm^{-1} and characteristic peak at 3122 cm^{-1} are due to O-H stretching vibrations from solvent of electrodeposition and N-H asymmetric stretching in PANI. The 2928 cm^{-1} peak is due to stretching of aromatic C-H group and a less intense peak at 2856 cm^{-1} is formed by other C-H vibrations. Also aromatic C-C stretching give rise to 1636 cm^{-1} peak. The peak at 1383 cm^{-1} is characteristic of C-H vibrations.

Considering the FTIR spectra of composite nanofibers we see in three of the samples PP20, PP50 and PP100, a peak around 3406 cm^{-1} which is due to the O-H stretching vibrations. A peak at 3194 cm^{-1} in PP20, and around ~ 3154 for both PP50 and PP100 is due to N-H stretching vibrations of PANI. It is seen that this peak broadens as the concentration of PANI in fibers increases. In pure PVA fiber a more intense peak due to C-H asymmetric stretching is found at 2927 cm^{-1} . This peak diminishes in intensity almost equally for all the composite fibers containing PANI, and found around $\sim 2930\text{ cm}^{-1}$. This is due to

stretching of aromatic C-H group in PANI that forms a less intense peak at the same position. A peak positioned around 1635 cm^{-1} in PVA fiber correspond to C-C group and also due to inter or intra molecular hydrogen bonding with adjacent O-H groups in PVA. In the three composite samples a peak positioned around ~ 1634 has less intensity than in pure PVA fiber. This is due to aromatic C-C stretching in PANI. There is no intensity variation for C-H symmetric vibrations peak of PVA fiber at 2855 cm^{-1} comparing with composite fibres. A peak around $\sim 1461\text{ cm}^{-1}$ due to C=N stretching in aromatic compounds and absorption by benzene ring is seen in PP20, PP50 and PP100 fibers. A fairly more intense peak at 1388 cm^{-1} for PVA fiber and $\sim 1382\text{ cm}^{-1}$ for composite fibers comes from C-H vibrations. The characteristic peak of PVA fiber at 1094 is attributed to presence of terminal polyvinyl groups. This peak broadens as concentration of PANI increases. Thus FTIR spectral studies suggest that PVA is incorporated in PVA fiber, PANI is electrodeposited on the PET substrate and presence of both PVA and PANI are detected in PP20, PP50 and PP100 samples. The incorporation of PANI in the PVA fiber is established by the intensity variation in peaks of pure PVA fiber as well as composite fibers.

3.3 Cyclic Voltammetry (CV) Analysis

The PVA-PANI composite nanofibers electrospun onto pieces of PET substrates, PANI electrodeposited on PET substrates are taken as electrode material for

supercapacitor application. The nanofiber electrode formed with 20 μ l, 50 μ l and 100 μ l of PANI are named PP20, PP50 and PP100 respectively and that of deposited PANI as EP. Two of such electrodes of EP, PP20, PP50, PP100 are separately taken and a polymer gel electrolyte of thickness = 1.858 mm is sandwiched in between them and sealed to form a supercapacitor prototype. The thickness of EP, PP20, PP50 and PP100 were measured using MITUTOYO VL 50 Profilometer and found to be 2.63 μ m, 1.13 μ m, 3.96 μ m and 4.34 μ m respectively[9]

Cyclic voltammetry studies of the supercapacitor prototypes were done with a potential window of 1V (-0.5V to 0.5 V) at different scan rates of 20mV/s , 50mV/s, 100mV/s, 500mV/s and 1000 mV/s.[figure 5]

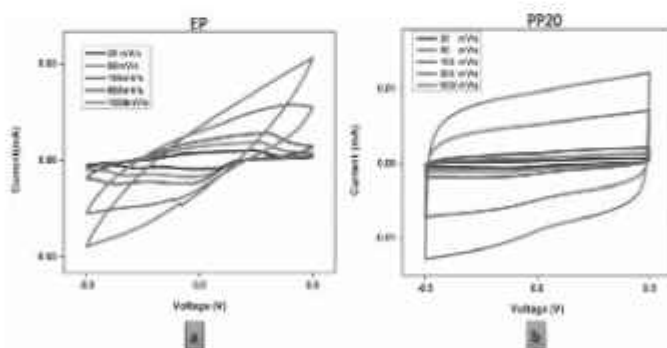


Figure 5

(a) I-V characteristics of electrodeposited PANI (EP) at different scan rates (b) I-V characteristics of PP20 at different scan rates.

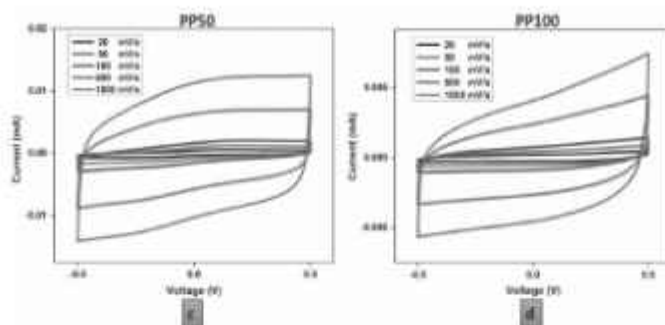


Figure 5 (c) I-V characteristics of PP50 at different scan rates. (d) I-V characteristics of PP100 at different scan rates.

The shape of CV plots suggests a good pseudocapacitance behaviour for PP20, PP50 and PP100 samples and they can be excellent for use as supercapacitor electrode material. The nanofiber electrode show stability on repeated scanning.

Figure 6 shows the I-V characteristics of all the sample electrodes at scan rate of 20 mV/s. The area under the C-V curve for EP, PP20, PP50 and PP100 were found and the specific capacitance of each electrode in two- electrode system is calculated using the equation

$$C_{sp} = 4C/S$$

where $C = (\int I(V)dV) / 2(dV/dt) V$, $\int I(V)dV$ is the area enclosed by the CV curve. dV/dt is the scan rate and V is the potential window. S is the mass (g) and specific capacitance obtained is called Gravimetric capacitance (F/g).

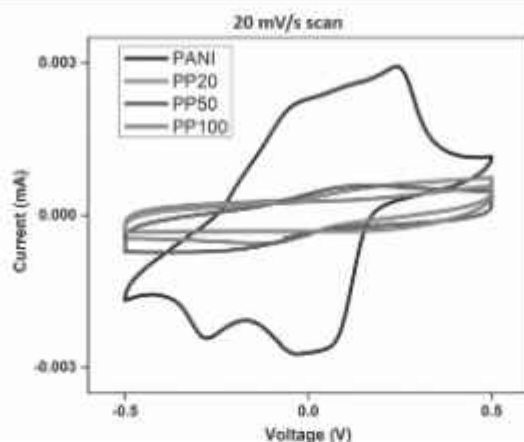


Figure 6:
The I-V characteristics of all samples at a scan rate of 20 mV/s.

For a scan rate of 20 mV/s, the area under the I-V graphs for EP, PP20, PP50 and PP100 are 0.003 cm^2 , $7.1913 \times 10^{-4} \text{ cm}^2$, $7.503 \times 10^{-4} \text{ cm}^2$ and $5.462 \times 10^{-4} \text{ cm}^2$ respectively. The mass of EP electrode is 0.0016 g and mass of nanofiber electrodes is 0.000366 g.

We observed that the super capacitance is well enhanced when For a scan rate of 20 mV/s, the area under the I-V graphs for EP, PP20, PP50 and PP100 are 0.003 cm^2 , $7.1913 \times 10^{-4} \text{ cm}^2$, $7.503 \times 10^{-4} \text{ cm}^2$ and $5.462 \times 10^{-4} \text{ cm}^2$ respectively. The mass of EP electrode is 0.0016 g and mass of nanofiber electrodes is 0.000366 g.

We observed that the supercapacitance is well enhanced when nanofiber electrodes are used. The PP20 electrode shows a comparable supercapacitance as with EP electrode. When a nanofiber electrode is used, even with reduced doping level of PANI, a specific capacitance as comparable with EP is obtained. Also we find as the concentration of PANI in nanofibers increases the supercapacitance first

increases and then decreases. This can be explained by examining the SEM images of PP50 nanofiber shown in figure 7

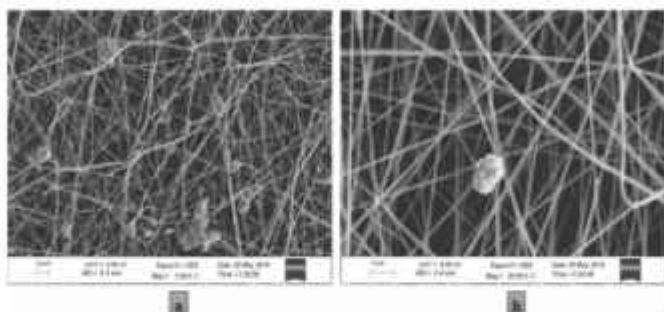


Figure 7

(a) The SEM image of PP50 fiber with agglomerations of PANI (b) Magnified image of (a)

Figure 8 shows the photographs of polymer solution used for electrospinning of composite fibers. The agglomerations of PANI can be also seen in solution as black dots.

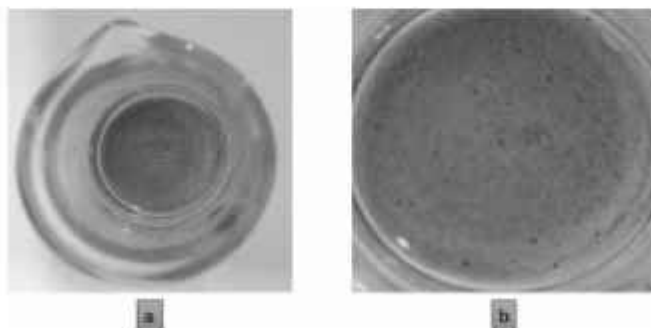


Figure 8 (a) The solution used for E-spinning PP100 fibers (b) The agglomeration of PANI seen as black dots in solution.

The addition of PANI (emeraldine salt) into PVA solution creates an agglomeration of PANI in fiber. We confirm that PANI has not completely dispersed in PVA solution. These agglomerations appear in the nanofibers also. As SEM images indicate an increase in concentration can increase the number of agglomerated structures in the nanofiber and thus reducing the surface area of the electrode. This is the reason for decrease in supercapacitance as concentration of PANI increases.

To eliminate the agglomerations in fibers we can use a method by which PANI completely disperses in PVA matrix and we expect an increase in supercapacitance as concentration increases.

3.4 Electrochemical Impedance Spectroscopy Analysis (EIS)

The EIS analysis was done using electrochemical workstation. In this measurement the voltage amplitude range is low and in the range 5 -10 mV and with wide frequency range 0.01 Hz – 100 KHz .The effective impedance of the supercapacitor prototypes were found from the graph shown below (figure 9). It was found that the impedance for supercapacitor with nanofiber electrode was very less compared to electrodeposited PANI electrode. [7]

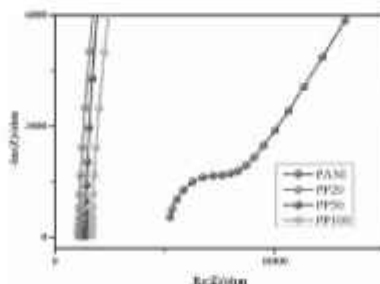


Figure 9: EIS spectra of PP20, PP50, PP100 and EP prototypes

The sheet resistance for the PP20, PP50 and PP100 fiber prototypes is around 950 ohms and that for EP (electrodeposited PANI) prototype is 5222 ohms. The charge transfer resistance of EP is around 3096 ohms and that of PP20, PP50 and PP100 is seen to be very small.

CONCLUSION

The PVA, PVA-PANI composite nanofibers were formed by electrospinning. The composite fibers electrospun onto conducting PET substrates and electrodeposited PANI on PET substrates are taken as supercapacitor electrode material. The supercapacitance is enhanced using composite nanofiber electrodes due to higher surface area as compared to electrodeposited PANI electrode. The specific capacitance of nanofiber electrode increases as doping level of PANI increases and then decreases, because higher concentration of PANI leads to more number of agglomerated structures in fibers reducing the surface area of electrode.

REFERENCES:

1. Huanhuan Wang, Jianyi Lin, Ze Xiang Shen –“Polyaniline (PANI) based electrode materials for energy storage and conversion”-*Journal of science: Advanced materials and devices* 1(2016) 225-255.
2. K Vinotha, V.Senthilkumar, S.Muruganand, K. Sriram-“Fabrication of electrospun PVA-KCL nanofibers as EDLC and electrochemical analysis for application as solid polymer electrolyte”-*IJPAM-Vol 119 n0:15(2018)*, 1145-1153.
3. Chaim-Wen Liew, S .Ramesh ,A.K.Arof –“Good prospect of ionic liquid based -polyvinyl alcohol polymer electrolytes for supercapacitors with excellent electrical, electrochemical and thermal properties”- *Int. J. Hydrog. Energy* (2013)
4. Sudeshnachaudari, Yogeshsharma “Electrospun polyaniline nanofibers web electrodes for supercapacitors” –*J. Appl. Polym. Sci* (2012)
5. Principles of Instrumental analysis- Skoog, Holler ,Crouch.
6. Hop tranthi than, Phuoacanh le, Mai dang thi, Tuan le quang and Tung ngotrinh-“Effect of gel polymer electrolyte based on polyvinyl alcohol/ poly

- ethylene oxide blend and sodium salts on the performance of solid state supercapacitor”-Bull Mater. Sci.(2018)41-145
7. IshaGawri, Swati Katta,K.P Singh and S.K Tripathi-“Synthesis and characterization of polyaniline as emeraldine salt”- AIP conference proceedings 1728,020287(2016).
 8. B Kavitha , K. Prabhakar, K. Sivakumar-“Spectroscopic studies of nano size crystalline conducting polyaniline”- IOSRJAC Vol 2 issue:1 (2012) 16-19.
 9. SharonaA.Melchoir, Kumar Raju, Innocent S .Ike-“High voltage symmetric supercapacitor based on 2D titanium carbide/ carbon nanosphere composites in a neutral aqueous electrolyte.”- ECS. J, 165(3)A501-A511 (2018).

ON STRENGTH OF FUZZY GRAPHS

Reshmi K M

Department of Mathematics

Govt.Engineering College, Kozhikode-673010

reshmikm@gmail.com

Abstract

Fuzzy Graphs has generated interest in many researchers in mathematics as well as engineers. It is a fast growing field with applications in many fields of engineering and technology. In this paper some basic definitions and terminologies of fuzzy graphs are studied.

Keywords: Fuzzy graphs, weight matrix, strength of a fuzzy graphs

1 Introduction

The paper written by Leonhard Euler on the Seven Bridges of Königsberg and published in 1736 is regarded as the first paper in the history of graph theory. Graphs can be used to model many types of relations and processes in physical, biological, social and information systems. Many practical problems can be represented by graphs. In computer science, graphs are used to represent networks of communication, data organization, computational devices, the flow of computation, etc. In mathematics, graphs are useful in geometry and certain parts of topology such as knot theory. Algebraic graph theory has close links with group theory. A graph structure can be extended by assigning a weight to each edge of the graph. Graphs with weights, or weighted graphs, are used to represent structures in which pairwise connections have some numerical values.

The theory of fuzzy sets finds its origin in the pioneering paper of Zadeh. Since then this philosophy had tremendous

impact on logic, information theory etc. and finds its applications in many branches of engineering and technology .

Fuzzy graph theory was introduced by Azriel Rosenfeld in 1975. Though it is very young, it has been growing fast and has numerous applications in various fields. Fuzzy analogues of many structures in crisp graph theory, like bridges, cut nodes, connectedness, trees and cycles etc. were developed after that.

2 Fuzzy Sets and Relations

Throughout this paper we use \vee for Supremum and \wedge for Infimum.

Definition 2.1. A *Fuzzy subset* of a nonempty set S is a mapping $\sigma : S \rightarrow [0, 1]$, where $[0, 1]$ denote the set $\{t \in \mathbb{R}/0 \leq t \leq 1\}$

Here σ assigns to each element $x \in S$ a degree of membership ,
 $0 \leq \sigma(x) \leq 1$.

Definition 2.2. The *support* of a fuzzy set σ is

$$\text{supp}(\sigma) = \{x \in S/\sigma(x) > 0\}$$

and σ is said to be non trivial if $\text{supp}(\sigma) \neq \Phi$

Definition 2.3. Let S and T be two sets and σ and ν be fuzzy subsets of S and T , respectively. Then a *fuzzy relation* μ from the fuzzy subset σ into the fuzzy subset ν is a fuzzy subset μ of $S \times T$ such that $\mu(x, y) \leq \sigma(x) \wedge \nu(y)$, $\forall x \in S$ and $\forall y \in T$.

That is, for μ to be a fuzzy relation, the degree of membership of a pair of elements never exceeds the degree of membership of either of the elements themselves.

The fuzzy relation μ can be represented by means of a matrix $M = (m_{xy})$, where $m_{xy} = \mu(x, y)$, $x \in S$ and $y \in T$.

There are three special cases of fuzzy relations. They are

1. $S = T$ and $\sigma = \nu$. In this case, μ is said to be a fuzzy relation on σ . That is μ is a fuzzy subset of $S \times S$ such that $\mu(x, y) \leq \sigma(x) \wedge \sigma(y)$.

2. $\sigma(x) = 1.0, \forall x \in S$ and $\nu(y) = 1.0, \forall y \in T$. In this case, μ is said to be a fuzzy relation from S into T .
3. $S = T, \sigma(x) = 1.0, \forall x \in S$ and $\nu(x) = 1.0, \forall x \in T$. In this case, μ is said to be a fuzzy relation on S .

Definition 2.4. Let μ be a fuzzy relation on σ . Then μ is called the *strongest fuzzy relation* on σ if and only if for all fuzzy relations ϖ on σ , and for all $x, y \in S, \varpi(x, y) \leq \mu(x, y)$. Thus if μ is the strongest fuzzy relation on σ then $\mu(x, y) = \sigma(x) \wedge \sigma(y), \forall x, y \in S$

Definition 2.5. Let $\mu : S \times T \rightarrow [0, 1]$ be a fuzzy relation from a fuzzy subset σ of S into fuzzy subset ν of T and $\varpi : T \times U \rightarrow [0, 1]$ be a fuzzy relation from a fuzzy subset ν of T into a fuzzy subset ξ of U . Define $\mu \circ \varpi : S \times U \rightarrow [0, 1]$ by

$$\mu \circ \varpi(x, z) = \vee \{ \mu(x, y) \wedge \varpi(y, z) / y \in T \}$$

for all $x \in S, z \in U$. Then $\mu \circ \varpi$ is called the *composite* of μ with ϖ .

The composition of μ with ϖ is a fuzzy relation from a fuzzy subset σ of S into a fuzzy subset ξ of U . The definition of the composition operation reveals that $\mu \circ \varpi$ can be computed similar to a matrix multiplication, where the addition is replaced by \vee and multiplication by \wedge . Since composition is associative, we use the notation μ^2 to denote the composition $\mu \circ \mu, \mu^k$ to denote $\mu^{k-1} \circ \mu, k > 1$.

Define $\mu^\infty(x, y) = \vee \{ \mu^k(x, y) | k = 1, 2, \dots \}$ for all $x, y \in S$. Define $\mu^0(x, y) = 0$ if $x \neq y$ and $\mu^0(x, y) = \sigma(x)$ otherwise, for all $x, y \in S$. Given a fuzzy relation μ on a fuzzy subset σ of S , define the fuzzy relation μ^c on σ by $\mu^c(x, y) = 1 - \mu(x, y)$ for all $x, y \in S$.

Definition 2.6. Let $\mu : S \times T \rightarrow [0, 1]$ be a fuzzy subset of σ of S into a fuzzy subset ν of T . The fuzzy relation $\mu^{-1} : T \times S \rightarrow [0, 1]$ of ν into σ is defined as $\mu^{-1}(x, y) = \mu(y, x)$ for all $(y, x) \in T \times S$.

Let μ and ϖ be fuzzy relations on a fuzzy subset σ of S .

Definition 2.7. A fuzzy relation μ is said to be reflexive (on a fuzzy subset σ of S) if $\mu(x, x) = \sigma(x), \forall x \in S$.

Definition 2.8. A fuzzy relation μ is said to be symmetric if $\mu(x, y) = \mu(y, x), \forall x, y \in S$. In other words, μ is symmetric if the matrix representation of μ is symmetric (with respect to the diagonal).

Definition 2.9. A fuzzy relation μ is said to be transitive if $\mu^2 \subseteq \mu$. Hence μ^∞ is transitive for any fuzzy relation μ .

3 Fuzzy graphs

Any fuzzy relation μ on a fuzzy subset σ , of a set V can be regarded as defining a weighted graph, or fuzzy graph, where the vertex $v \in V$ has weight $\sigma(x) \in [0, 1]$ and edge $(x, y) \in V \times V$ has weight or strength $\mu(x, y) \in [0, 1]$. Since we are considering only simple graphs, all fuzzy relations are symmetric and all edges are regarded as unordered pairs of vertices.

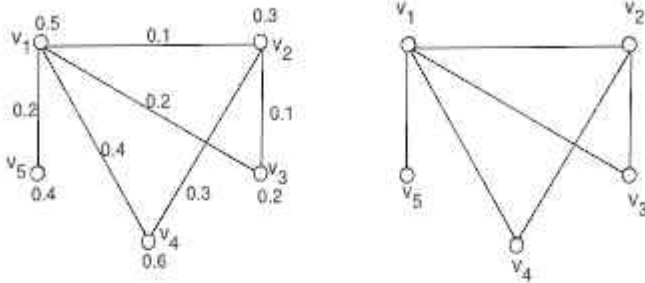
Definition 3.1. A *fuzzy graph* $G = (V, \sigma, \mu)$ is a nonempty set V together with a pair of functions $\sigma : V \rightarrow [0, 1]$ and $\mu : V \times V \rightarrow [0, 1]$ such that for all x, y in $V, \mu(x, y) \leq \sigma(x) \wedge \sigma(y)$.

We call σ , the fuzzy vertex set of G and μ the fuzzy edge set of G , respectively. Note that μ is a fuzzy relation on σ . We will assume that, unless otherwise specified, the underlying set is V and that it is finite. Therefore, for the sake of notational convenience, we omit V in the sequel and use the notation $G = (\sigma, \mu)$. Thus in the most general case, both vertices and edges have membership value. However, in the special case where $\sigma(x) = 1, \forall x \in V$, edges alone have fuzzy membership. So, in this case, we use the abbreviated notation $G = (V, \mu)$.

Any fuzzy graph $G = (\sigma, \mu)$ can be represented diagrammatically like the crisp graph. Each vertex is indicated by a point with weight $\sigma(x)$ and each edge (x, y) by a line joining the points x and y with weight $\mu(x, y)$.

Example 3.1. We give an example of a fuzzy graph and its associated crisp graph in figure 2.1.

We denote the underlying (crisp) graph of $G = (\sigma, \mu)$ by $G^*(V, E)$. Note that a crisp graph $G^*(V, E)$ is a special case of a fuzzy graph with each vertex and edge of G^* having membership value 1.

Figure 1: Fuzzy graph G and its crisp graph

4 Paths and Connectedness

Definition 4.1. A path P in a fuzzy graph $G = (\sigma, \mu)$ is a sequence of distinct vertices x_0, x_1, \dots, x_n (except possibly x_0 and x_n) such that $\mu(x_{i-1}, x_i) > 0, 1 \leq i \leq n$

Here $n \geq 1$ is called the length of the path P .

The consecutive pairs (x_{i-1}, x_i) are called the edges of the path.

The diameter of $x, y \in V$, written as $diam(x, y)$, is the length of the longest path joining x to y .

Definition 4.2. The strength of P is defined as $\wedge_{i=1}^n \mu(x_{i-1}, x_i)$. In other words, the strength of a path is defined to be the weight of the weakest edge of the path. A single vertex x may also be considered as a path. In this case, the path is of length 0.

If the path has length 0, it is convenient to define its strength to be $\sigma(x_0)$.

Definition 4.1. A strongest path joining any two vertices x and y is that path which has strength $\mu^\infty(x, y)$, which is usually called the strength of connectedness between the vertices x and y .

Example 4.1. Consider the example given below.

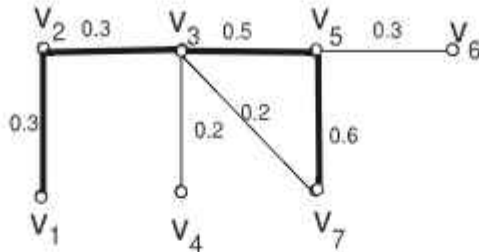


Figure 2: Strongest path from v_1 to v_7

Here v_1, v_2, v_3, v_7 is a path from v_1 to v_7 of length 3. The strongest path joining v_1 to v_7 is the darkened path shown in the figure.

Definition 4.2. A fuzzy graph $G(\sigma, \mu)$ is called a complete fuzzy graph if $\mu(uv) = \sigma(u) \wedge \sigma(v)$, for all $u, v \in V$

Also if G is a complete fuzzy graph then G^* is a complete graph.

5 Weight Matrix of a Fuzzy Graph

Definition 5.1. Let $G(\sigma, \mu)$ be a fuzzy graph with underlying crisp graph $G^*(V, E)$ with order n , and size m . Let x and y be two distinct vertices of G . If there exists at least one path between x and y of length less than or equal to k then the connectedness of strength k between x and y is defined as the maximum of the strength of all paths between them of length less than or equal to k . Otherwise it is defined as zero.

Example 5.1. In the fuzzy graph G in figure3, the connectedness of strength three between the vertices v_1 and v_8 is 0.3. Also the connectedness of strength two between the vertices v_1 and v_5 is 0.3.

Definition 5.2. Let $G(\sigma, \mu)$ be a fuzzy graph with underlying crisp graph $G^*(V, E)$ with $|V| = n$ and $|E| = m$. The $n \times n$

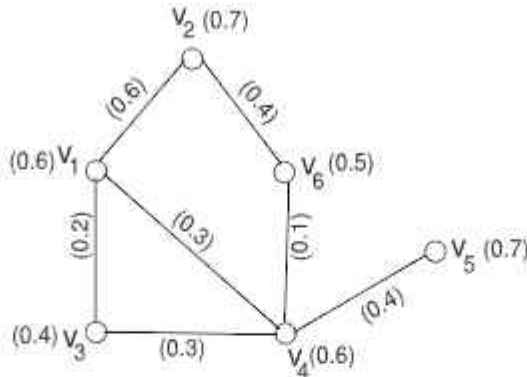


Figure 3: Fuzzy graph G

matrix $A = (a_{ij})$ defined by

$$a_{ij} = \begin{cases} \mu(v_i v_j) & \text{when } i \neq j \\ \sigma(v_i) & \text{when } i = j \end{cases}$$

is called the weight matrix associated with the graph G .

For $i \neq j$ the $(i, j)^{th}$ entry of the weight matrix of the fuzzy graph G represents the weight (membership value) of the edge $v_i v_j$ and a_{ii} represents the weight (membership value) of the vertex v_i . By the definition of a fuzzy graph $a_{ii} \geq a_{ij} = a_{ji}$ for all i, j .

Example 5.2. The weight matrix A of the fuzzy graph G in figure3 is given by

$$A = \begin{bmatrix} 0.6 & 0.6 & 0.2 & 0.3 & 0.0 & 0.0 \\ 0.6 & 0.7 & 0.0 & 0.0 & 0.0 & 0.4 \\ 0.2 & 0.0 & 0.4 & 0.3 & 0.0 & 0.0 \\ 0.3 & 0.0 & 0.3 & 0.6 & 0.4 & 0.1 \\ 0.0 & 0.0 & 0.0 & 0.4 & 0.7 & 0.0 \\ 0.0 & 0.4 & 0.0 & 0.1 & 0.0 & 0.5 \end{bmatrix}$$

6 Properties of the Weight Matrix of fuzzy graphs

Definition 6.1. A symmetric matrix $A = (a_{ij})$ with $a_{ii} \geq a_{ij}$ for all i, j is called a strong diagonal matrix.

Properties of the Weight Matrix associated with fuzzy graphs

1. The weight matrix A of any fuzzy graph is symmetric.
2. The sum of entries in a row or column is equal to the total degree of the corresponding vertex.
3. If A_1 and A_2 are two weight matrices which corresponds to two different labelling of the same fuzzy graph G , then for some permutation matrix P , $PA_1 = A_2P$.
4. Weight matrix of a fuzzy graph with respect to any labelling is strong diagonal.

Suppose $A = (a_{ij})$ is an $n \times n$ strong diagonal matrix with entries in $[0, 1]$. Then there exists a unique fuzzy graph (upto isomorphism) $G(\sigma, \mu)$ with vertices say $\{v_1, v_2, \dots, v_n\}$ such that $\sigma(v_i) = a_{ii}$ and for each pair i, j , ($i \neq j$), $\mu(v_i v_j) = \mu(v_j v_i) = a_{ij}$.

Let $A = (a_{ij})$ and $B = (b_{ij})$ be the given strong diagonal matrices with entries in $[0, 1]$. We define the product AB of A and B as the matrix $C = (c_{ij})$ where c_{ij} is the join of the meet of the corresponding entries of i^{th} row of A and the corresponding entries of j^{th} column of B . We define A^n , for $n \geq 2$, by $A^{n-1}A$.

In general the matrix multiplication defined above on the class of $n \times n$ strong diagonal matrices is not a binary operation. For example consider the matrices A and B given by

$$A = \begin{bmatrix} 0.4 & 0.3 & 0.2 & 0.2 \\ 0.3 & 0.5 & 0 & 0.2 \\ 0.2 & 0.4 & 0.6 & 0.1 \\ 0.2 & 0.2 & 0.1 & 0.3 \end{bmatrix} \quad B = \begin{bmatrix} 0.3 & 0.2 & 0.1 & 0.2 \\ 0.2 & 0.4 & 0.3 & 0.1 \\ 0.1 & 0.3 & 0.3 & 0.0 \\ 0.2 & 0.1 & 0.0 & 0.5 \end{bmatrix}$$

then the product C of A and B is

$$C = \begin{bmatrix} 0.3 & 0.3 & 0.3 & 0.2 \\ 0.3 & 0.4 & 0.3 & 0.2 \\ 0.2 & 0.4 & 0.3 & 0.2 \\ 0.2 & 0.2 & 0.2 & 0.3 \end{bmatrix}$$

But if we restrict the class by considering only the strong diagonal $n \times n$ matrices with fixed diagonal entries, then the matrix multiplication defined above is a binary operation.

Proposition 6.1. Let $A = (a_{ij})$ and $B = (b_{ij})$ be two strong diagonal matrices of the same order. Suppose that $a_{ii} = b_{jj}$, for all i, j . Then their product is again a strong diagonal matrix.

Proof. Suppose $A = (a_{ij})$ and $B = (b_{ij})$ be two strong diagonal matrices with $a_{ii} = b_{ii}$ for every i . Since A and B are strong diagonal matrices we have, $a_{ii} \geq a_{ij} = a_{ji}$ and $b_{ii} \geq b_{ij} = b_{ji}$ for all i, j . Suppose $AB = C = (c_{ij})$. Then

$$c_{ij} = \bigvee_{k=1}^n (a_{ik} \wedge b_{kj}) \leq (a_{ii} \wedge b_{jj}) = a_{ii} = b_{jj}.$$

Thus $c_{ii} \geq c_{ij} \forall i, j$ □

Definition 6.2. Given an $n \times n$ matrix A , the least positive integer n such that $A^n = A^i$, for all $i \geq n$, is called its strength.

Definition 6.3. If G is a fuzzy graph with weight matrix A , then the strength of G is defined as the strength of its weight matrix.

Illustration

Consider the following fuzzy graph.

Here Its weight matrix A is given by

$$\begin{bmatrix} 0.4 & 0.3 & 0.3 & 0.1 & 0 \\ 0.3 & 0.3 & 0.2 & 0.1 & 0 \\ 0.3 & 0.2 & 0.4 & 0.2 & 0.3 \\ 0.1 & 0.1 & 0.2 & 0.2 & 0 \\ 0 & 0 & 0.3 & 0 & 0.5 \end{bmatrix}$$

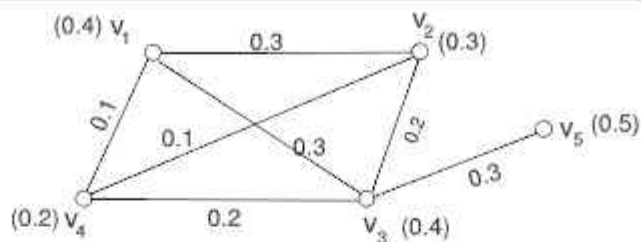


Figure 4: Fuzzy graph G

A^3 is given by the following matrix.

$$\begin{bmatrix} 0.4 & 0.3 & 0.3 & 0.3 & 0.3 \\ 0.3 & 0.3 & 0.3 & 0.2 & 0.3 \\ 0.3 & 0.3 & 0.4 & 0.2 & 0.3 \\ 0.2 & 0.2 & 0.2 & 0.2 & 0.2 \\ 0.3 & 0.3 & 0.3 & 0.2 & 0.5 \end{bmatrix}$$

For every $n \geq 3$, $A^n = A^3$. Hence its strength is 3.

References

1. A.Kaufmann ; *Introduction to Theory of Fuzzy Sets*, AcademicPress Inc, Orlando, Florida, Volume 1,1973.
2. A. Rosenfeld; *Fuzzy Sets and Their Applications to Cognitive and Decision Process*, Academic Press, New York (1975), 75-95.
3. D.B.West; *Introduction to Graph Theory* Prentice Hall of India Pvt Ltd - New Delhi, 1999.
4. D. Dubois and H. Parade; *Fuzzy Sets and Systems, Theory and Applications*,Academic Press, New York, 1980.
5. F. Harary; *Graph Theory* Narosa Addison Wesley Publishing Company, 1988. *Fuzzy Sets*, J.Math Anal.Application 18, 145-173.
6. H.J Zimmerman ; *Fuzzy Set Theory and its Application* Kluwer Academic Publishers, Boston, 1991.
7. J.Clark and D.A.Holton; *A first look at Graph Theory*, Allied Publishers Ltd.1999.
8. J. Harris; *An Introduction to Fuzzy Logic and Applications*, Springer International Edition, 2010.
9. J. A. Bondy, U.S.R. Murty; *Graph Theory*; Springer, 2008.
10. J.N. Mordeson and P.S Nair; *Fuzzy Graphs and Fuzzy Hypergraphs*Physica-verlag, Heidelberg 2000.
11. L.A. Zadeh; *Fuzzy sets ,Information and control* 8.338-353.
12. L. R. Foulds; *Graph Theory Applications*; Narosa Publishing House, 1993.
13. M.B Sheeba and P. Raji; *Strength of fuzzy graphs*, Far east journal of Mathematics, Pushpa publishing company.(accepted).
14. R. Balakrishnan, K. Ranganathan; *A Text Book of Graph Theory*; Springer. 2000.
15. R. Diestel; *Graph Theory*; Third Edn., Springer 2005.

STRENGTH OF A FUZZY GRAPH AS ITS STRENGTH OF CONNECTIVITY

Reshmi K M

Department of Mathematics

Govt.Engineering College, Kozhikode-673010

reshmikm@gmail.com

Abstract

Connectedness of strength k between two distinct vertices of a fuzzy graph, strength of a fuzzy graph and strength of connectivity of a fuzzy graph were introduced by Sheeba M.B and Raji Pilakkat (11). It was also proved that the strength of connectivity of the graph is the strength of the graph (11). In this paper the strength of various fuzzy graphs are determined in terms of order of the graph/ the number of its weakest edge, using the concept of strength of connectivity.

Keywords: Strength, extra strong path, strength of connectivity

1 Introduction

Strength of a path in a fuzzy graph is defined as the membership value of the weakest edge. The concept of a strongest path plays an important role in the structure of fuzzy graphs. In (11) strength of different fuzzy graphs were determined by analysing different powers of its weight matrix. Also the relation between the strength of connectivity of a fuzzy graph and its strength was established in the same paper. Consider the following definitions :

Definition 1.1. Let G be a fuzzy graph with underlying crisp graph G^* . A path P is said to connect the vertices v_i and v_j of G strongly if its strength is maximum among all paths between v_i and v_j . Such paths are called strong paths. i.e. a path is strong if it connect any two vertices strongly.

Given a fuzzy graph G there may exist more than one strong path between two distinct vertices.

Definition 1.2 (11). Any strong path between two distinct vertices v_i and v_j in G with minimum length is called an extra strong path between them.

Definition 1.3 (11). The maximum length of extra strong paths between every pair of distinct vertices in G is called the strength of connectivity of the graph.

Theorem 1.1 (11). Let G be a fuzzy graph with underlying crisp graph G^* and A its weight matrix. Let k denote the strength of connectivity of the graph G . Then the strength of G is k .

We use Theorem (1.1) to establish the relationship between strength of connectivity and strength of a graph. Here we try to prove the same results by Raji Pilakkat and M B Sheeba (10) & (11) analysing the lengths of the extra strong paths in the case of every pair of vertices $(v_i, v_j) \in V \times V$.

As stated earlier, Strength of a fuzzy graph is the maximum of the lengths of all extra strong paths connecting different pairs of vertices in G .

2 Strength of Fuzzy Graphs

Theorem 2.1. Consider a fuzzy graph G . Suppose that G^* is the path $P = v_1 v_2 v_3 \dots v_n$. Then the strength of the graph G is the length $n - 1$ of the path P .

Proof. Consider the vertices v_1 and v_n .



Figure 1: The $n - 1$ path P

The only path connecting v_1 to v_n is P itself. Hence P is the extra strong path between v_1 and v_n , which is of length $n - 1$. Also there exists no path in P of greater length. Hence the strength of G is $n - 1$. \square

Theorem 2.2. If G is not a fuzzy cycle but G^* is a cycle of length n then the strength of the graph G is $n - 1$.

Proof. Since G is not a fuzzy cycle there exists exactly one edge say, uv with minimum membership value.



Figure 2: Fuzzy cycle G

The two paths in G^* joining u to v are the edge uv and the the path $G - \{uv\}$. The strongest of which is the latter. Length of $G - \{uv\}$ is $n - 1$. Again there are no paths of length greater than $n - 1$ in G . Hence strength of G is $n - 1$. \square

Theorem 2.3. Let G be a complete fuzzy graph. Then the strength of the graph G is one.

Proof. Being a complete fuzzy graph, every pair of vertices in G^* is connected by an edge. Also for every edge uv , $\mu(uv) = \sigma(u) \wedge \sigma(v) = \mu^\infty(uv)$. Hence every extra strong path in G is of length one. So the strength of G is one. \square

Theorem 2.4. Let G be a regular fuzzy graph with crisp graph G^* a cycle of length n . Then the strength of G is $\lfloor \frac{n}{2} \rfloor$.

Proof. We consider two cases.

Case:1 n is odd

G being a regular fuzzy graph with G^* a cycle, there exists $k \in [0, 1]$ such that $\mu(v_i v_j) = k$ for all i and j . Hence every path is a strong path. Hence the length of extra strong path is less than or equal to the diameter of $G^* = \lfloor \frac{n}{2} \rfloor$.

Case:2 n is even.

In this case the membership value of either all edges are the same or alternate edges are the same. The first case is same as above. In the second case the strength of any path connecting two vertices v_i and v_j will be the same unless they are adjacent. Hence the length of extra strong path will be less than or equal to $\lfloor \frac{n}{2} \rfloor$.

If they are adjacent the extra strong path will be the edge connecting v_i and v_j . Hence in any case the length of extra strong path is either $\lfloor \frac{n}{2} \rfloor$ or less than $\lfloor \frac{n}{2} \rfloor$. So the strength is $\lfloor \frac{n}{2} \rfloor$. \square

Theorem 2.5. In a fuzzy cycle G of length n , suppose there are l weakest edges where $l \leq \lfloor \frac{n+1}{2} \rfloor$. If these weakest edges form altogether a subpath, then the strength of the graph G is $n - l$.

Proof. Let W denote the subpath formed by the l weakest edges. Let v_i, v_j be any two vertices of G . Then we consider the following cases.

Case : 1

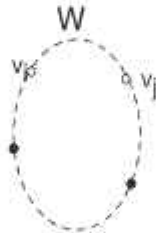


Figure 3: Fuzzy cycle G

The vertices v_i and v_j are internal vertices of W . Since G is a cycle, there are two different paths connecting v_i to v_j . But both have the same strength. Hence the length of extra strong path will be less than or equal to $\lfloor \frac{n}{2} \rfloor$. As $l \leq \lfloor \frac{n+1}{2} \rfloor$, we have $\lfloor \frac{n}{2} \rfloor \leq n - l$.

Case : 2

The vertices v_i and v_j are the internal vertices of W^c . In this case the strongest path will be contained in W^c . Hence the length of extra strong path will be less than or equal to

$n - l$.

Case : 3



Figure 4: Fuzzy cycle G

$v_i \in W$ and $v_j \in W^c$. One of the vertices say, v_i is an internal vertex of W and the other vertex v_j is an internal vertex of W^c . (v_i, v_j are not the end vertices.) Again the two paths connecting v_i to v_j are of equal strength. Hence the length of extra strong path is less than or equal to $\lfloor \frac{n}{2} \rfloor \leq n - l$.

Case : 4



Figure 5: Fuzzy cycle G

The vertices v_i and v_j are end vertices of W . Then W^c is the extra strong path and its length is $n - l$.

Hence considering all the four cases we find that the strength of G is $n - l$. \square

Theorem 2.6. Let G be a fuzzy cycle with crisp graph G^* a cycle of length n , having l weakest edges which form altogether a subpath where $l > [(n+1)/2]$. Then the strength of the graph is $\lfloor \frac{n}{2} \rfloor$.

Proof. Let W denote the subpath of l weakest edges. Then G^* being a cycle any two vertices are connected exactly by two paths. Consider the following cases where $v_i, v_j \in V$

Case : 1

When v_i and v_j are the internal vertices of W or $v_i \in W$ and $v_j \in W^c$. In both of these cases the two paths connecting v_i to v_j are of equal strength. Hence the length of extra strong path is either $\lfloor \frac{n}{2} \rfloor$ or less than $\lfloor \frac{n}{2} \rfloor$.

Case : 2

When v_i and v_j are the end vertices or when v_i and v_j are the internal vertices of W^c . In this case the length of the extra strong path is either less than $\lfloor \frac{n}{2} \rfloor$ or equal to $\lfloor \frac{n}{2} \rfloor$. Hence the strength of G is $\lfloor \frac{n}{2} \rfloor$. \square

Next we try to give a generalized result for a fuzzy graph G having l weakest edges that do not altogether form a subpath.

Theorem 2.7. In a fuzzy cycle G of length n suppose there are l weakest edges which do not altogether form a subpath. Let s denote the maximum length of the subpath which do not contain any weakest edge. Then the strength of the graph is maximum of $\lfloor \frac{n}{2} \rfloor$ and s .

Proof. Let W denote the minimal subpath in G that contains all the l weakest edges. Then W^c will be the maximal subpath in G that contains no weakest edges. Hence length of W^c is s .

Let $v_i, v_j \in V$. Let v_i or v_j but not both happens to be the internal vertices of W . Then both the paths from v_i to v_j have the same strength. Hence the length of the extra strong path is either $\lfloor \frac{n}{2} \rfloor$ or less than $\lfloor \frac{n}{2} \rfloor$.

If both v_i and v_j are the internal vertices of W then two cases arise.

Case:1 When both the edges incident with v_i or v_j are the weakest edges, as illustrated in the following figure. The darken edges are the weakest edges.

Then the two paths connecting v_i to v_j have the same strength. Hence its length is less than or equal to $\lfloor \frac{n}{2} \rfloor$.

Case: 2 When exactly one edge incident with v_i and v_j is a weakest edge, as illustrated in the following figure. In this case

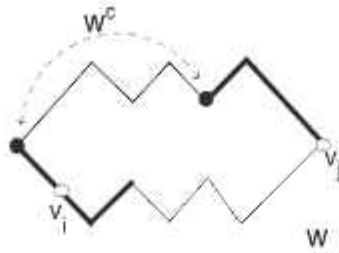


Figure 6: Fuzzy cycle G

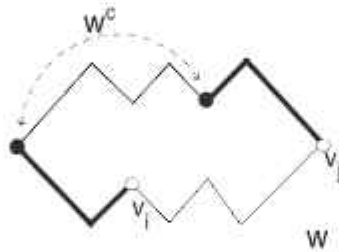


Figure 7: Fuzzy cycle G

the length of the extra strong path will be less than or equal to s .

If both v_i and v_j are the internal vertices of W^c . Then the extra strong path will be a subpath of W^c . Hence its length is less than s .

If both v_i and v_j are end vertices of W or if one is an end vertex and the other an internal vertex of W^c then the extra strong path is a subpath of W^c . Hence the length of it is less than or equal to s .

Considering all the cases we see that strength of $G = \vee\{\lfloor \frac{n}{2} \rfloor, s\}$ \square

Corollary 2.1. Let G be a fuzzy cycle of length n . Suppose

there are l weakest edges which do not altogether form a sub-path. If $l > \lfloor n/2 \rfloor - 1$ then the strength of the graph is $\lfloor n/2 \rfloor$.

Corollary 2.2. Let G be a fuzzy cycle of length n . Suppose there are l weakest edges which do not altogether form a sub-path, but these edges forms part of a $l + 1$ path in G . If $l = \lfloor n/2 \rfloor - 1$ then the strength of the graph is $\lfloor (n+1)/2 \rfloor$.

Example 2.1. Consider the graph given below. Here $n =$

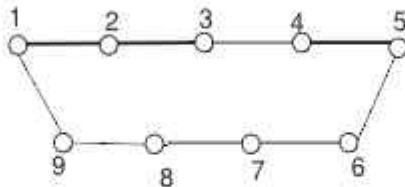


Figure 8: Fuzzy cycle G with $n = 9$, $l = 3$, $s = 4$

9 , $l = 3$, $s = 4$, $\lfloor \frac{9}{2} \rfloor = 4$. So strength = 4

Example 2.2. Consider graph given below. Here $n = 10$, $l =$

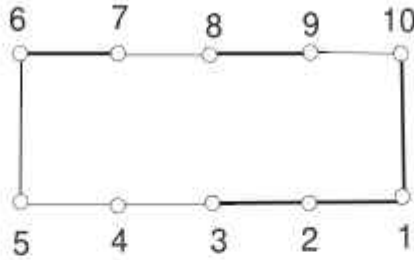


Figure 9: Fuzzy cycle G with $n = 10$, $l = 5$, $s = 3$

5 , $s = 3$, $\lfloor \frac{n}{2} \rfloor = 5$. So strength = $5 = \lfloor \frac{n}{2} \rfloor$

Example 2.3. Consider the graph given below. Here $n =$

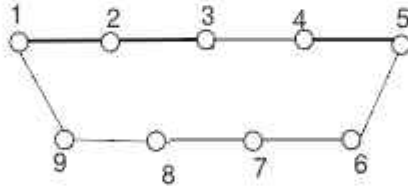


Figure 10: Fuzzy cycle G with $n = 9$, $l = 3$, $s = 5$

9 , $l = 3$, $s = 5$, $\lfloor \frac{n}{2} \rfloor = 4$. So strength = $5 = \lfloor \frac{n+1}{2} \rfloor$

References

1. A Nagoorgani and K. Radha; *On Regular Fuzzy Graphs*; Journal of Physical Sciences Volume 12, 2008, 33-40.
2. A. Nagoorgani and S.R Latha; *On Irregular Fuzzy Graphs* Applied Mathematical Sciences, Volume 6, 2012, 517-523.
3. A. Nagoorgani and V.T Chandrashekarani; *A First Look at Graph Theory*, Allied Publishers, 2010.
4. D.B.West; *Introduction to Graph Theory* Prentice Hall of India Pvt Ltd - New Delhi, 1999.
5. D. Dubois and H. Parade; *Fuzzy Sets and Systems, Theory and Applications*, Academic Press, New York, 1980.
6. F. Harary; *Graph Theory* Narosa Addison Wesley Publishing Company, 1988.
7. J. A. Bondy, U.S.R. Murty; *Graph Theory*; Springer, 2008.
8. J.N. Mordeson and P.S Nair; *Fuzzy Graphs and Fuzzy Hypergraphs* Physica-verlag, Heidelberg 2000.
9. L.A. Zadeh; *Fuzzy sets, Information and control* 8,338-353. Narosa Publishing House, 1993.
10. M.B Sheeba and P. Raji; *Strength of fuzzy graphs*, Far east journal of Mathematics, Pushpa publishing company. (accepted).
11. M.B Sheeba and P. Raji ; *Strength of fuzzy cycles*, SAJM, Vol 1, 2013.
12. R. Balakrishnan, K. Ranganathan; *A Text Book of Graph Theory*; Springer, 2000.

COMPLEMENT TREE DOMINATION NUMBER

■ Raji Pilakkat¹, Roopa.V.K²

¹Professor, Department of mathematics University of Calicut
rajiunical@rediffmail.com

²Asst.professor, Department of Mathematics,
Govt.College, Madappally,
jk.roopa.jk@gmail.com

Abstract

A dominating set $S \subseteq V$ of a graph $G = (V, E)$ is a complement tree dominating set if the induced graph $\langle V - S \rangle$ is a tree. A complement tree dominating set S is a minimal complement tree dominating set if no proper subset $S' \subset S$ is a complement tree dominating set. The complement tree domination number $\gamma_{ct}(G)$ of $G = (V, E)$ is the minimum cardinality of a minimal complement tree dominating set. In this paper, bounds on $\gamma_{ct}(G)$ are obtained and its exact values for some standard graphs are found.

Keywords: wheel graph, wounded spider, dominating set, domination number, γ - set, dominating tree set, nonsplit dominating set, nonsplit domination number, γ_{ns} -set, complement dominating set, complement tree dominating set, complement tree domination number, γ_{ct} - set.

2000 Mathematics Subject Classification: 05C69

1. INTRODUCTION:

All graphs considered here are finite, simple and undirected. Any undefined term in this paper may be found in Haynes et al [4].

For $n \geq 4$, the *Wheel Graph* W_n is $K_1 + C_{n-1}$.

A *Wounded Spider* is the graph K_1 or the graph formed by subdividing at most $t - 1$ of the edges of a star $K_{1,t}$, $t \geq 1$.

The *Star* $K_{1,n-1}$ has one vertex v of degree $n - 1$ and $n - 1$ vertices of degree one.

The *Connectivity* $\kappa(G)$ of G is the minimum number of vertices whose removal results in a trivial or disconnected graph.

For a graph $G = (V, E)$, a set $S \subset V$ is *Independent* if no two vertices in S are adjacent. The *Independence Number* $\beta_0(G)$ is the maximum cardinality of an independent set in G .

The *Open Neighborhood* $N(v)$ of the vertex v consists of the set of vertices adjacent to v .

A set $S \subseteq V$ of vertices in a graph $G = (V, E)$ is called a *Dominating Set* if every vertex $v \in V$ is either an element of S or is adjacent to an element of S . The *Domination Number* $\gamma(G)$ of a graph G equals the minimum cardinality of a dominating set in G .

A dominating set S of a graph $G = (V, E)$ forms a *Dominating Tree Set* if the induced graph $\langle S \rangle$ forms a tree.

A dominating set $S \subseteq V$ of a graph $G = (V, E)$ is a *Nonsplit Dominating Set* if the induced graph $\langle V - S \rangle$ is connected. A nonsplit dominating set S is a *Minimal Nonsplit Dominating Set* if no proper subset $S' \subset S$ is a nonsplit dominating set. The *Nonsplit Domination Number* $\gamma_{ns}(G)$ is the minimum cardinality of a minimal nonsplit dominating set.

A dominating set $S \subseteq V$ of a graph $G = (V, E)$ is a *Complement Tree Dominating Set* if the induced graph $\langle V - S \rangle$ is a tree. A complement tree dominating set S is a *Minimal Complement Tree Dominating Set* if no proper subset $S' \subset S$ is a complement tree dominating set. The *Complement Tree Domination Number* $\gamma_{ct}(G)$ of $G = (V, E)$ is the minimum cardinality of a minimal complement tree dominating set.

We define a set of vertices a γ -set if it is a dominating set with cardinality $\gamma(G)$. Similarly, a γ_{ns} -set and γ_{ct} -set are defined. Unless otherwise stated, a graph has n vertices and m edges.

2. MAIN RESULTS:

Theorem 1: A complement tree dominating set of a graph $G = (V, E)$ exists only if G has exactly one nontrivial component. Thus, a graph G having no isolated vertices has a complement tree dominating

set if and only if G is connected.

Note that, $\gamma_{ct}(G) =$ number of isolated vertices in $G + \gamma_{ct}(G_1)$, Where G_1 is the nontrivial component of G .

Note: Every complement tree dominating set in a connected graph G is a nonsplit dominating set. That is, $\gamma(G) \leq \gamma_{ns}(G) \leq \gamma_{ct}(G)$.

Theorem 2: A complement tree dominating set D of a graph G is minimal if and only if for each vertex $v \in D$ one of the following conditions is satisfied. (i) there exists a vertex $u \in V - D$ such that $N(u) \cap D = \{v\}$.
 (ii) v is an isolated vertex in $\langle D \rangle$.
 (iii) $|N(v) \cap V - D| \neq 1$.

Proof: Let D be a minimal complement tree dominating set of minimum cardinality. Suppose \exists a vertex $v \in D$ such that v does not satisfy any of the conditions. Then conditions (i) and (ii) imply that $D' = D - \{v\}$ is a dominating set. The condition (iii) implies that $\langle V - D' \rangle$ is a tree. Hence, D' is a complement tree dominating set of G , a contradiction. So, for any vertex $v \in D$ one of the three stated conditions hold.

For the converse, assume that D is a complement tree dominating set and for each vertex $v \in D$, one of the three stated conditions holds. Then D is a minimal complement tree dominating set.

For, let v be any vertex of D . If condition (i) holds, then the vertex $u \in V - D$ is dominated by

v only. Hence, $D' = D - \{v\}$ is not a dominating set.

If condition (ii) holds, then $D' = D - \{v\}$ cannot be a dominating set. If third condition holds, then $|N(v) \cap V - D| = 0$ or $|N(v) \cap V - D| \geq 2$. If $|N(v) \cap V - D| = 0$, then $\langle V - (D - \{v\}) \rangle$ is disconnected. Otherwise, $\langle V - (D - \{v\}) \rangle$ is cyclic. Hence, in any case $D' = D - \{v\}$ is not a complement tree dominating set.

Since $v \in V(G)$ is arbitrary, D is a minimal complement tree dominating set. •

Theorem 3: For any complete graph K_n with $n \geq 2$ vertices,

$$\gamma_{ct}(K_n) = \begin{cases} 1 & \text{if } n = 2 \\ n - 2 & \text{if } n \geq 3. \end{cases}$$

Proof: Let K_n be a complete graph on n vertices. For $n = 2$ and 3 the single vertex v of K_n forms a complement tree dominating set of minimum cardinality.

So let us suppose that $n \geq 4$. Let D be any non trivial subset of $V(K_n)$. If $|D| = n - 2$, then D is a complement tree dominating set.

On the other hand, if $|D| = m < n - 2$, then $\langle V - D \rangle$ is K_{n-m} with $n - m \geq 3$. So in this case D is not a complement tree dominating set. Therefore, $\gamma_{ct}(K_n) = n - 2 \forall n \geq 4$.

Hence,

$$\gamma_{ct}(K_n) = \begin{cases} 1 & \text{if } n = 2 \\ n - 2 & \text{if } n \geq 3. \end{cases}$$

Theorem 4: For the graphs C_n and P_n on n vertices,

$$(a) \quad \gamma_{ct}(C_n) = n - 2 \quad \forall n \geq 3$$

$$(b) \quad \gamma_{ct}(P_n) = \begin{cases} n - 1 & \text{if } n = 2, 3 \\ n - 2 & \text{if } n \geq 4. \end{cases}$$

Proof: (a): For $n = 3$, using Theorem 3, •

$$\gamma_{ct}(C_n) = n - 2.$$

So suppose that $n \geq 4$. In this case, any set D of $n - 2$ vertices with $\langle D \rangle = P_{n-2}$ will form a complement tree dominating set. Therefore,

$$\gamma_{ct}(C_n) \leq n - 2.$$

To prove that $\gamma_{ct}(C_n) = n - 2$, let D be any complement tree dominating set for C_n with $|D| = m < n - 2$. Then $\langle V - D \rangle$ is disconnected. If not, then $\langle V - D \rangle$ is a path on $n - m$ vertices with $n - m \geq 3$. In that case the internal vertices of $\langle V - D \rangle$ are not dominated by D , a contradiction. Therefore, D cannot be a complement tree dominating set. So,

$$\gamma_{ct}(C_n) = n - 2 \quad \forall n \geq 4.$$

Hence the result.

(b) A similar proof holds for P_n . •

Theorem 5: For any tree T , $\gamma_{ct}(T) = \Delta(T)$ if and only if T is a wounded spider, where $\Delta(T)$ is the maximum degree of T .

Proof: Let T be the wounded spider obtained by the subdivision of at most $(t - 1)$ edges of $K_{1,t}$ for $t \geq 1$.

If $t = 1$, then $T = K_2$ and the result follows.

Now let D be any complement tree dominating set of T with $|D| = m < \Delta(T)$.

Let v be the vertex of maximum degree in T .

Case 1: $v \in D$.

In this case D contains at most $\Delta(T) - 2$ pendant vertices. Therefore, $\langle V - D \rangle$ is disconnected.

Case 2: $v \notin D$.

In this case D contains at most $\Delta(T) - 1$ pendant vertices. i.e., at least one pendant vertex is left out by D , and not dominated by D . So, D is not a dominating set of T .

Therefore, in any case $\gamma_{ct}(T) \geq \Delta(T)$. Also the set of all pendant vertices will form a complement tree dominating set of cardinality $\Delta(T)$.

Therefore, $\gamma_{ct}(T) \leq \Delta(T)$. Hence,

$$\gamma_{ct}(T) = \Delta(T).$$

Conversely assume that for a tree T , $\gamma_{ct}(T) = \Delta(T)$. If $T \neq K_{1,n}$ the result holds. So assume that $T \neq K_{1,n}$. Let D be a γ_{ct} -set of T and let v be an end vertex of T . Assume that v does not belong to D . Then its support vertex must be in D . Otherwise D would not be a dominating set. Therefore $\langle V - D \rangle$ contains at least two components, a contradiction. So,

$$\gamma_{ct}(T) \geq \text{number of end vertices.}$$

Given that, $\gamma_{ct}(T) = \Delta(T)$. Therefore,

$$\Delta(T) \geq \text{number of end vertices.}$$

Since T is a tree,

$$\Delta(T) \leq \text{number of end vertices.}$$

So, $\gamma_{ct}(T) = \Delta(T) = \text{number of end vertices}$. Since $T \neq K_{1,n}$, this implies that T is the wounded spider.

Note: The converse of this result does not hold for general graph. For example, consider the cycle C_4 . For that, $\gamma_{ct}(G) = 2 = \Delta(G)$.

Theorem 6: For the Wheel graph W_n on $n \geq 4$, vertices, $\gamma_{ct}(G) = 2$.

Theorem 7: For any complete bipartite graph $K_{m,n}$ with $2 \leq m \leq n$,

$$\gamma_{ct}(K_{m,n}) = m.$$

Proof: Let $K_{m,n}$ $2 \leq m \leq n$ be the complete bipartite graph with bipartition (V_1, V_2) . Let $V_1 = \{v_1, v_2, \dots, v_m\}$ and $V_2 = \{u_1, u_2, \dots, u_n\}$. Then

$D = \{v_1, v_2, \dots, v_{m-1}, u_1\}$ forms a complement tree dominating set for $K_{m,n}$. Therefore,

$$\gamma_{ct}(K_{m,n}) \leq m.$$

If $m = 2$, then,

$$\begin{aligned} \gamma(K_{m,n}) &= 2 \\ &\leq \gamma_{ct}(K_{m,n}) \\ &\leq 2. \end{aligned}$$

Therefore, $\gamma_{ct}(K_{m,n}) = 2$, if $m = 2$.

Assume that $3 \leq m \leq n$. Let D be a complement tree dominating set of cardinality k . Suppose $|D| = k \leq m - 1$. Since D is a dominating set of $K_{m,n}$, D must contain vertices from both V_1 and V_2 . Therefore, D contains at most $m - 2$ vertices from each component. Hence, $V - D$ contains at least two vertices from each of V_1 and V_2 . Hence $\langle V - D \rangle$ contains a cycle, which is a contradiction. So,

$$\begin{aligned} |D| &\geq m, \text{ and } \gamma_{ct}(K_{m,n}) \geq m. \text{ Hence,} \\ \gamma_{ct}(K_{m,n}) &= m, \forall 2 \leq m \leq n. \end{aligned} \quad \bullet$$

Theorem 8: A dominating set D of a graph G is a complement tree dominating set if and only if for any pair of vertices $w_1, w_2 \in V - D$, \exists a unique $w_1 - w_2$ path containing vertices of $V - D$ only.

References

- [1] F.Harary; *Graph Theory*, Addison - Wesley, Reading, Massachusetts(1969).
- [2] V. R. Kulli and B.Janakiram, *The Split Domination Number Of A Graph*, Graph Theory Notes of new York XXXII(1997), 16-19.
- [3] V. R. Kulli and B.Janakiram, *The Nonsplit Domination Number of a Graph*, Indian J.Pure appl. Math.,31(4)(2000) 441-447.
- [4] Teresa W.Haynes, Stephen T.Hedetniemi, Peter J.Slater; *Fundamentals of domination in graphs*; Marcel Dekker, Inc (1998).

SOME MORE RESULTS ON COMPLEMENT TREE DOMINATION NUMBER

■ Raji Pilakkat¹, Roopa.V.K²

¹Professor, Department of mathematics University of Calicut
rajiunical@rediffmail.com

²Asst.professor, Department of Mathematics,
Govt.College, Madappally,
jk.roopa.jk@gmail.com

Abstract

A dominating set $S \subseteq V$ of a graph $G=(V,E)$ is a complement tree dominating set if the induced graph $\langle V - S \rangle$ is a tree. A complement tree dominating set S is a minimal complement tree dominating set if no proper subset $S' \subset S$ is a complement tree dominating set. The complement tree domination number $\gamma_{ct}(G)$ of $G = (V, E)$ is the minimum cardinality of a minimal complement tree dominating set. In this paper, bounds on $\gamma_{ct}(G)$ are obtained and its exact values for some more standard graphs are found.

Keywords: wheel graph, wounded spider, dominating set, domination number, γ - set, dominating tree set, nonsplit dominating set, nonsplit domination number, γ_{ns} -set, complement dominating set, complement tree dominating set, complement tree domination number, γ_{ct} - set.

2000 Mathematics Subject Classification: 05C69

1. INTRODUCTION:

All graphs considered here are finite, simple and undirected. Any undefined term in this paper may be found in Haynes et al [4].

For $n \geq 4$, the *Wheel Graph* W_n is $K_1 + C_{n-1}$.

A *Wounded Spider* is the graph K_1 or the graph formed by subdividing at most $t - 1$ of the edges of a star $K_{1,t}$, $t \geq 1$.

The *Star* $K_{1,n-1}$ has one vertex v of degree $n - 1$ and $n - 1$ vertices of degree one.

The *Connectivity* $\kappa(G)$ of G is the minimum number of vertices whose removal results in a trivial or disconnected graph.

For a graph $G = (V, E)$, a set $S \subset V$ is *Independent* if no two vertices in S are adjacent. The *Independence Number* $\beta_0(G)$ is the maximum cardinality of an independent set in G .

The *Open Neighborhood* $N(v)$ of the vertex v consists of the set of vertices adjacent to v .

A set $S \subseteq V$ of vertices in a graph $G = (V, E)$ is called a *Dominating Set* if every vertex $v \in V$ is either an element of S or is adjacent to an element of S .

The *Domination Number* $\gamma(G)$ of a graph G equals the minimum cardinality of a dominating set in G .

A dominating set S of a graph $G = (V, E)$ forms a *Dominating Tree Set* if the induced graph $\langle S \rangle$ forms a tree.

A dominating set $S \subseteq V$ of a graph $G = (V, E)$ is a *Nonsplit Dominating Set* if the induced graph $\langle V - S \rangle$ is connected. A nonsplit dominating set S is a *Minimal Nonsplit Dominating Set* if no proper subset $S' \subset S$ is a nonsplit dominating set. The *Nonsplit Domination Number* $\gamma_{ns}(G)$ is the minimum cardinality of a minimal nonsplit dominating set.

A dominating set $S \subseteq V$ of a graph $G = (V, E)$ is a *Complement Tree Dominating Set* if the induced graph $\langle V - S \rangle$ is a tree. A complement tree dominating set S is a *Minimal Complement Tree Dominating Set* if no proper subset $S' \subset S$ is a complement tree dominating set. The *Complement Tree Domination Number* $\gamma_{ct}(G)$ of $G = (V, E)$ is the minimum cardinality of a minimal complement tree dominating set.

We define a set of vertices a γ - set if it is a dominating set with cardinality $\gamma(G)$. Similarly, a γ_{ns} - set and γ_{ct} - set are defined. Unless otherwise stated, a graph has n vertices and m edges.

2. MAIN RESULTS:

Theorem 1: Every tree T except for star $\gamma_{ct}(T) \leq n - 2$.

Proof: If T is a tree, which is not a star, then \exists two adjacent cut vertices u and v with degrees \geq

2. Therefore, $V - \{u, v\}$ is a complement tree dominating set of T .

So, $\gamma_{ct}(T) \leq n - 2$. •

Theorem 2: If G is a tree such that $\kappa(G) > \beta_0(G)$, then $\gamma_{ct}(G) = \gamma(G)$, where $\kappa(G)$ is the connectivity of G and $\beta_0(G)$ is the independence number of G .

Proof: Let D be a γ -set of G . Since $\kappa(G) > \beta_0(G) \geq \gamma(G)$, $\langle V - D \rangle$ is connected.

Hence, $\gamma_{ct}(G) \leq |D| = \gamma(G)$.

But $\gamma(G) \leq \gamma_{ct}(G)$. Therefore, $\gamma(G) = \gamma_{ct}(G)$. •

Theorem 3: For a connected graph G , the complement tree dominating set S of G is a dominating tree set if S is a γ -set of G .

Proof: Let S be a complement tree dominating set of G . Assume that S is a γ -set. Then $\forall v \in S$ at least one of the following conditions holds.

(a) v is an isolate in S .

(b) $\exists u \in V - S$ such that $N(u) \cap S = \{v\}$. Then we assert that $V - S$ is a dominating tree set for G .

Since S is a complement tree dominating set, $\langle V - S \rangle$ is a tree. Also $V - S$ is a dominating set.

Suppose not. Then $\exists u \in S$ such that u is not dominated by $V - S$. Therefore,

$$N(u) \cap V - S = \emptyset. \quad (1)$$

Since G is a connected graph, u is not an isolate in S . Then using condition (b), $\exists v \in V - S$ such that $N(v) \cap S = \{u\}$ a contradiction to (1). Thus S is not a γ -set of G , which is again a contradiction. Therefore, $V - S$ is a dominating set of G . •

Theorem 4: If a graph $G = (V, E)$ has order ≥ 4 and $\gamma_{ct}(G) = 1$, then G contains $K_{1,2}$ as an induced graph.

Proof: Let $G = (V, E)$ be a graph of order $n \geq 4$ and $\gamma_{ct}(G) = 1$. Let $S = \{v\} \subset V$ be a γ_{ct} -set of G . Then $V - S$ contains $N(v)$ and the graph induced by $N(v)$ is a tree. Since $|V(G)| \geq 4$, $|V - S| \geq 3$. Hence $V - S$ contains $K_{1,2}$ as an induced subgraph. •

Let G be a graph on n vertices and let v be any vertex of G . Then $V - \{v\}$ forms a complement tree dominating set. The next result is a consequence of this.

Result: For any graph on n vertices, $\gamma_{ct} \leq n - 1$.

Result: If a graph G contains two adjacent vertices of degree ≥ 2 , then $\gamma_{ct}(G) \leq n - 2$.

Result: If G is a graph with $\delta(G) \geq 2$, then $\gamma_{ct}(G) \leq n - 2$.

Theorem 5: In a graph G , $\gamma_{ct}(G) < n - 1$, if and only if G contains K_3 or $K_{1,2}$ having at least two of its vertices as non pendant vertices of G as an induced subgraph.

Proof: Let G be a graph such that $\gamma_{ct}(G) < n - 1$ and let D be a γ_{ct} -set with $|D| = k < n - 1$. Then $|V - D| \geq 2$ and hence $V - D$ contains K_2

as an induced subgraph. Let it be $v_1 v_2$. Then, either \exists a vertex $v_3 \in D$ which is adjacent to v_1 and v_2 or \exists two distinct vertices $w_1, w_2 \in D$ such that $v_1 w_1 \in E(G)$ and $v_2 w_2 \in E(G)$. Hence the result.

Conversely assume that G is a graph with K_3 or $K_{-1,2}$ having at least two of its vertices are non pendant vertices of G as an induced subgraph.

Case 1: The graph G contains K_3 as an induced subgraph.

Let u, v be any two vertices of K_3 . Then $V' = V - \{u, v\}$ forms a complement tree dominating set for G . Therefore, $\gamma_{ct}(G) \leq n - 2$.

Case 2: The graph G contains $K_{1,2}$ with the above mentioned property as an induced subgraph.

Let the vertices inducing $K_{1,2}$ be x, u, v , where x is the center of $K_{1,2}$ and v a non pendant vertex in G . Then $V' = V - \{x, v\}$ forms a complement tree dominating set for G . Therefore, $\gamma_{ct}(G) \leq n - 2 < n - 1$. Hence the result. \bullet

Theorem 6: Let T be a tree with at least one cut vertex such that each cut vertex is adjacent to at least one end vertex. Then, $\gamma_{ct}(T) = n - \gamma(T)$, where $\gamma(T)$ is the minimum cardinality dominating set.

Proof: Assume that T is a tree with at least one cut vertex such that each cut vertex is adjacent to at least one end vertex. Let S be the set of all cut vertices of T . Then S is a γ -set for T .

$$\begin{aligned} \gamma(T) &= \text{number of cut vertices of } T \\ &= n - \text{number of pendant vertices of } T. \end{aligned}$$

We assert that the set S' of all pendant vertices of T forms a γ_{ct} -set for T .

Clearly, the set S' forms a complement tree dominating set for T . Therefore, $\gamma_{ct}(T) \leq$ number of pendant vertices, p .

Let D be a γ_{ct} -set for T with cardinality k . Suppose that $k < p$. Since D is a dominating set D must contain at least one support vertex. So, $V - D$ contains at least two pendant vertices of T . If their support vertices are in D , then $V - D$ is disconnected. Otherwise D fails to be a dominating set. Therefore, in either case we have a contradiction. So, $\gamma_{ct}(T) \geq p$.

Hence, $\gamma_{ct}(T) = p$, where p is the number of pendant vertices of T .

$$\begin{aligned}\gamma_{ct}(T) &= n - \text{number of cut vertices of } T \\ &= n - \gamma(T).\end{aligned}$$

Therefore, $\gamma_{ct}(T) = n - \gamma(T)$. •

We have for any graph G , $\gamma_{ct}(G) \leq n - 1$.

Theorem 7: For a graph G , $\gamma_{ct}(G) = n - 1$ if and only if the non trivial component of G is a star.

Proof: Let $G = (V, E)$ be a graph having only one non trivial component G_1 .

Suppose that $G_1 = K_{1,t}$, $t \geq 1$.

$$\gamma_{ct}(G) = |\text{isolated vertices}| + \gamma_{ct}(G_1)$$

$$\begin{aligned}
 &= |\text{isolated vertices}| + t \\
 &= |\text{isolated vertices}| + n - (|\text{isolated vertices}| + 1.)
 \end{aligned}$$

Therefore, $\gamma_{ct}(G) = n - 1$.

For the converse part, assume $\gamma_{ct}(G) = n - 1$. Complement tree dominating set exists only if G has exactly one non trivial component G_1 . Then, we have to show that G_1 is the star $K_{1,t}$, $t \geq 1$. Let D be a γ_{ct} -set for G . Then D contains all isolated vertices in G . Here $|D| = n - 1$. Therefore, $|V - D| = 1$. Let $V - D = \{u\}$. Then $u \in G_1$. If we add another vertex v from G_1 to u , then $D - \{v\}$ is not a complement tree dominating set. But $\langle u, v \rangle$ is connected and hence a tree. Therefore, $D - \{v\}$ is not a dominating set. So, either v is an isolated vertex in D or $N(u) \cap D = \{v\}$. Therefore in any case v is an isolated vertex in D . Since $v \in D$ is arbitrary, D contains isolated vertices only. Hence G_1 is the star $K_{1,t}$, $t \geq 1$.

References

- [1] F.Harary; *Graph Theory*, Addison - Wesley, Reading, Massachusetts(1969).
- [2] V. R. Kulli and B.Janakiram, *The Split Domination Number Of A Graph*, Graph Theory Notes of new York XXXII(1997), 16-19.
- [3] V. R. Kulli and B.Janakiram, *The Nonsplit Domination Number of a Graph*, Indian J.Pure appl. Math.,31(4)(2000) 441-447.
- [4] Teresa W.Haynes, Stephen T.Hedetniemi, Peter J.Slater; *Fundamentals of domination in graphs*; Marcel Dekker, Inc (1998).

CALCULATION OF BETWEENNESS CENTRALITY OF SOME GRAPHS

I Shiny Joseph

Asst. Professor, Department of Mathematics
Govt. Polytechnic College, Meenangadi
shinyjoseph314@gmail.com

Abstract

The betweenness centrality of a graph measures the tendency of a single vertex to be more central than all other vertices in the graph. In many real world situation it has quite a significant role. In this paper we study about the betweenness centrality of graphs obtained by some graph operations in the star graph and study some construction of betweenness uniform graphs.

1. INTRODUCTION

The common way to express the importance of network objects is to quantify it by evaluating a specific centrality index on the vertices of the graph representing a given network ; where the vertices with the higher values of centrality are perceived as being more important [9].

Betweenness centrality plays an important role in analysis of social networks, computer networks and many other types of network data models [7,8,9].

Betweenness centrality measures the extent to which a vertex lies on the shortest paths between pairs of other vertices [4].

Let $G(V, E)$ be a simple connected undirected graph with vertex set V and edge set E , n and m denote the number of its vertices and edges respectively. For every vertex $v \in V$, the open neighbourhood of v is the set $N(v) = \{u \in V : uv \in E\}$ and the closed neighbourhood of v is the set $N[v] = N(v) \cup \{v\}$. The degree of a vertex $v \in V$ is $deg(v) = |N(v)|$. For any two vertices $u, v \in V$, the distance $d(u, v)$ between u and v is the length of a shortest path between u and v in G . The eccentricity of a vertex u is the number $e(u) = \max\{d(u, v) : v \in V\}$. The maximum eccentricity of the vertices of G is called the diameter of G and is denoted by D .

Definition 1.1 [8] : Let $G(V, E)$ be a simple connected undirected graph with vertex set V . The betweenness centrality of a vertex $v \in V$ is given by

$$B(v) = \sum_{s \neq v \neq t} \frac{\sigma_{st}(v)}{\sigma_{st}}, \text{ where } \sigma_{st} \text{ is the number}$$

of shortest paths with vertices s and t as their end vertices and $\sigma_{st}(v)$ is the number of those shortest paths that include vertex v .

Definition 1.2 [8] : The average vertex betweenness centrality of a graph $G(V, E)$ of order

n is defined as $B(G) = \frac{1}{n} \sum_{v \in V} B(v)$.

2. BETWEENNESS CENTRALITY OF SOME GRAPH OPERATIONS.

For any vertex $v \in V$ of a graph G of order n , $B(v)$ lies between 0 and $\binom{n-1}{2}$, where the value 0 is reached if and only if all neighbours of v induce a clique in G and $\binom{n-1}{2}$ is the case where G is the star graph S_n with v as its central vertex [9].

In this section we calculate the betweenness centrality of the vertices of the graph obtained by the join of the star graph and a vertex, the betweenness centrality of the vertices of the graph $K_2 \times S_n$, the betweenness centrality of the graph obtained by joining a vertex to the pendant vertices of S_n and the betweenness centrality of the vertices of the lexicographic product $S_n \cdot K_2$ and $K_2 \cdot S_n$.

Theorem 2.1. [1] : If diameter D of a graph G is 2, then the betweenness centrality of a vertex

$v \in G$ is given by $B(v) = \sum_{\substack{s, t \in N(v) \\ st \in E(G), s \neq t}} \frac{1}{\sigma_{st}}$.

Theorem 2.2 : The betweenness centrality of the vertices of the join of the star graph S_n and the vertex a , is given by

$$B(v) = \frac{1}{2} \binom{n-1}{2}; \text{ if } v = a \text{ or } v \text{ is the central vertex}$$

$$= 0 \quad ; \quad \text{otherwise}$$

Proof : Consider the star graph S_n with vertex set $u, v_1, v_2, \dots, v_{n-1}$ where u is the central vertex and K_1 with vertex a . Consider $S_n \wedge K_1$.

$$N(u) = \{a, v_1, v_2, \dots, v_{n-1}\}, a v_i \in E(S_n) \text{ for } i = 1, 2, \dots, n-1$$

$$N(a) = \{u, v_1, v_2, \dots, v_{n-1}\}, u v_i \in E(S_n) \text{ for } i = 1, 2, \dots, n-1$$

There are two paths connecting v_i and v_j through u and a . Thus each nonadjacent pair (v_i, v_j) , $i < j$ contributes two shortest paths. Since there are $\binom{n-1}{2}$ such combinations, by Theorem 2.1,

$$B(v) = B(a) = \frac{1}{2} \binom{n-1}{2}.$$

Now $N(v_i) = \{u, a\}$, for $i = 1, 2, \dots, n-1$ and $au \in E(S_n)$

Hence by Theorem 2.1, $B(v_i) = 0$, for $i = 1, 2, \dots, n-1$.

Theorem 2.3 : The betweenness centrality of the graph $K_2 \times S_n$ is given by

$$B(u, v_i) = \frac{(n-1)(7n-11)}{6}, \quad i = 1, 2 ;$$
 if u is the central vertex of S_n

$$B(u_j, v_i) = \frac{(2n-1)}{6}, \quad j = 1, 2, \dots, n-1, i = 1, 2.$$

Proof : Consider the graph S_n with vertex set $u, u_1, u_2, \dots, u_{n-1}$ where u is the central vertex and the graph K_2 with vertex set v_1, v_2 .

There is only one shortest path connecting (u_i, v_1) and (u_j, v_1) for $i \neq j$ and which passes through (u, v_1) . There are $\binom{n-1}{2}$ such combinations.

Hence
$$\sum_{\substack{i \neq j \\ (u_i, v_1), (u_j, v_1) \in V(K_2 \times S_n)}} \frac{\sigma_{(u_i, v_1), (u_j, v_1)}((u, v_1))}{\sigma_{(u_i, v_1), (u_j, v_1)}} = \binom{n-1}{2}$$

There are three shortest paths connecting (u_i, v_1) and (u_j, v_2) for $i \neq j$ and two of them passing through the vertex (u, v_1) . There are $((n-1)(n-2))$ such combinations.

Hence
$$\sum_{\substack{i \neq j \\ (u_i, v_1), (u_j, v_2) \in V(K_2 \times S_n)}} \frac{\sigma_{(u_i, v_1), (u_j, v_2)}((u, v_1))}{\sigma_{(u_i, v_1), (u_j, v_2)}} = ((n-1)(n-2)) \frac{2}{3}.$$

There are two shortest paths from (u_i, v_1) to (u, v_2) of which one is passing through the vertex (u, v_1) . There are $(n-1)$ such combinations.

$$\sum_{\{u_i, v_1\}, \{u, v_2\} \in V(K_2 \times S_n)} \frac{\sigma_{\{u_i, v_1\}, \{u, v_2\}}(\{u, v_1\})}{\sigma_{\{u_i, v_1\}, \{u, v_2\}}} = ((n-1)) \frac{1}{2}$$

There is no shortest path from (u_i, v_2) to (u_j, v_2) which passes through (u, v_1) .

$$\text{Hence } B(u, v_1) = \binom{n-1}{2} + \frac{n-1}{2} + (n-1)(n-2) \frac{2}{3}$$

Similarly

$$\sum_{\substack{i \neq j \\ \{u_i, v_2\}, \{u_j, v_2\} \in V(K_2 \times S_n)}} \frac{\sigma_{\{u_i, v_2\}, \{u_j, v_2\}}(\{u, v_2\})}{\sigma_{\{u_i, v_2\}, \{u_j, v_2\}}} = \binom{n-1}{2}$$

$$\sum_{\{u_i, v_2\}, \{u, v_1\} \in V(K_2 \times S_n)} \frac{\sigma_{\{u_i, v_2\}, \{u, v_1\}}(\{u, v_2\})}{\sigma_{\{u_i, v_2\}, \{u, v_1\}}} = ((n-1)) \frac{1}{2}$$

$$\sum_{\substack{i \neq j \\ \{u_i, v_2\}, \{u_j, v_1\} \in V(K_2 \times S_n)}} \frac{\sigma_{\{u_i, v_2\}, \{u_j, v_1\}}(\{u, v_2\})}{\sigma_{\{u_i, v_2\}, \{u_j, v_1\}}} = ((n-1)(n-2)) \frac{2}{3}$$

$$\sum_{\substack{i \neq j \\ \{u_i, v_2\}, \{u_j, v_2\} \in V(K_2 \times S_n)}} \frac{\sigma_{\{u_i, v_2\}, \{u_j, v_2\}}(\{u, v_2\})}{\sigma_{\{u_i, v_2\}, \{u_j, v_2\}}} = 0$$

$$\text{Hence } B(u, v_2) = \binom{n-1}{2} + \frac{n-1}{2} + (n-1)(n-2)\frac{2}{3}$$

$$\text{Thus } B(u, v_i) = \frac{(n-1)(7n-11)}{6}, \text{ for } i = 1, 2.$$

There are two shortest paths connecting (u, v_1) and (u_i, v_2) of which one is passing through the vertex (u_i, v_1) . There are three shortest paths connecting (u_j, v_1) to (u_i, v_2) for $i \neq j$ of which one is passing through the vertex (u_i, v_1) . There are $(n-2)$ such combinations for a fixed i .

$$\text{Hence } B((u_i, v_1)) = \frac{1}{2} + (n-2)\frac{1}{3}, \text{ for } i = 1, 2, \dots, n-1.$$

$$\text{Similarly we get } B((u_i, v_2)) = \frac{1}{2} + (n-2)\frac{1}{3}, \text{ for } i = 1, 2, \dots, n-1.$$

Theorem 2.4 : The betweenness centrality of the vertices of the graph obtained by joining the vertex a to every pendant vertices of S_n is given by

$$\begin{aligned} B(v) &= \frac{(n-1)(n-2)}{4}; \text{ if } v \text{ is the central vertex or} \\ &\quad v = a \\ &= \frac{1}{n-1}; \text{ otherwise.} \end{aligned}$$

Proof : Consider the star graph S_n with vertex set $u, v_1, v_2, \dots, v_{n-1}$ where u is the central

vertex and consider the vertex a . Now join the vertex a to every pendant vertices v_1, v_2, \dots, v_{n-1} . $N(u) = N(a) = \{v_1, v_2, \dots, v_{n-1}\}$. There are two paths connecting v_i and v_j through u and a . Hence for each nonadjacent pair (v_i, v_j) , $i < j$, contributes two shortest paths. Since there are $\binom{n-1}{2}$ such combinations, by Theorem 2.1

$$B(v) = B(a) = \frac{1}{2} \binom{n-1}{2} \cdot N(v_i) = \{u, a\} \text{ for } i = 1, 2, \dots, n-1.$$

There are $n-1$ paths connecting u and a through v_1, v_2, \dots, v_{n-1} .

Hence by Theorem 2.1, $B(v_i) = \frac{1}{n-1}$, for $i = 1, 2, \dots, n-1$.

Theorem 2. 5 : The betweenness centrality of the vertices of the lexicographic product

$S_n \cdot K_2$ is given by

$B(u, v_i) = \binom{n-1}{2} \frac{3}{2}$, $i = 1, 2$; if u is the central vertex of S_n

$$B(u_j, v_i) = 0, j = 1, 2, \dots, n-1, i = 1, 2.$$

Proof : Consider the graph S_n with vertex set $u, u_1, u_2, \dots, u_{n-1}$ where u is the central vertex and the graph K_2 with vertex set v_1, v_2 . $N((u, v_i)) = V(S_n \cdot K_2) - |(u, v_i)|$, $i = 1, 2$. There are two shortest paths connecting each nonadjacent pair of vertices in $N((u, v_i))$. Since there are $\binom{n-1}{2} + (n-1)(n-2)$ such combinations, by theorem 2.1

$B(u, v_i) = \binom{n-1}{2} \frac{3}{2}$, $i = 1, 2$. Since all the vertices in $N(u_j, v_i)$ are adjacent $B(u_j, v_i) = 0$, $j = 1, 2, \dots, n-1$, $i = 1, 2$.

Theorem 2. 5 : The betweenness centrality of the vertices of the lexicographic product

$K_2 \cdot S_n$ is given by

$$B(v_i, u) = \frac{(n-1)(n-2)}{n+1}, \quad i = 1, 2; \text{ if } u$$

is the central vertex of S_n

$$B(v_j, v_i) = \frac{(n-1)(n-2)}{2(n+1)}, \quad j = 1, 2, \dots, n-1,$$

$i = 1, 2$.

Proof : Consider the graph S_n with vertex set $u, u_1, u_2, \dots, u_{n-1}$ where u is the central vertex and the graph K_2 with vertex set v_1, v_2 .

$N((v_i, u)) = V(K_2.S_n) - |(v_i, u)|$, $i = 1, 2$. Each nonadjacent pair of vertices in $N((v_i, u))$ contributes $(n+1)$ paths.

Since there are $2 \binom{n-1}{2}$ such pairs, by theorem 2.1,

$$B(v_i, u) = \frac{(n-1)(n-2)}{n+1}, \quad i = 1, 2.$$

$$N((v_i, u_j)) = |(v_k, u_s)_{k \neq i, s=1,2,\dots,n-1}, (v_1, u), (v_2, u)|, \\ i = 1, 2, \quad j = 1, 2, \dots, n-1.$$

Each nonadjacent pair of vertices in $N((v_i, u_j))$ contributes $(n+1)$ paths.

Since there are $\binom{n-1}{2}$ such pairs, by theorem 2.1

$$B(v_i, u_j) = \frac{(n-1)(n-2)}{2(n+1)}, \quad i = 1, 2,$$

$$j = 1, 2, \dots, n-1.$$

3. SOME RESULTS ON BETWEENNESS UNIFORM GRAPHS

Definition 3.1. [1] : Graphs with vertices having the same betweenness centrality are called betweenness uniform graphs. In this section we try to construct some betweenness uniform graphs with given betweenness centrality.

Theorem 3. 1 : For any given integer $n > 2$, there exists a betweenness uniform graph with betweenness centrality 1.

Proof : Construct the graph G with vertex set v_1, v_2, \dots, v_n such that join the vertex v_i to all other vertices except v_{i-1} and v_{i+1} . If $i = 1$ take $v_{i-1} = v_n$ and if $i = n$ take $v_{i+1} = v_1$. There are $(n-4)$ shortest paths connecting v_j and v_{j+1} and exactly one of them passing through each v_i except $i = j-1, j, j+1, j+2$.

That is
$$\sum_{\substack{v_j, v_{j+1} \in V(G) \\ i \neq j}} \frac{\sigma_{v_j, v_{j+1}}(v_i)}{\sigma_{v_j, v_{j+1}}} = (n-4) \frac{1}{n-4} \quad , \text{ for}$$

$i = 1, 2, \dots, n$. Hence $B(v_i) = 1$, for $i = 1, 2, \dots, n$. Therefore G is a betweenness uniform graph with betweenness centrality 1 .

Theorem 3. 2 : For any given integer n , there exists a betweenness uniform graph with betweenness centrality $\frac{n-1}{2}$.

Proof : Consider two complete graphs , K_n with vertices u_1, u_2, \dots, u_n and vertices v_1, v_2, \dots, v_n . Join the vertex u_i to the vertex v_i for $i = 1, 2, \dots, n$. $N(u_i) = \{u_1, u_2, \dots, u_{i-1}, u_{i+1}, \dots, u_n, v_i\}$, $u_i u_j \in E(G)$ for $i, j = 1, 2, \dots, n$ and $u_i v_i \in E(G)$. There are two paths connecting u_j and v_i through v_j and u_i for $j = 1, 2, \dots, i-1, i+1, \dots, n$. Since there are $(n-1)$ such combinations by Theorem 2.1

$$B(u_i) = \frac{n-1}{2}, \quad i = 1, 2, \dots, n.$$
 Now,

$$N(v_j) = \{v_1, v_2, \dots, v_{i-1}, v_{i+1}, \dots, v_n, u_j\}$$

$$v_i v_j \in E(G) \text{ for } i, j = 1, 2, \dots, n \text{ and } v_j u_j \in E(G).$$

There are two shortest paths connecting v_i and u_j through u_j and v_j for $i = 1, 2, \dots, j-1, j+1, \dots, n$. Since there are $(n-1)$ such combinations by Theorem 2.1

$$B(v_j) = \frac{n-1}{2}, \quad j = 1, 2, \dots, n.$$

Thus the graph constructed with $2n$ vertices is a betweenness uniform graph with betweenness centrality $\frac{n-1}{2}$.

REFERENCES

- [1] Jana Coroničová Hurajová, Tomas Madaras, Kosice, "More on betweenness-uniform graphs," *Czechoslovak Mathematical Journal*, 68(143) (2018), 293-306.
- [2] S. Gago, J. Coroničová Hurajová, and T. Madaras, "On betweenness-uniform graphs," *Czechoslovak Mathematical Journal*, vol. 63, no. 3, pp.629–642, 2013.
- [3] S. Gago, J. Hurajová, T. Madaras, "Notes on the betweenness centrality of a graph", *Math. Slovaca* 62 (1) (2012) 1–12.
- [4] Sunil Kumar Raghavan Unnithan, Balakrishnan Kannan, and Madambi Jathavedan, "Betweenness Centrality in Some Classes of Graphs" *International Journal of Combinatorics*, Vol.2014
- [5] L. C. Freeman, "A set of measures of centrality based on betweenness," *Sociometry*, vol. 40, pp. 35–41, 1977.
- [6] L. C. Freeman, "Centrality in social networks conceptual clarification," *Social Networks* vol. 1, no. 3, pp. 215–239, 1979.
- [7] W. Imrich, S. Klavzar, and Douglas F.R., Topics in graph theory : Graphs and their cartesian product, *Wiley-Interscience, New York*, 2000.

- [8] Riste Skrekovski, Ivan Gutman, Vertex version of the Wiener Theorem, *MATCH Communications in Mathematical and in Computer Chemistry*, 72 (2014)295-300
- [9] "Quantitative Graph Theory Mathematical foundations and applications", Matthias Dehmer and Frank Emmert Streib, CRC press Taylor and Francis group.

DIRECT SUM OF WEAK SPECTRAL SYNTHESIS SETS

MURALEEDHARAN T K

Department of Mathematics,
St. Josephs College Devagiri, Kozhikode - 673008, India.
muralreedharandevagiri@gmail.com

ABSTRACT

A result on weak spectral synthesis of direct sum which is a generalisation of a result of R. Lasser on spectral synthesis sets, is proved.

Key words: Spectral synthesis, C-Set, S-Set.

MSC 2010: 43A45

Let G be a locally compact abelian group, \hat{G} be its dual group. For a subset E of G , Let $I(E) = \{f \in L^1(G) : \hat{f} = 0 \text{ on } E\}$ and $J(E) = \{f \in L^1(G) : \text{supp } f \cap E = \emptyset\}$ and $\overline{J(E)} = \overline{J(E)}$. Then both $I(E)$ and $\overline{J(E)}$ are the biggest and smallest closed ideal of $L^1(G)$ with zero set E . Then E is said to be a weak synthesis set or weak S-Set of characteristic n if $f^n \in J(E)$ for every $f \in I(E)$, see[3]. In this paper we generalise a result of R. Lasser [2] for weak spectral synthesis sets. Notations are from [1]

We need the following lemma which is proved as a part of the theorem in [2].

Lemma Let G be a locally compact abelian group, \hat{G} be its dual group and H a closed subgroup of \hat{G} . Let $r : G \rightarrow \hat{H}$ be the restriction map of $G = \hat{\hat{G}}$ on \hat{H} . Let $K \subset G$ be the dual of \hat{G}/H . Let T be a compact set in G such that r is one-to-one on T and let $S \subset K$ be a closed set with scattered boundary ∂S (i) Suppose that

I_1 is a closed ideal in $A(G)$ with zero set $S + T$. If $f \in A(G)$ satisfies the following two conditions,

then $f \in I_1 + I(K + T)$.

(1) there exist a compact set $C \subset K$ and $g \in I_1$ such that

$$f - g \in I((K \setminus C) + T);$$

(2) for each $y \in K$ there exist an open neighbourhood V of y in K and $a \in I_1$ such that $f - a \in I(V + T)$.

(ii) Let $f \in I(S + T)$ and $\Delta(f, I_1) = \{y \in K, \text{for which there do not exist } V \text{ and } g \text{ as in (i)}\}$. Then $\Delta(f, I_1)$ is closed and is a subset of the boundary of S .

Theorem Let G be a locally compact abelian group, \hat{G} its dual group and H a closed subgroup of \hat{G} . Let $r: G \rightarrow \hat{H}$ be the restriction map of G on \hat{H} . Let T be a compact weak S -set in G such that r is one-to-one on T (so that $K + T$ is a direct sum). Let $S \subset K$ be a closed set with scattered boundary ∂S where $K = H^\perp \subset \hat{G}$ is the dual group of \hat{G}/H . If $K + T$ is a weak S -set, then $S + T$ is a weak S -set.

Proof: Let I_1 be as in the above lemma and let $f \in A(G)$ satisfy the conditions (1) and (2) mentioned in the lemma.

Then $f \in I_1 + I(K + T)$. Given that $K + T$ is a weak S -set; let n be its characteristic. Then $I^n(K + T) \subset \overline{I(K + T)} \subset I(S + T) \subset I_1$. We have $f = g + h$ where $g \in I_1$ and $h \in I(K + T)$. So $f^n = (g + h)^n = g_1 + h^n$ where $g_1 \in I_1$. So $f^n \in I_1$.

Let $m - 1$ be the characteristic of T and let $f \in I(S + T)$. Then we Prove $\Delta(f^{mn}, I_1) = \emptyset$. From part (ii) of lemma it is enough to prove that $\Delta(f^{mn}, I_1)$ has no isolated points. Suppose y is an isolated point of $\Delta(f^{mn}, I_1)$. Then there exists an open neighbourhood U of y in K such that $U \setminus \{y\} \subset K \setminus \Delta(f^{mn}, I_1)$. Since $I_1 + I(y + T) = I(y + T) \supset I(S + T)$, there is a $g \in I_1$, such that $f - g \in I(y + T)$. T is a weak S -set of characteristic $m - 1$, so

$y + T$ is a weak S -set of the same characteristic. So there exists a function f_k vanishing in a neighborhood W_k of $y + T$ such that $(f - g)^{m-1} = \lim f_k$. So $(f - g)^m = \lim f_k + (f - g)$. Then there are open $V_k \subset K$ such that $y \in V_k$ and $V_k + T \subset W_k$ therefore f_k is zero on $V_k + T$. Choose open neighbourhoods V, W of y in K such that $V \subset \bar{V} \subset W \subset \bar{W} \subset U$ with \bar{V}, \bar{W} compact. Then $(\bar{V} + T) \cap ((K \setminus W) + T) = \emptyset$ and there is an $h \in A(G)$ such that $h(x) = 1$ for all $x \in \bar{V} + T$ and $h(z) = 0$ for all $z \in (K \setminus W) + T$. Now we can apply the first part of the lemma. Thus $[hf_k(f - g)]^n \in I_1, h^n(f - g)^{mn} \in I_1$, so $h^n f^{mn} \in I_1$. Then $f^{mn} = h^n f^{mn} - (h^n f^{mn} - f^{mn}) \in I_1 + I(V + T)$. So $y \notin \Delta(f^{mn}, I_1)$ a contradiction. Hence $\Delta(f^{mn}, I) = \emptyset$.

When K is compact, f^{mn} satisfies the conditions in lemma(i) and so $f^{mn} \in I_1 + I(K + T)$. As before this implies $(f^{mn})^n \in I_1$. Suppose that K is not compact. For $f \in I(S + T)$, choose $g_k \in A(G)$ such that $\text{supp } g_k$ is compact and $\lim f g_k = f$. Further for each $k \in N$ there is a compact $C \subset K$ such that $\text{supp } g_k \cap K + T \subset C + T$, hence $f + g_k \in I((K \setminus C) + T)$ so $(f + g_k)^{mn} \in I((K \setminus C) + T)$ thus $\Delta((f + g_k)^{mn}, I_1) = \emptyset$, thus $((f + g_k)^{mn})^n \in I_1$, so $f^{mn^2} \in I_1$ thus $S + T$ is a weak S -set.

Corollary In the statement of the theorem assume T is a C -set; then characteristic of $S + T$ is less than or equal to n^2 , where n is the characteristic of $K + T$.

REFERENCE

1. J.J. Benedetto, Spectral synthesis, Academic Press, New York (1975).
2. R. Lasser, A result on spectral synthesis of direct products, Math. Scand. 44(1979), 335-338
3. C.R. Warner, Weak spectral synthesis, Proc. Amer. Math. Soc. 99(1987), 244-248.